

**International
Progress Report**

IPR-03-34

Äspö Hard Rock Laboratory

Update of the geological model 2002

Johan Berglund, SwedPower AB

Philip Curtis, FB Engineering AB

Thomas Eliasson, Sveriges Geologiska Undersökning

Tommy Olsson, I&T Olsson AB

Peter Starzec, Statens geotekniska institut

Eva-Lena Tullborg, Terralogica AB

December 2003

Svensk Kärnbränslehantering AB

Swedish Nuclear Fuel

and Waste Management Co

Box 5864

SE-102 40 Stockholm Sweden

Tel 08-459 84 00

+46 8 459 84 00

Fax 08-661 57 19

+46 8 661 57 19



**Äspö Hard Rock
Laboratory**

Report no.	No.
IPR-03-34	F117K
Author	Date
Johan Berglund	Dec. 2003
Philip Curtis	
Thomas Eliasson	
Tommy Olsson	
Peter Starzec	
Eva-Lena Tullborg	
Checked by	Date
Rolf Christiansson	2005-03-07
Approved	Date
Christer Svemar	2005-03-30

Äspö Hard Rock Laboratory

Update of the geological model 2002

Johan Berglund, SwedPower AB
Philip Curtis, FB Engineering AB
Thomas Eliasson, Sveriges Geologiska Undersökning
Tommy Olsson, I&T Olsson AB
Peter Starzec, Statens geotekniska institut
Eva-Lena Tullborg, Terralogica AB

December 2003

Keywords: Äspö descriptive model, GeoMod, Geology, Geological model, Fractures, Fracture statistics, Fracture zones, Deformation zones, Ductile deformation, Brittle deformation

This report concerns a study which was conducted for SKB. The conclusions and viewpoints presented in the report are those of the author(s) and do not necessarily coincide with those of the client.

Preface

The main purpose of the GeoMod project, which initiated in the beginning of 2002, was to update the previous geoscientific model of Äspö (Äspö96), mainly by incorporate additional data collected after 1995. The updated model (Äspö02) was meant to, as far as possible, be integrated in a three dimensional digital model and to be documented in a single technical report.

The geoscientific disciplines: geology, rock mechanics, hydrogeology and hydrogeochemistry, were supposed to be integrated into a common understanding of the site. However it became obvious, during the spring 2003, that the necessary integration efforts far exceeded the expected. As a result of this, the GeoMod project was temporarily terminated in May 2003.

The result obtained within geology, when the project was terminated, is presented in this report. The other progress reports are:

- IPR-03-35
Äspö Hard Rock Laboratory
Update of the hydrogeological model 2002
- IPR-03-36
Äspö Hard Rock Laboratory
Update of the hydrogeochemical model 2002
- IPR-03-37
Äspö Hard Rock Laboratory
Update of the rock mechanical model 2002

Recommendations of further work are presented in the reports.

The helpful comments, suggestions and reviewing from Johan Andersson, Mel Cascoyne, Richard Everitt, John A Hudson, Bill Lanyon and Anders Winberg are acknowledged. The support and help from: Mansueto Morosini, Tommy Olsson and Roger Taringer are acknowledged.

Rolf Christiansson

Abstract

The Äspö Hard Rock Laboratory (HRL) was established in the end of the eighties as a full scale laboratory for constructing, building and operating a deep repository for spent nuclear fuel and for developing and testing equipment and methods for characterization of possible repository sites.

The work with the Äspö HRL has been divided into three phases. These are the pre-investigation phase, the construction phase and the operative phase. At present the activities are performed in the latter, operative phase. After the construction phase SKB presented a 2D geological model, Äspö96 / Rhén et al., 1997 /, which was based on the investigations made in the first two phases. In GeoMod, the Äspö96-model has been updated to 3D. It also includes results from complementary investigations performed during the operative phase. The present report is a progress report in the GeoMod-project.

Hydrological pathways in- and around a planned deep repository and in a hard rock laboratory as the one at Äspö are in focus in many of the SKB investigations, as circulating fluids are a probable transporting agent for radioactive nuclides in a potential leakage from a deep repository. Genesis, geometry and other features of open fractures in the rock volume, both the present one as well as possible forthcoming ones, is thereby essential when describing and modelling the geology. In the present report the geology is described briefly on a regional scale and on a local Äspö scale. The individual objects of the 3D geological model are described in more detail. The descriptions are mainly based on existing reports and on data from the SKB databases SICADA and TMS (Tunnel Mapping System). Also data achieved in the present project are included, such as interpretations of magnetic survey maps, interpretations of BIPS-images, analyses and descriptions of water conducting features and judgements of reliabilities.

All regional structural zones from the former model (Äspö96) are present also in the present model (Äspö02), with only minor geometric revisions. Concerning the local zones, major and minor, two of four zones from Äspö96 are present also in Äspö02. The two zones not modelled in Äspö02 have been observed at only one locality in the tunnel and was not extrapolated to a major, continuous zone. All zones in the Äspö96-model were termed “fracture zones”. However, since all zones except one (NNW4), are known to be brittle reactivations of initially ductile zones, the general term “deformation zones” has been applied for the zones in this report. The frequency of fracturing in, and between these zones varies strongly.

On a regional scale, a network of semi-ductile shear zones exists. Some of the zones in this network have been localised in the Äspö tunnel and on the surface of Äspö Island, but also southwards on Ävrö Island and on the Simpevarp peninsula. Interpretations of airborne magnetic surveys indicate that the network constitute a three km wide zone along the coastline. The general strike of the zone is NE-SW, while individual shear zones in the network appear to strike in NE-SW, ENE-WSW and E-W. Minor ductile zones are common on Äspö Island, frequently also with a NW-SE strike. Relations between different deformation zones have so far not been described or investigated.

NW-SE is not only a common orientation for minor ductile shear zones, but is also the most frequent strike for brittle fractures. While fractures occur, however, in most orientations, other prominent orientations are N-S/steeply dipping, NE-SW/steeply dipping and a sub horizontal set. The majority of the zones that have been modelled have higher water conductivity than the surrounding bedrock. In the rock volumes between the zones a dominance of water conductive fractures with orientation NW-SE/steeply dipping has been revealed. Some of these fractures are gathered into minor fracture zones (elsewhere called “Water Conducting Features and “High Permeability Features”). It has not been judged possible to interpolate these fractures to major units in the present model. Thus, they are only visualized at the observation localities, with position and orientation.

The relation between the shear zone network and fracture systems has not been established, regionally or locally, at Äspö. In and around the Äspö HRL the majority of the shear zones are striking in NE-SW with steep dips, while the dominating brittle fracture set strikes in NW-SE with a steep dip. The difference is remarkable. Comparing fracture orientations in the different blocks of the geological model and in the zones do not support the hypothesis that they belong to the same fracture systems, even though the visual impression from the stereographic projections seem to indicate a correlation between many of the blocks. Stereographic projections of fracture orientations in several zones clearly show deviant orientations compared to adjacent blocks.

In order to show the geometry and characteristics of the zones in an informative way, a proposal for an “atlas” has been presented. The purpose with this atlas is to describe each zone in a brief and simplified manner, visually and in tables, with references to the source of information.

Sammanfattning

Äspölaboratoriet tillkom i slutet av 80-talet för att fungera som fullskalelaboratorium för SKB:s arbete att konstruera, bygga och driva ett djupförvar för använt kärnbränsle och för att utveckla och testa utrustning och metoder för att karaktärisera tilltänkta förvarsområden.

Arbetet med Äspölaboratoriet har indelats i tre faser: förundersökningsfasen, konstruktionsfasen och den operativa fasen, som vi befinner oss i nu. Efter konstruktionsfasen presenterade SKB en geologisk modell i 2D, Äspö96 /Rhén et al., 1997/, baserad på undersökningar gjorda i de två första faserna. I GeoMod uppdateras denna modell till 3D, med komplettering av undersökningar gjorda under den operativa fasen. Denna rapport är en lägesrapport för projektet.

Vattnets transportvägar i och runt ett tilltänkt djupförvar, och i ett laboratorium av det slag som finns på Äspö, ligger i fokus för de flesta undersökningar SKB genomför eftersom det är detta medium som skulle kunna tänkas utgöra bärare för radioaktiva nukleider vid ett eventuellt läckage från förvaret. Genes, geometri och övrig karaktär på den öppna sprickvolymen i berget, den nu existerande och den eventuella framtida, är därför ett huvudmål när geologin och dess geometrier modelleras och beskrivs. I denna rapport beskrivs geologin allmänt i regionen och på Äspö, samt mer ingående för den tredimensionella modellens objekt. Beskrivningarna är i huvudsak baserade på befintliga publikationer och på data hämtat från SKB:s databaser SICADA och TMS, men delvis också på data som tagits fram i detta projekt. Exempel på det senare är tolkningar av magnetiska kartor, tolkningar av BIPS-bilder, analys och beskrivning av ”Water Conducting Features” och osäkerhetsbedömningar.

Av de zoner som fanns med i tidigare modell (Äspö96) så är alla större, regionala, inkluderade även i Äspö02, med endast smärre geometriska förändringar. Av de lokala, större och lokala, mindre zonerna fanns två av fyra med i Äspö96, medan de två övriga var lokaliserade i tunneln utan att extrapoleras till en större sammanhängande zon. Alla zoner modellerade i Äspö96 var benämnda sprickzoner, medan vi i denna rapport valt att mer generellt kalla zonerna defomationszoner, eftersom alla utom en (NNW4) har påvisad äldre, duktil deformation som föregångare till senare spröd deformation. Graden av uppsprickning längs och runt dessa zoner varierar starkt.

I regional skala finns ett nätverk av semi-duktila skjuvzoner. Individuella zoner i nätverket är lokaliserade på Äspö (markytan och tunnel) och mot söder på Ävrö/Simpevarp. Tolknings av flygburna mätningar av jordmagnetfältet indikerar att nätverket existerar i en tre km bred zon längs kusten. Zonen stryker i sydväst-nordost, medan individuella zoner i nätverket dessutom tycks stryka i ost-nordost och ost-väst. Små duktila zoner förekommer på Äspö och frekvent även i nordväst-sydostlig riktning. Korsningar eller relationer mellan defomationszoner, har tyvärr inte beskrivits eller observerats.

Nordväst-sydost är också den mest frekventa sprickriktningen. Sprickor förekommer dock i de flesta riktningar och andra framträdande sprickriktningar är brant i nord-syd, brant i sydväst-nordost samt flacka sprickor. De flesta modellerade zonerna är vattenförande i högre grad än omgivande berggrund. I mellanliggande berggrundsblock finns en tydlig dominans av vattenförande sprickor i en brant sydost-nordvästlig riktning. En del av dessa ligger ansamlade i mindre sprickzoner ("Water Conducting Features" eller "High Permeability Features"). Det har dock inte i dagsläget bedömts möjligt att med tillräcklig hög säkerhet kunna sammanbinda dessa sprickor och strukturer till större enheter i modellen. Dessa finns därför enbart visualiserade vid observationsplatsen, med angivet läge och orientering.

Relationen mellan nätverket av skjuvzoner och existerande spricksystem har inte fastlagts regionalt eller på Äspö. I och runt Äspö HRL är de flesta större skjuvzoner branta och stryker i sydväst-nordost, medan det dominerande spricksystemet är brant och stryker i sydost-nordväst. Kontrasten är slående. Den jämförande sprickstatistiken mellan de olika blocken i den geologiska modellen och i zonerna kan inte styrka att det är samma spricksystem i de olika delarna. Det visuella intrycket av de stereografiska projektionerna är annars att en sån likhet existerar mellan flera av blocken, medan sprickriktningarna i flera av zonerna har uppenbart avvikande riktningar, jämfört med angränsande block.

För att överskådligt förmedla zoners geometri och egenskaper har ett förslag till "atlas" tagits fram. Denna syftar till att på ett kortfattat och något förenklat sätt beskriva respektive zon visuellt och i tabellform, med referens till källinformation.

Contents

1	Introduction	11
1.1	The GeoMod project	12
1.1.1	Objectives	12
1.1.2	This report and other GeoMod related reports	13
1.1.3	Reviewing	13
2	Site location and overview of existing data	15
2.1	Overview	15
2.2	Co-ordinate system	16
2.3	Geoscientific investigations and experiments made	17
2.3.1	The data used in the modelling	18
2.3.2	Experiments in Äspö HRL	18
3	Evaluation of primary data	19
3.1	Introduction	19
3.2	Terminology	19
3.3	Input data	20
3.3.1	Geological mapping	20
3.3.2	TMS	21
3.3.3	Core mapping	23
3.3.4	Magnetic data	25
3.3.5	Other data	29
3.4	Äspö bedrock geology	29
3.4.1	Introduction	29
3.4.2	Geological evolution	30
4	Tree-dimensional site descriptive modelling, geology and geometries	41
4.1	Introduction	41
4.2	RVS	42
4.2.1	Introduction	42
4.2.2	Overview of the modelling process	42
4.2.3	Constructing and visualising surfaces	45
4.3	Modelling of deformation zones in GeoMod	48
4.3.1	Conceptual models	48
4.3.2	General assumptions made	49
4.3.3	Prerequisite for modelling zones	49
4.3.4	Extent of modelled zones	50
4.3.5	Characterisation	51
4.3.6	Visualized parameters in RVS	53

5	The Äspö02 site descriptive model	55
5.1	Base model	55
5.2	Sub-model	56
5.3	Lithology	56
5.4	Zone description	57
5.4.1	ZAS0002A0 (NE1)	58
5.4.2	ZAS0003A0 (EW3)	64
5.4.3	ZAS0004A0 (NE2)	67
5.4.4	ZAS0007A0 (NW1)	71
5.4.5	ZAS0005A0 (NNW4)	74
5.4.6	ZAS0008A0 (NW2)	77
5.4.7	ZAS0006A0 (NEHQ3)	78
5.4.8	ZAS0001A0 (EW1)	82
5.4.9	Atlas of Deformation Zone	87
5.5	Rock blocks	91
5.6	Fractures	91
5.6.1	High Permeability Features	91
5.6.2	Fracture mineralogy	97
5.6.3	Fracture statistics	100
5.7	Comparison with Äspö96	122
6	Recommendation for further work	123
7	References	125

Appendices

1. Waterbearing fractures.

2. Protocols over observations of deformation zones.

1 Introduction

The Swedish Nuclear Fuel and Waste Management Company (SKB) established the Äspö Hard Rock Laboratory in late 1980th in order serve as a test area for SKB's work to design and construct a deep geological repository for spent fuel and to develop and test methods for characterization of selected repository site.

The role of the Äspö Hard Rock Laboratory is to provide input to the performance assessments that have to be supplied as part of each license application and to develop, test, and evaluate methods for site investigations, detailed investigations, repository construction as well as disposal and backfilling of tunnels before they are applied within the deep repository programme. The work with the Äspö HRL has been divided into three phases: the pre-investigation phase, the construction phase, and the operating phase.

During the Pre-investigation phase, 1986–1990, studies were made to provide background material for the decision to locate the laboratory to a suitable site. The natural conditions of the bedrock were described and predictions made of geological, hydrogeological, geochemical etc conditions to be observed during excavation of the laboratory. This phase also included planning for the construction and operating phases.

During the Construction phase, 1990–1995, comprehensive investigations and experiments were performed in parallel with construction of the laboratory. The excavation of the main access tunnel to a depth of 450 m and the construction of the Äspö Research Village were completed. Excavation started on October 1st, 1990 after approval had been obtained from the authorities concerned, and was completed in February 1995.

At the end of the construction stage, the different models used during the site characterization were compiled and evaluated as a first attempt to establish a multidisciplinary site descriptive model, where the results were published in a series of technical reports:

- Stanfors, R, Erlström, M, Markström I. Äspö HRL – Geoscientific evaluation 1997/1. Overview of site characterization 1986 – 1995. SKB TR 97-02.
- Rhen, I (ed), Bäckblom G., Gustafson, G, Stanfors, R, Wikberg, P. Äspö HRL – Geoscientific evaluation 1997/2. Results from pre-investigations and detailed site characterization. Summary Report. SKB TR 97-03.
- Stanfors, R, Olsson, P, Stille, H. Äspö HRL – Geoscientific evaluation 1997/3. Results from pre-investigations and detailed site characterization. Comparison of predictions and observations. Geology and Mechanical stability. SKB TR 97-04.
- Rhen, I, Gustafson, G, Wikberg, P. Äspö HRL – Geoscientific evaluation 1997/2. Results from pre-investigations and detailed site characterization. Comparison of predictions and observations. Hydrogeology, Groundwater chemistry and Transport of solutes. SKB TR 97-04.

- Rhen, I (ed.), Gustafson, G, Stanfors, R, Wikberg, P. Äspö HRL – Geoscientific evaluation 1997/2. Models based on site characterization 1986 – 1995. SKB TR 97-05.
- Almén K-E (ed), Olsson P, Rhen I, Stanfors R, Wikberg P. Äspö Hard Rock Laboratory. Feasibility and usefulness of site investigation methods. Experience from the pre-investigation phase. SKB TR 94-24.

The Operating phase began in 1995. A preliminary outline of the programme for the Operating phase was given in SKB's Research, Development and Demonstration (RD&D) Program 1992. Since then the programme has been revised and the basis for the current programme is described in SKB's RD&D Program 1998.

During the operating stage a number of different experiments and studies have been executed in Äspö HRL, which provides additional information compared to the experience obtained and presented in the previous reports. In order to update the geoscientific models, SKB initiated the project GeoMod to compile the results from the operating period 1995-2002.

1.1 The GeoMod project

1.1.1 Objectives

The GeoMod project was aiming at updating the existing model by integrating new data collected since 1995. The major part of the new data has been produced in the lower part of the Äspö tunnel spiral. The updated model is contained in a 1 km³ cube with focus on a volume including the tunnel spiral volume from about –200 metres to about –500 metres.

The specific objectives in the GeoMod project were to:

- Describe the geoscientific properties of a prescribed rock volume containing the tunnel spiral.
- Identify relevant processes to explain the geoscientific properties.
- Define the boundary conditions of importance to the rock volume processes.
- Develop methodology to integrate the knowledge from the different geoscientific disciplines.
- Develop a coherent integrated geoscientific model of Äspö.

The project started January 2002. Before the integration of the models finished the GeoMod project was temporarily terminated in May 2003. Finally, SKB decided to reduce the content of the project by omitting the fully integration between the different geoscientific disciplines. It was decided that the work with the completed integration was postponed until 2005.

As a consequence, the different geoscientific models; i.e. geological, hydrogeological, rock mechanics and hydrogeochemical, are published in four separate reports, one for each discipline.

The objectives of this report are to present the result within geology.

1.1.2 This report and other GeoMod related reports

This report presents the updating of the geological part of the GeoMod project.

Three other reports are produced with in GeoMod:

- IPR-03-35
Äspö Hard Rock Laboratory
Update of the hydrogeological model 2002
Patrik Vidstrand
December 2003
- IPR-03-36
Äspö Hard Rock Laboratory
Update of the hydrogeochemical model 2002
Marcus Laaksoharju, Ioana Gurban
December 2003
- IPR-03-37
Äspö Hard Rock Laboratory
Update of the rock mechanical model 2002
Hossein Hakami
December 2003

1.1.3 Reviewing

Although, a complete integration between the disciplines have not been accomplished in the current version of the geoscientific modelling, the relation and interaction between the disciplines have been addressed with respect to the scientific content. The Scientific Content Issues are:

- Is the scientific content complete, given the objectives and current level of the work?
- Is the science clearly explained?
- Is the model adequate, given the current state of play?
- Is it clear how updating can be accomplished?
- Is the presented information traceable?
- Are the conclusions justified and adequate?
- Confidence in the model and robustness

The evaluation and it's robustness for the different disciplines have been in focus and the statements put forward in the individual reports are not contradictive unless this is clearly stated.

2 Site location and overview of existing data

2.1 Overview

The Äspö HRL is located on the Äspö Island which is located near to the Simpevarp nuclear site. A great number of investigations have been made both on Äspö and in adjacent areas, such as Laxemar and Ävrö, c.f. Figure 2-1.

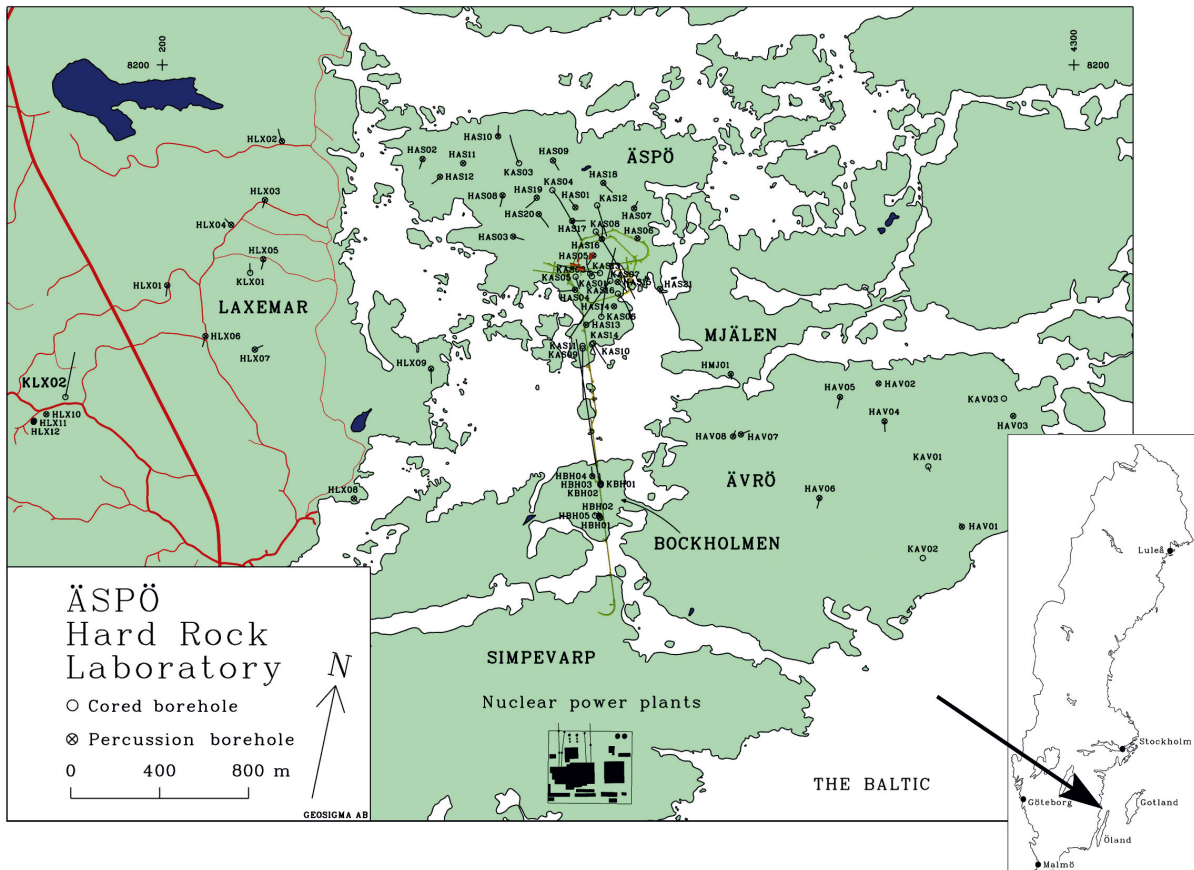


Figure 2-1. Overview of the Äspö Island and the adjacent areas. The selected model domain is shown in Figure 2-2.

The GeoMod-project will update the existing model by integrating new data collected since 1995. Most new data have been collected during the operational phase for different experiments conducted in the tunnel. The majority of the new information originates from the experimental sites in the lower part of the Äspö HRL. The updated model will focus on a volume including the tunnel spiral (c.f. Figure 2-2.).

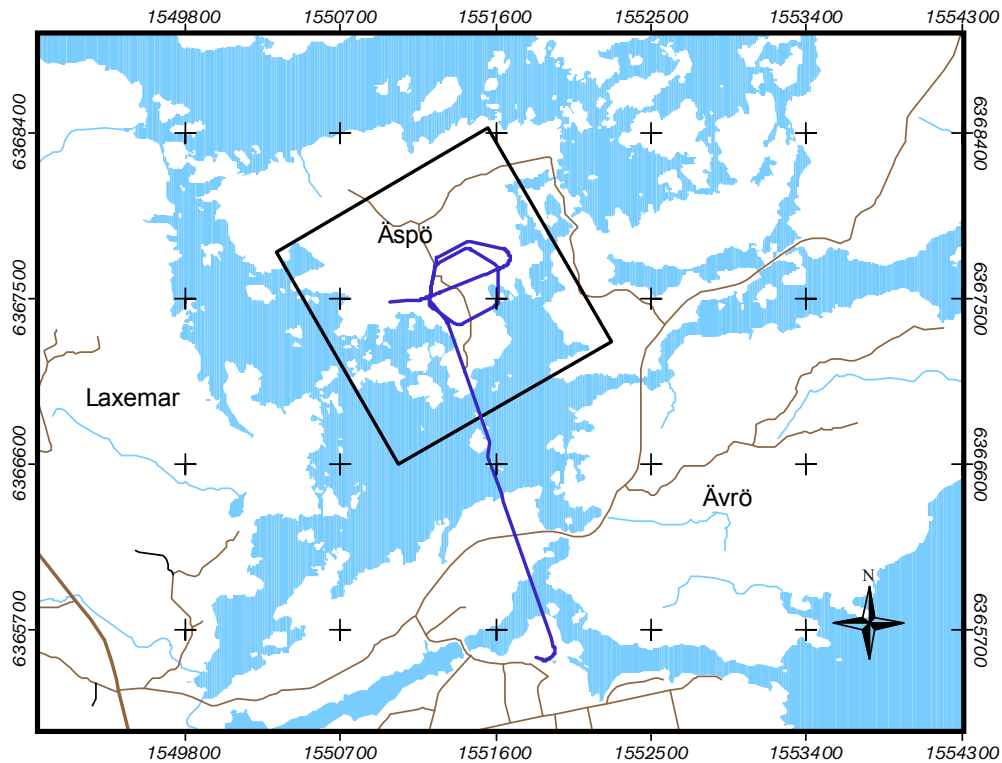


Figure 2-2. Map showing the GeoMod model area along with the horizontal projection of the Äspö tunnel (RT90 coordinate system).

2.2 Co-ordinate system

The corner coordinates of the model volume are defined by the virtual cube with following corner coordinates.

Table 2-1. Model volume coordinates.

Äspö 1km Cube Coordinates			
RT90-RHB70			
	Easting	Northing	Elevation
	[m]	[m]	[mamsl]
Top square			
1	1551200.046	6367099.181	50
2	1550700.046	6367965.206	50
3	1551566.071	6368465.206	50
4	1552066.071	6367599.181	50
Bottom square			
5	1551200.046	6367099.181	-1000
6	1550700.046	6367965.206	-1000
7	1551566.071	6368465.206	-1000
8	1552066.071	6367599.181	-1000

The modelling is contained within a common virtual cube with 1 km side length extending from +50m to -1000 mamsl (meter above mean sea level) in elevation to which appropriate boundary conditions have to be set. This volume is to be tied to its regional context based on the previous model, Äspö96.

2.3 Geoscientific investigations and experiments made

The underground part of the laboratory consists of a tunnel from the Simpevarp peninsula to the southern part of Äspö where the tunnel continues in a spiral down to a depth of 450 m (Figure 2-3). The total length of the tunnel is 3600 m where approximately 400 m at the end have been excavated by a tunnel boring machine (TBM) with a diameter of 5 m. The first part of the tunnel has been excavated by conventional drill and blast technique. The underground tunnel is connected to the ground surface through a hoist shaft and two ventilation shafts. Äspö Research Village is located at the surface on the Äspö Island and it comprises office facilities, storage facilities, and machinery for hoist and ventilation (Figure 2-3).

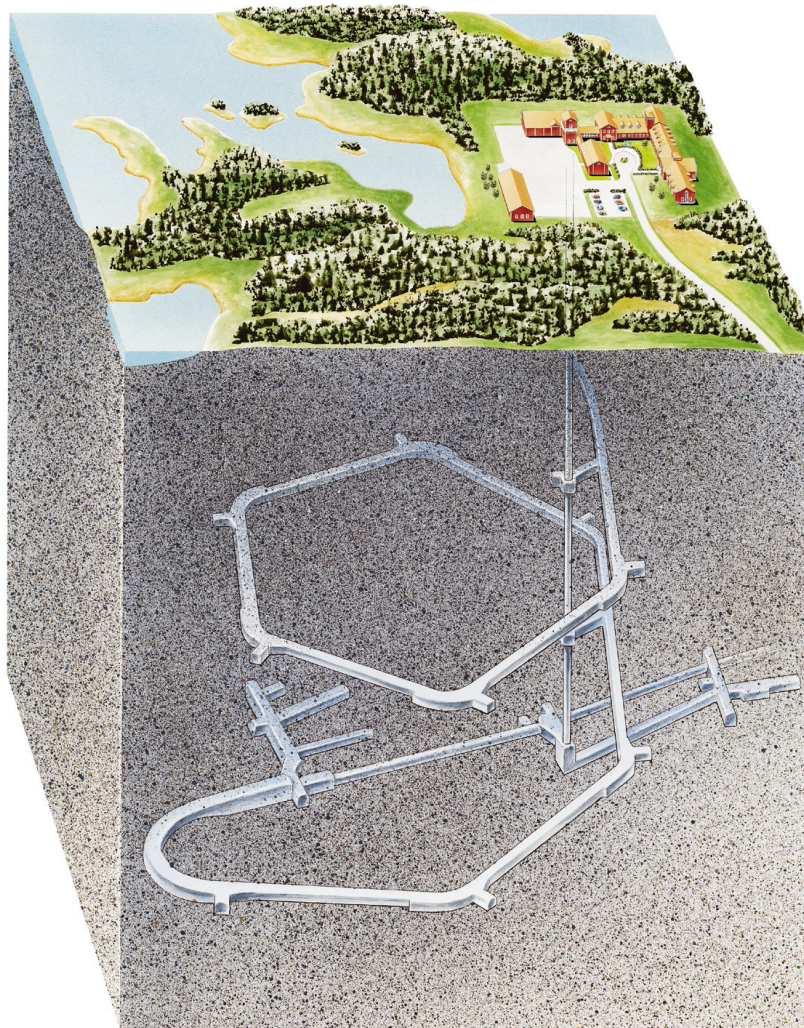


Figure 2-3. Overview of the Äspö Hard Rock Laboratory Facilities within GeoMod's virtual volume.

2.3.1 The data used in the modelling

All data used for the modelling were quality assured data, received from SKB:s database SICADA. The database contains all tests, sampling and analyses obtained from percussion and core drilled boreholes at surface or in the underground experimental areas of Äspö HRL.

2.3.2 Experiments in Äspö HRL

A great number of experiments have been executed in Äspö HRL since the start of the operating phase. Examples of experiments where relevant data was collected are e.g., REX, TRUE, TRUE BS, HQ, ZEDEX, JADE, MICROBE, COLLOID, PROTOTYPE REPOSITORY, MATRIX and other experiments.

3 Evaluation of primary data

3.1 Introduction

The input data to the geometrical and geological modelling work in Äspö02 focus on observed, geological data and the spatial distribution and geometry of these, and thus only to a lesser extent on interpreted data from e.g. geophysical data. In this chapter the used data are discussed as well as biases related to these.

3.2 Terminology

In order to get a better understanding of the presented model, regarding what has been modelled, levels of uncertainty, variability, etc, there is a need to describe how certain geological terminology has been used, during field work, analysis and in this report. The present guidelines from SKB concerning definition of geological parameters as reported in /Strähle, 2001/ are in accordance with the terminology used in this report.

Deformation zone is in this report used to denote any kind of zone in the rock that display signs of having been deformed in the geological past, both in the brittle and ductile state. A “zone” is regarded as such when there is evidence that it has a considerable extension in three dimensions and has a high length/width ratio.

Deformation zones include different sizes as classified by SKB /Andersson et al., 2000/ as shown in Table 3-1 and Table 3-2.

Table 3-1. Size classification of ductile deformation zones.

Type	Length	Width
Regional deformation zone	>10 km	>100 m
Local major deformation zone	1 – 10 km	5 – 100 m
Local minor deformation zone	10 m – 1 km	0.1 – 5 m

Table 3-2. Size classification of brittle deformation zones.

Type	Length	Width
Regional fracture zone	>10 km	>100 m
Local major fracture zone	1 – 10 km	5 – 100 km
Local minor fracture zone	10 m – 1 km	0.1 – 5 m
Fracture	<10 m	<0.1 m

There have been changes in the use of rock terminology at Äspö in a partly confusing way. The composition of the predominant rock type span from granite to quartz diorite (see Figure 3-11 and chapter 3.4). It has a slightly inhomogeneous texture, with variable grain-size and amount of megacrysts. At Äspö these rocks have been separated into the “Ävrö granite” (or Småland granite) and “Äspö diorite”. The visible difference is defined as /Annertz K, 1994 and Munier et al., 1988/:

1. Ävrö granite: Grey to greyish red (to red), finely medium-grained (1-3 mm) granite.
2. Äspö diorite: Dark grey to greyish red, fine medium-grained (1-3 mm) granodiorite to quartz monzodiorite, generally with megacrysts of microcline.

In the tunnel mapping the distinction was made primarily on the basis of the colour and the content of megacrysts. During the early core-mapping (KAS02-04) these two rock types were divided into seven different units on the basis of their mineralogical composition, colour and content of megacrysts. The boundaries between them were normally considered as gradational.

Later the separation between Ävrö granite and Äspö diorite was made on the basis of their density, as follows, with the calculated content of magnetite subtracted. The boundaries of these, so-called silica densities was: granite 2.641-2.7 kg/dm³ and diorite 2.701-2.8 kg/dm³. The rocks in boreholes KAS02-KAS04 were also separated accordingly.

In this report granite and granodiorite are used synonymously with Ävrö granite and Äspö diorite, respectively, because this is the current terminology used for these rocks in the Boremap database.

3.3 Input data

3.3.1 Geological mapping

The geology at Äspö, including excavated trenches across the island, has been mapped by the Geological Survey of Sweden /Kornfält and Wikman, 1987b/. These data are used as 2D reference design-files during modelling in RVS put at z=0 masl. A brief summary of the regional and local bedrock geology is given in chapter 3.4.

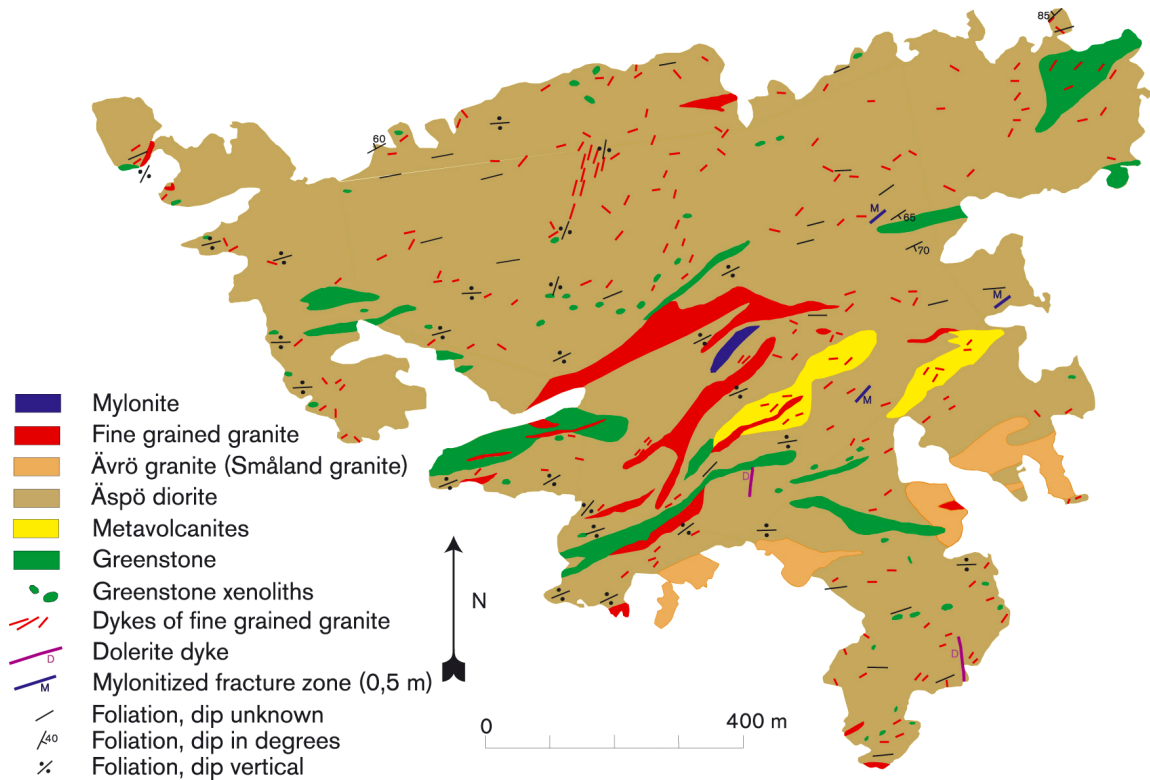


Figure 3-1. Bedrock map of Äspö /Rhen et al., 1997/ (modified from /Kornfält and Wikman, 1988/).

3.3.2 TMS

The Tunnel Mapping System (TMS) used at Äspö is a CAD-based system utilising Microstation[®] software, with a database linkage. The TMS database was delivered to the project in august 2002 as Microsoft Access[®] files together with the drawings of the tunnel mapping in design (Microstation[®]) format.

Although most basic parameters in TMS have been measured consistently, the system has been refined, changed and partly used in an inconsistent way through time. As an example labels have been changed (e.g. some niches have become tunnels and the others renamed from TASA chainage to NASA chainage), new sub-parameters have been added (such as aperture, width and oxidation zone for table “Fracture”) and measurements of some parameters have only been made sporadically (such as the sub-parameter “water” that should have the value Y or N, but are often empty, which in this project is interpreted as N). The remark field is a column in each table of the database that offers an opportunity for the mapping geologist or other administrator of the database to comment on characteristics not possible to describe with existing parameters. The remark field has, however, no standardized nomenclature and is used inconsistently. It is therefore often quit difficult to comprehend. It is also evident from looking at the database from different tunnels that different mappers have measured different parameters, except for the basic ones.

The 1972 separate posts occurring in the rock table in the database are mapped as only five different rock types in the tunnel. The intention has been to simplify the lithology as far as possible and focus on rock mechanical characteristics. The major rock types are granite and granodiorite (Småland granite and Äspö dirorite, respectively are also used as synonyms), basic volcanics and rocks primarily appearing as dykes, pegmatite and fine-grained granite. Mylonite and breccia have been mapped at seven locations. Of the nine different structural types to choose from (Table 3-3), six have been used. The values “shear”, “fold” and “lineation” have not been used. Mylonitized have been used at ten localities.

Table 3-3. Rock structure types in TMS.

Code	Description
1	Homogeneous
2	Schistified
3	Gneissified
4	Stratified
5	Mylonitized
6	Brecciated
7	Shear
8	Fold
9	Lineation



3.3.3 Core mapping

Several systems have been used for the geological mapping of drill cores at Äspö. The two primary systems considered here are the Petrocore system and the Boremap system. Both systems have developed considerably during the years of drilling and core mapping at Äspö HRL. These developments have been made both in methodology, terminology and also involve the usage of equipment. Unfortunately these changes are not always fully documented.

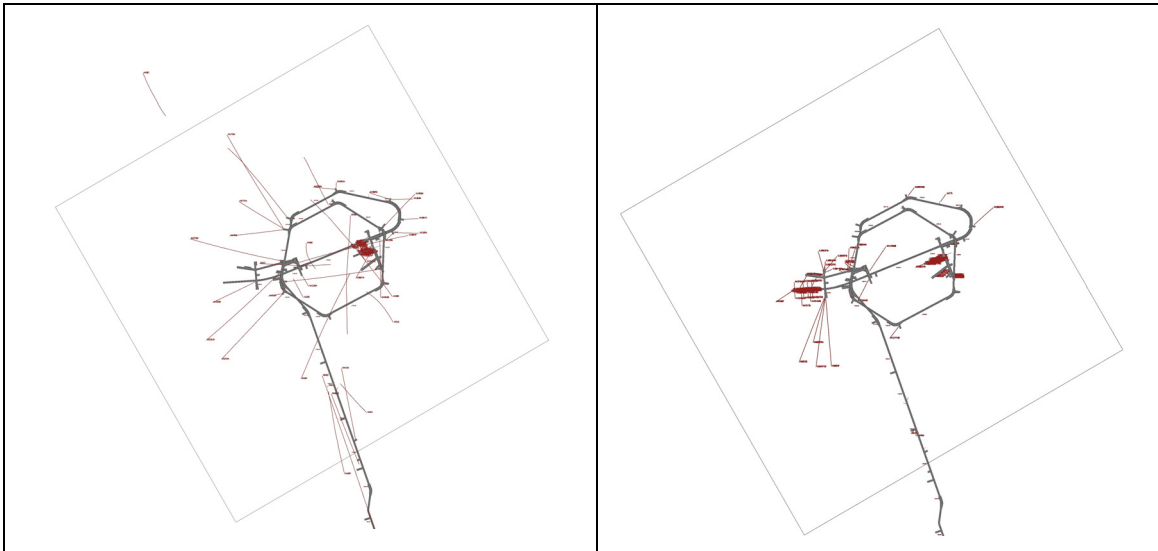


Figure 3-3. Borehole mapped in a) the Petrocore system and b) the Boremap system respectively. Note the concentration of boreholes in a few areas (Boremap in particular) and the relatively small volumes investigated through drilling compared to the total model volume.

Most of the cores from boreholes at the Äspö site have been mapped with the Petrocore system. From about year 1997 and onwards the mapping has, however, basically been done in the Boremap system. 226 boreholes have been mapped in this system (Figure 3-3) and 204 have been scanned with BIPS (Borehole Image Processing System), of which 8 are percussion drilled holes. A majority of these boreholes are concentrated around two detailed investigated areas related to the projects “Prototype” and “Long Term Test of buffer material” (at the end of the A-tunnel and in the G-tunnel), the “Canistar Retrieval”, “ZEDEX”, “Backfill & plug” and “Demo repository” (in the D, K and Z tunnels) (see Figure 3-4). Most of the boreholes in these areas are rather short.

Only cored boreholes longer than ca 15 m have been used in the modelling. With the use of BIPS-images the Boremap system can give true orientation of visible fractures and other structures, whereas this is not the case in Petrocore. The equipment and methodology used in the BIPS system as used at Äspö has developed since 1995, when the first logging was done. Generally, most of the images created today have better resolution. A few of the images (stored in archives at Äspö) from boreholes in fact have so low quality that it is impossible to judge the rock type and to measure lithological contacts and structures. In SICADA there are also several boreholes mapped in Boremap that do not have information regarding orientation or only partly so (strike or dip).

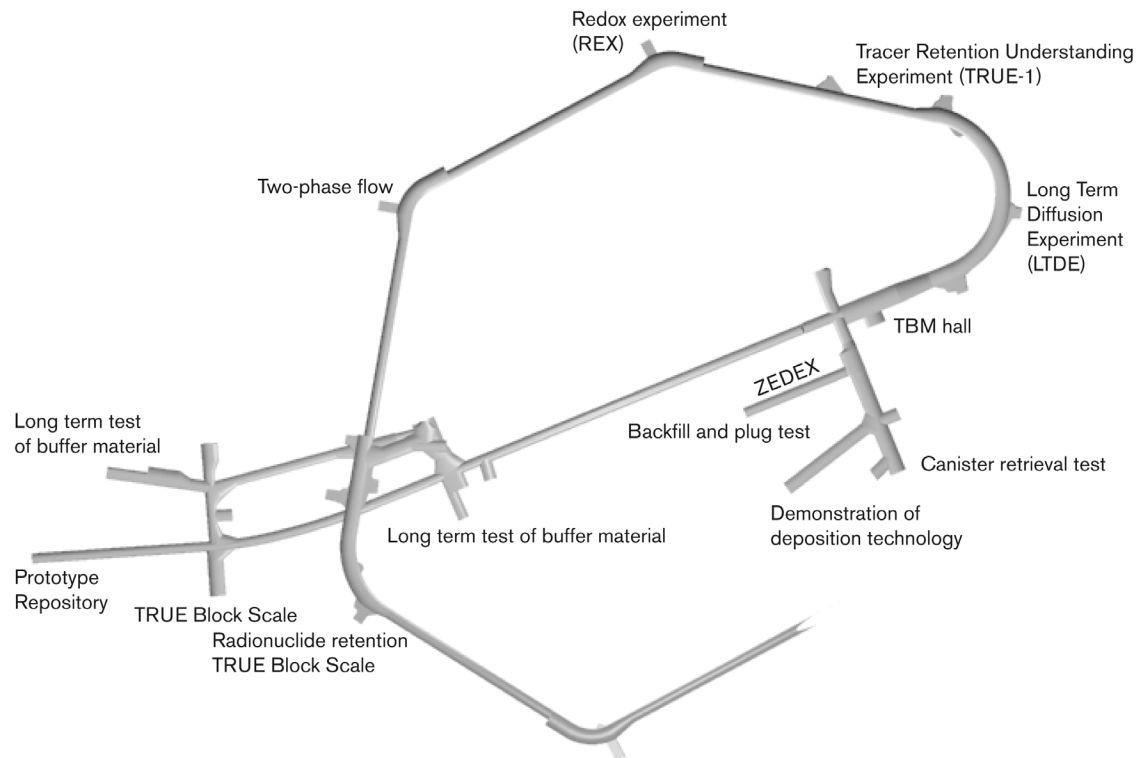


Figure 3-4. Project areas in the lower part of the Äspö tunnel.

Because there is no true orientation of mapped objects in Petrocore, it is only the location of objects that can be used in the 3D modelling. A few of the Petrocore boreholes have been scanned, partly or fully with different kind of photographic equipment after their first mapping in order to get an orientation of fractures, but also these orientations have errors considered to be rather large and unpredictable /Stråhle A, pers. com 2003/.

In Figure 3-3 all boreholes mapped in this system are shown. As can be seen in this figure there are only a few boreholes mapped in Boremap outside the Zedex and the Prototype areas, where the density of boreholes on the other hand is very high. In fact only two of the modelled zones are penetrated by any borehole mapped in Boremap.

Fractures, lithological contacts, “rock occurrences” (xenoliths and veins) and structures have generally been oriented in the Boremap system, but not zone structures or zone boundaries. The only actual zones mapped, and named as such in the database, are “crush zones”. These are sections in the core where the size of the pieces in the core is so small that individual fractures had not been able to measure. The orientations of crush zones have not been measured. The cause of the crushing in zone is not stated in the database. There is thus a possibility that many of these zones initially were sealed fractures that broke during the drilling process.

In Boremap only 10, thin crush zones exists in the database, whereas there are 847 crush zones in Petrocore. A few of these are several m wide, but a majority are less than 1 m wide and most of them only a few cm or dm wide.

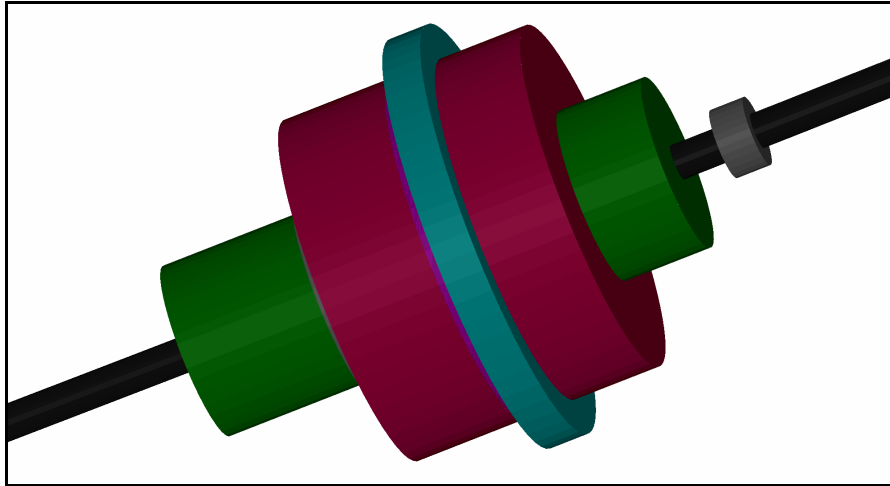


Figure 3-5. The geological parameters have been visualized in RVS with selected colours and shape. This shows the interpreted intersection of EW1a in borehole KA1755A, between 202.5-216.8 borehole length. Here green discs represent chloritic alteration, red discs are tectonized sections and light blue represent a crushed section in the core. There is also a narrow purple disc behind the blue one, representing mylonite.

3.3.4 Magnetic data

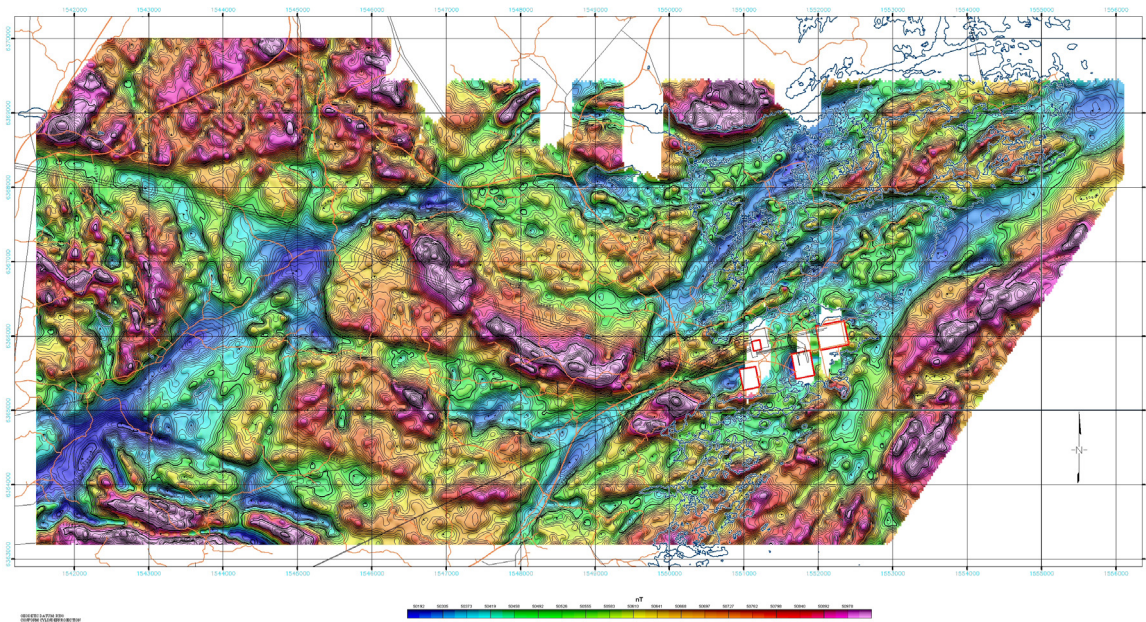


Figure 3-6. Regional aeromagnetic map. The figure comes from /Rønning et al., 2003/ and shows the magnetic field for the Äspö-Simpevarp-Laxemar area. Each square in the figure represents one km² and the orange squares to the right are buildings at the nuclear plant at Simpevarp.

The magnetic signature of rock often show significant differences, both with respect to the level of total magnetic field (measured in nanoTesla, nT) and to the pattern that the variability of the magnetic field displays on magnetic maps. The variation in the Äspö-Simpevarp-Laxemar region, between highs and lows is ca +/- 500 nT about the average at ca 50 000, neglecting rare peak anomalies. Recent helicopter borne magnetic measurements have been performed as an activity in the site investigation program (PLU) /Rønning et al., 2003/. The resulting data have been processed and published e.g. as anomaly maps of the total magnetic field (Figure 3-6). The methodology and equipment used is described in /Rønning et al., 2003/ and interpretation of the data is reported by /Triumf et al., in press/. Earlier aeromagnetic data in the region has been analysed in /Nisca, 1987/ and /Bergman et al., 1998/.

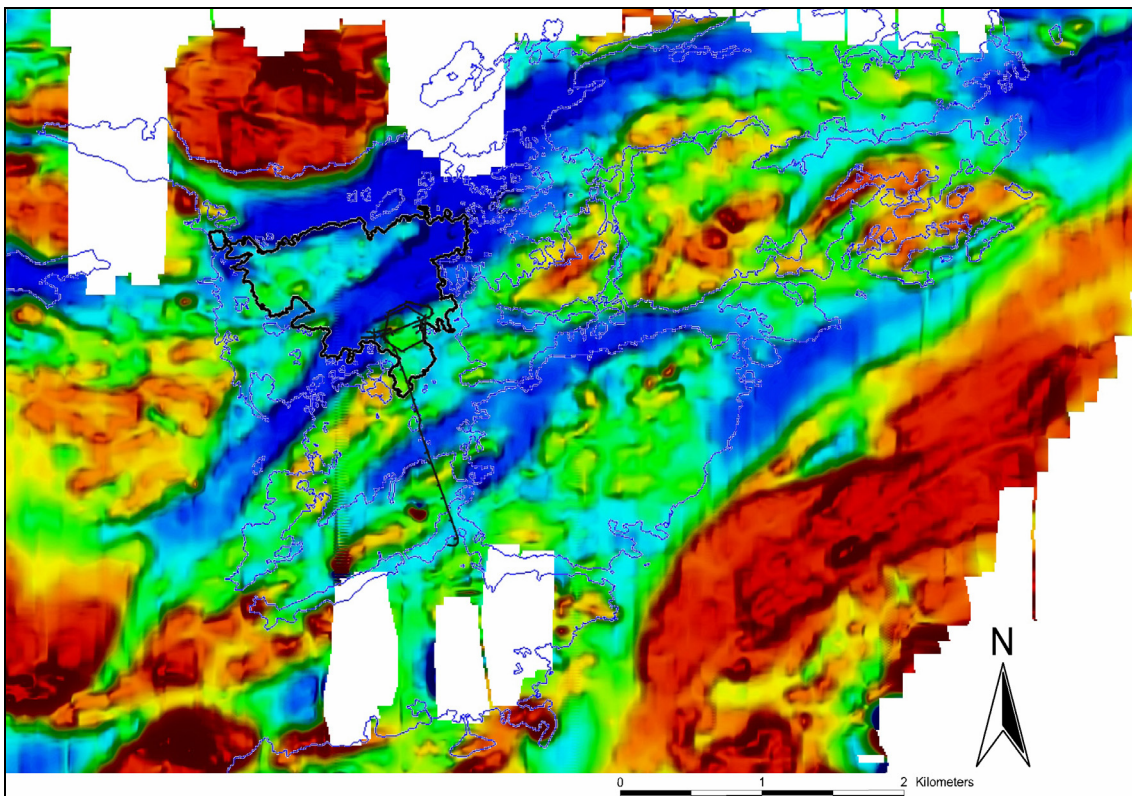


Figure 3-7. Blow-up of the eastern part of Figure 3-6. Here Äspö and the Äspö tunnel are outlined. No data is available from white areas; those in the south correspond to buildings at the power plant.

The differences in magnetic properties between rocks make magnetic maps, like the ones in Figure 3-6, Figure 3-7 and Figure 3-8, very useful tools as an aid to separate different rocks in areas of poor outcropping. However, secondary metamorphic alteration of magnetic minerals, especially magnetite to hematite and Fe-oxyhydroxides reduce the magnetic field strength. Such mineralogical changes take place in an oxidising environment that can occur both during dynamic metamorphism, hydrothermal alteration and weathering and are often related to ductile or brittle deformation along zones. These latter therefore show up as zones of magnetic low.

The magnetic field strength from a primary magmatic rock is roughly proportional to the amount of ferromagnetic minerals in the rock, primarily magnetite. Magnetite preferentially crystallizes early in a magmatic sequence and is therefore more common in mafic rocks than in felsic rocks. The unaided eye does not easily identify these minerals if they are small, but an indirect method that indicates the ability of a rock to become magnetic is the magnetic susceptibility, which is normally measured during regular geological mapping. The equipment normally used measures the amount of magnetic minerals in ca 1 dm² half sphere down in the rock and there is a need to do several measurements on each outcrop in order to get a representative average value to be used when aeromagnetic maps are being interpreted.

From Figure 3-6 certain characteristic patterns emerge. In the western part there are larger irregular areas with relatively homogeneous and higher magnetic field and areas with a lower magnetic field. These homogeneous areas most probably reflect the primary magnetic signature and possibly early, sub-solidus alteration. There are also narrow linear, low magnetic features referred to as magnetic lineaments. Such lineaments are generally interpreted as deformation zones in the bedrock /e.g. Bergman et al., 2000/, where the magnetic character of the primary rock have been metamorphosed or chemically altered as discussed above.

In the eastern part, on the other hand, a ca 3 km wide belt shows a more erratic pattern. The smooth magnetic pattern in the west is here disrupted and sliced into smaller scaled blocks separated by linear or sub-linear low magnetic zones. In the interpretation of these data by /Triumpf et al., in press, figure 5-9 and 5-11/, this data pattern is also obvious, with a disrupted magnetic pattern in the east, striking preferentially in NE-SW. This belt is best interpreted as a result of deformation of the crust, and thus of the primary magnetic pattern as it appears in the east (Figure 3-6). Linear, or sub-linear, zones of magnetic low frequently follow topographic lows, such as valleys or beneath the sea. At some places, however, they cross topographically higher areas. The most obvious example is the Äspö shear zone, running across Äspö Island and continues on the main land towards the southwest. The zone is exposed at Äspö, but also at several other location, and show up as a semi-ductile shear zone varying in width from a few metres to tenth of metres. The Äspö shear zone corresponds to the western boundary to the 3 km wide magnetic belt, discussed above.

A ground magnetic survey was conducted at Äspö during the pre-investigations. The data has been reprocessed by GeoVista AB for the Geomod project (Figure 3-8). This data was used together with geoelectric data to predict and locate smaller water bearing fracture zones and fractures /Nisca and Triumpf, 1989/. As can be seen in Figure 3-8 several of the zones at Äspö, besides the Äspö shear zone (EW1), follow zones of magnetic low. Especially noticeable are the NE1 and EW3 zones, but the width of the magnetic low zones is larger than the observed deformation zones. The same is also true for the EW1 (Äspö shear zone).

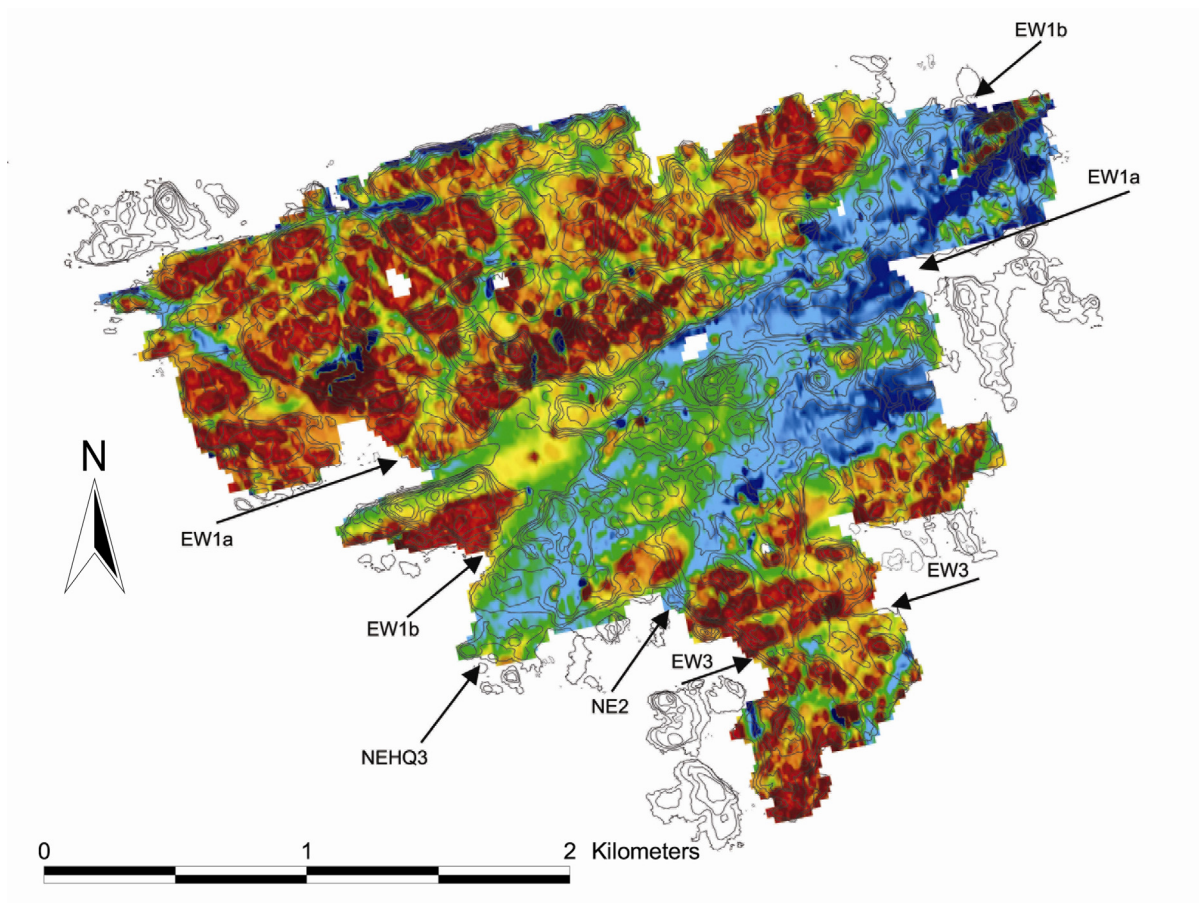


Figure 3-8. Topography and ground magnetic data from Äspö. The topographic equidistance is one m. Modelled zones, visible on the map as zones of magnetic low, are indicated.

The susceptibility across these magnetic low zones at Äspö is not systematically studied yet and therefore the correlation between them and the geology cannot be fully evaluated. Part of the magnetic low may thus be related to primary differences in the magmatic rocks along the zone and other parts to oxidation during metamorphic processes and hydrothermal alteration along the ductile zone and brittle reactivation along it. As an example, the red, fine-grained granites are especially frequent along the zone at Äspö and these generally have very low magnetic susceptibility. Until a detailed study of this topic has been carried out, it remains uncertain to what degree the different geological processes are responsible for the lower magnetic field. The strong correlation between the magnetic low and the regional shear zone indicate, however, that whatever the cause might be, it has a spatial and probably genetic relation to the zone.

3.3.5 Other data

As an input to the interpretation of the geometry of hydraulic structures at Äspö, besides the modelled deformation zones, the water bearing fractures cross-cutting the tunnel section and those longer than 5 m has been visualized in RVS. Also the database from /Mazurek et al., 1996/ has been re-evaluated considering hydraulic significance of the structures. These two sources have been compared and combined after a short field control (Appendix 1).

Some of the parameters visualized in RVS were not available in SICADA, when ordering via the program, but found when ordered separately from Äspö.

The BIPS images are stored on Compact Discs at Äspö. All images from boreholes longer than ca 15 m has been looked upon and commented. With this information as a basis, minor ductile deformation zones was located and visualised.

Other geophysical data have not been used directly in the modelling, but geophysical logging have been used in many boreholes as an aid to interpret the character of the bedrock (e.g. see chapter 3.2). Different reflecting equipment has been used in many boreholes, both radar (in 56 cored boreholes) and seismic methods. These have potential to be used as support for extrapolation and interpolation between actual observations of structures. The interpretation from such data is, however, often difficult to interpret without specialist competency, not at hand in this project. The predominance of reflexes with intermediate angles and rare occurrence of reflexes at high and very low angles to the borehole, even at localities where such structures are known to dominate, is an example of a bias and difficulties related to the interpretation of reflexes from the radar equipment (see for example the result from RAMAC measurements from the Oskarshamn site investigation /e.g. Aaltonen et al., 2003/).

3.4 Äspö bedrock geology

3.4.1 Introduction

The description of the bedrock geology from the regional area given in this chapter is a compilation based on earlier publications /Bergman et al., 1998; Bergman et al., 2000; Wikman and Kornfält, 1995; Kornfält et al., 1997; Kornfält and Wikman, 1987a; Kornfält and Wikman, 1987b and Kornfält and Wikman, 1988/ and much of the text is derived from /Andersson et al., 2002/.

To understand the geological development of the Äspö-Simpevarp region, it is necessary to consider not only the genesis of rocks during large-scale orogenies, when the majority of the rocks in the region were formed, but also processes when the region has had a more remote position to large-scale orogenies. The bedrock in the Äspö-Simpevarp-Laxemar region is dominated by intrusive rocks of the so-called Transscandinavian Igneous Belt (TIB). However, the geological development in the Oskarshamn region is complex and comprises not only the formation of igneous rocks, but also several periods of metamorphic overprinting, involving both structural, mineralogical and chemical changes, over a time period of ca 1900 million years. This chapter give a brief overview of the geological evolution in the region, from the intrusion of TIB to present day. For additional information of the geological evolution and processes that might have affected the bedrock in the region the reader is referred to e.g. /Larsson and Tullborg, 1993 and Milnes et al., 1998/.

3.4.2 Geological evolution

Lithological development

The major parts of the Precambrian bedrock of southeastern Sweden belong to the TIB, which was formed during repeated periods of intense alkali-calcic magmatism, between 1850 and 1650 Ma, i.e. during the waning stages of the Svecokarelian orogeny. In the Simpevarp region they intruded at ca 1810-1760 Ma /e.g. Kornfält et al., 1997/. The dominating rocks comprise granitoids to dioritoids and gabbroids, and related rocks, of possible volcanic origin, though not positively identified in the area. The dominating felsic portion of the granitoids to dioritoids are by tradition collectively referred to as “Småland granites”, although the latter comprise a variety of rock types regarding texture, mineralogy and chemical composition. Magma-mingling and mixing processes, exemplified by the occurrence of enclaves, hybridization and diffuse transitions between different lithologies etc., are typical for TIB rocks. In mesoscopic scale, these processes often result in a more or less inhomogeneous rock mass. However, if larger rock volumes are considered these may be regarded as being more or less homogeneous, despite some internal variations.

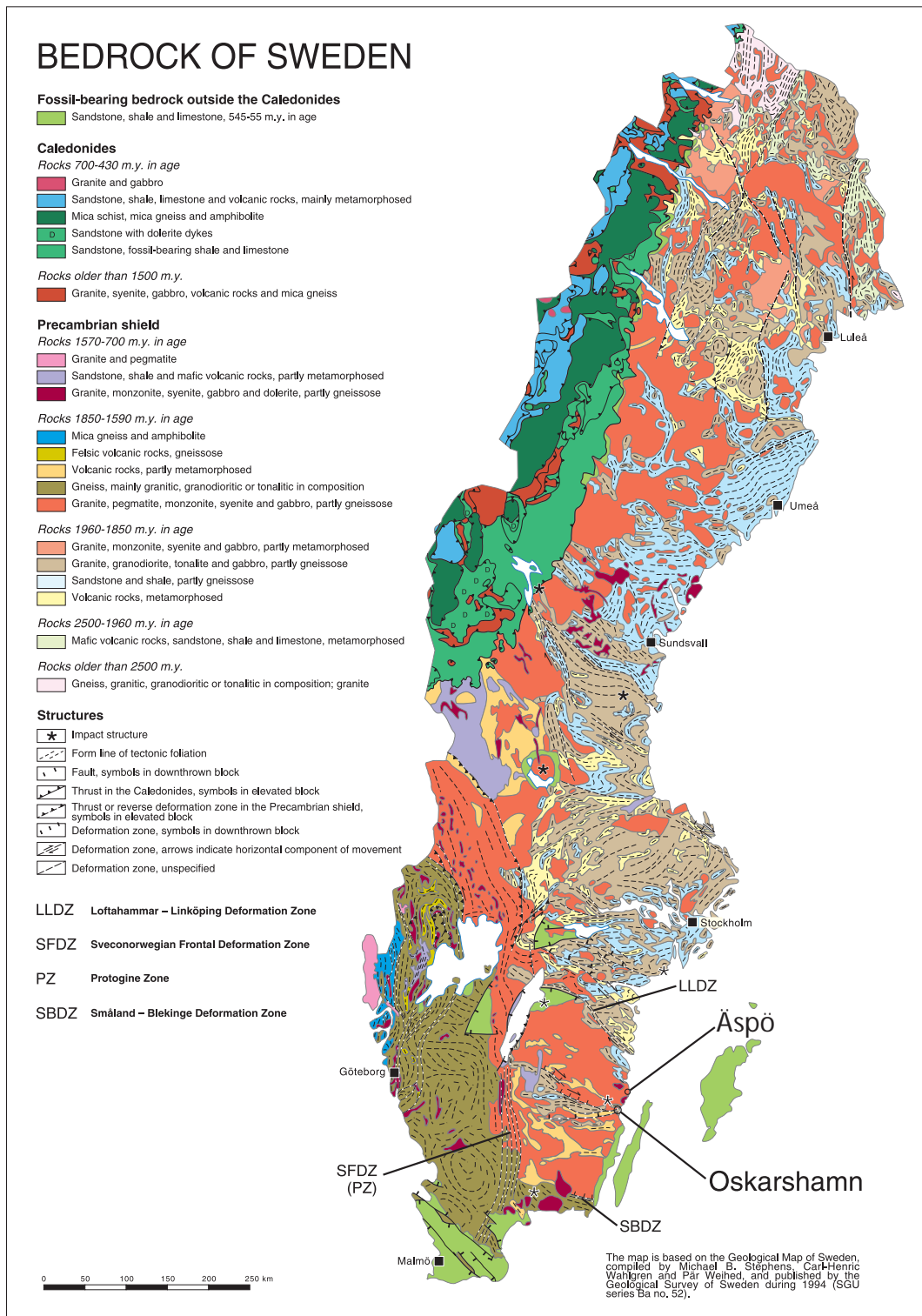


Figure 3-9. Bedrock map of Sweden.

Locally, fine-grained granitic or aplitic dykes and minor massifs are frequently occurring. Although volumetrically subordinate, these dykes constitute essential inhomogeneities in parts of the bedrock in the Oskarshamn region, especially in the Simpevarp area. These rocks are considered to be roughly coeval with the TIB host rock /Kornfält et al., 1997/, but have been intruded at a late stage in the magmatic process.

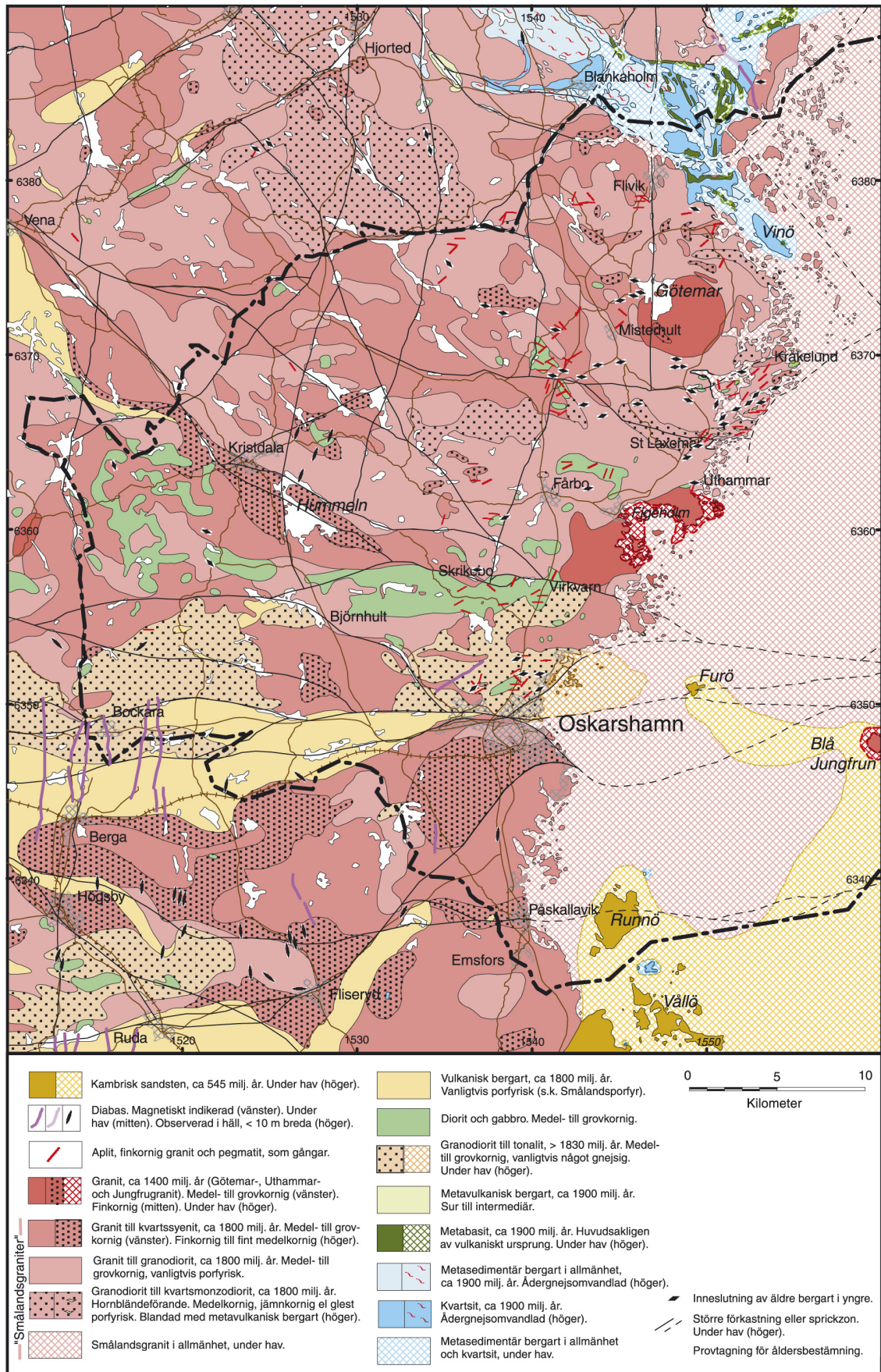


Figure 3-10. Bedrock map over Oskarshamn County.

The next rock-forming period in the Oskarshamn region took place at ca 1450 Ma, and is characterized by the local emplacement of granitic magmas in a more or less cratonized crust. This magmatism is exemplified by the occurrence of the Götemar, Uthammar and Jungfrun granites. Except for the occurrence of TIB-related granitic dykes in the Oskarshamn region, fine-grained granitic dykes and pegmatites that are related to the ca 1450 Ma granites occur as well, e.g. in the Götemar granite and the surrounding TIB rocks. However, these dykes are inferred to only occur within the granite proper and in the immediate surrounding.

West of the Laxemar-Simpevarp-Äspö area scattered dolerite dykes occur, ranging up to ca 10 m width. They are inferred to be related to the regional system of N-S trending dolerites intruding at ca 1000-900 Ma /Johansson and Johansson, 1990/. They are normally poorly exposed, but due to their generally more or less high content of magnetite, they usually constitute linear, positive magnetic anomalies, and their occurrence and extension may, thus, be identified on the magnetic anomaly maps. The intrusion of these dolerites is probably related to the ca 1100-900 Ma Sveconorwegian orogeny that caused strong reworking of the bedrock in southwestern Sweden.

In late Precambrian and/or early Cambrian time, i.e. between ca 600 and 550 Ma, arenitic sediments were deposited on a levelled bedrock surface, denoted the sub-Cambrian peneplain. The sediments were subsequently transformed to sandstones (in a wider sense), which constitute the youngest rocks in the region. The remainder of these former extensively occurring sedimentary rocks cover the Precambrian crystalline rocks along the coast of the Baltic Sea from the area south of Oskarshamn in the north to northeastern Blekinge in the south. Furthermore, fractures filled with Cambrian sandstone are documented in for example the Götemar granite, east of a N-S trending fault that transects the latter /Kresten and Chyssler, 1976/ and at Enudden, ca 4 km northeast of Simpevarp /Talbot and Ramberg, 1990/.

The bedrock at Äspö consists exclusively of magmatic rocks belonging to the ca 1.81-1.76 Ga generation of the TIB as described above. The main rock types that predominate in this generation are:

- 1) a medium-grained, equigranular granite to granodiorite, including subordinate quartz monzonite and monzodiorite (old name: Ävrö granite).
- 2) a medium-grained, sparsely to strongly porphyritic intrusive rock that varies in composition between granite and quartz diorite, including tonalitic, granodioritic, quartz monzonitic and quartz monzodioritic varieties (old name: Äspö diorite).
- 3) a grey, fine-grained, at places slightly porphyritic, intermediate rock.
- 4) Furthermore, dykes of fine-grained granite and pegmatite are frequently occurring.
- 5) Mafic rocks. These are undifferentiated amphibolites, but most of them are considered to be genetically related to the granitoids and dioritoids of TIB.

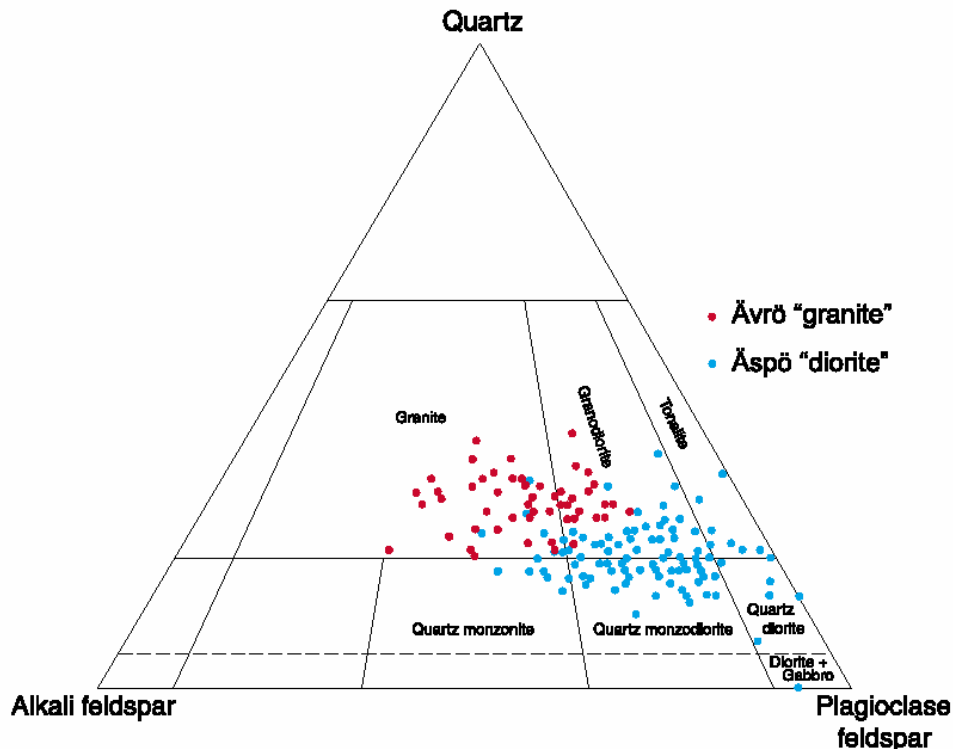


Figure 3-11. Modal composition of Småland “granites” from the Äspö area, i.e the granitoids and dioritoids, showing their large compositional variation. Based on Figures 3-13 and 3-14 in /Wikman and Kornfält, 1995/.

The dykes of fine-grained granites seem to be more common in the coastal areas than further inland, in the Laxemar area /Wahlgren et al., 2003 and Curtis et al., 2003/. The orientation of the dykes are predominately E-W and NE-SE in the coastal area, but more random in the Laxemar area. At Äspö they appear as dykes of varying width all over the island (red dashes in Figure 3-1), but in particular as larger bodies extended along the EW1 zone (Äspö shear zone).

Structural development

The bedrock of southeastern Sweden has gone through a long and complex structural development since the formation of the oldest ca 1890-1850 Ma supracrustal rocks, including both ductile and brittle deformation. The oldest deformation is of regional, penetrative character, and is recorded in the supracrustal rocks in the Blankaholm-Västervik area. It pre-dates the first generation of TIB rocks (i.e. the “Loftahammar granite”, ca 1850 Ma) in the area. The subsequent deformation that affected both the 1850 Ma generation of TIB rocks and the older supracrustals, is heterogeneous in character. This deformation is caused by dextral transpression in response to ca N-S to NNW-SSE regional compression and is constrained to the timeinterval ca 1850-1800 Ma. It can be exemplified by the dextral, strike-slip dominated Loftahammar-Linköping deformation zone (Figure 3-6) /Stephens and Wahlgren, 1996; Beunk and Page, 2001/.

The 1810-1760 Ma generations of TIB rocks, that dominates the bedrock in the Oskarshamn and Simpevarp region, is post-tectonic in relation to the regional, penetrative deformation that is related to the peak of the Svecokarelian orogeny. However, they are affected by a system of ductile deformation zones of the same

character as the Loftahammar-Linköping deformation zone, though developed during more low-grade conditions, i.e. at shallower levels in the crust, than the initial phase of shearing in the Loftahammar deformation zone. However, the Loftahammar deformation zone displays ductile reactivation during low-grade conditions, which presumably is contemporaneous with the shearing in the 1810-1760 Ma TIB rocks. In the Oskarshamn region, these deformation zones are exemplified by the E-W trending Oskarshamn-Bockara and NE-SW trending Oskarshamn-Fliseryd deformation zones /Bergman et al., 1998/. Presumably, also the ductile, NE-SW trending, so-called Äspö shear zone /Gustafsson et al., 1989/ belongs to this system of ductile deformation zones.

Independent of the syn-deformational metamorphic grade, the dextral and sinistral strike-slip component in the WNW-ESE to NW-SE and NE-SW trending ductile deformation zones, respectively, indicate that a regional, ca N-S to NNW-SSE compression prevailed during their formation and subsequent ductile reactivation. Consequently, this regional stress field is inferred to have prevailed for a considerable period of time, at least from the time of the intrusion of the 1850 Ma TIB generation, or possibly earlier, until ca 1750 Ma. Most of the lithological contacts in the region, and also in the whole of southeastern Sweden, are more or less concordant to the orientation of the ductile deformation zones, which indicate that the emplacement of the TIB magmas was facilitated by ongoing shear zone activity. Together with the subsequent deformation of the TIB rocks, this testifies for an important influence of the deformation zones for the present structural and lithological framework in the bedrock of southeastern Sweden.

Apart from the mylonitic foliation in the ductile deformation zones, the 1810-1760 Ma TIB rocks locally display a more or less well-developed internal fabric, e.g. preferred orientation of feldspar phenocrysts, mafic enclaves, biotite etc. However, it is often difficult to decide whether this fabric is syn-intrusive or caused by a subsequent tectonic overprinting. Both alternatives have been suggested /Wikström A, 1989 and e.g. Talbot et al., 1988, respectively/. The orientation of the foliation in the Simpevarp-Äspö region suggests that there might be a genetic relationship between fabric development outside the ductile deformation zones and the shear zone activity.

Most of the bedrock in the Simpevarp-Äspö area is only weakly deformed as described above and fairly homogeneous at outcrop scale. The coastal areas around Laxemar, Simpevarp, Ävrö, Hålö and Äspö are, however, located in a large-scale network of shear zones of ductile to semi-ductile character. They are of regional, local major and local minor scale. Exposed individual shear zones in the network rarely exceeds a width of 1 m, but e.g. the Äspö shear zone (EW1) is approximately 100 m wide in the central part of Äspö. The shear zone is the western boundary of this coastal shear belt and has been traced as a magnetic lineament from the Uthammar granite in the south to at least 1-2 km northeast of Äspö. In addition to the exposures at Äspö it is observed in outcrops at three localities along the lineament south of Äspö /Bergman et al., 2000/ (see also model description for EW1).

The aeromagnetic and ground magnetic map over the area /Triumpf et al., in press; Nisca and Triumpf, 1989/ and the topographic data has been used in the modelling to interpret the orientation and extent of the deformation zones (Figure 3-6 and Figure 3-8). A comparison between magnetic lineaments and topographic lineaments as they appear on the ground magnetic and topographic maps over Äspö (Figure 3-8) can give hints regarding the relation between brittle and ductile parts of deformation zones.

The transition from ductile to brittle deformation presumably took place during the time interval c.1750-1700 Ma, i.e. during uplift and stabilization of the crust after the Sveconorwegian orogeny /Larsson and Tullborg, 1993/. Since no ductile deformation has been observed in the ca 1450 Ma granites /e.g. Talbot and Ramberg, 1990/ or younger rocks, it is evident that only deformations during brittle conditions have affected the bedrock in the Oskarshamn region during at least the last ca 1450 Ma.

It is plausible that tectonic activities that are related to more or less remote large-scale processes, such as e.g. the Sveconorwegian and Caledonian orogenies, the intervening opening of the Iapetus Ocean, the Late Palaeozoic Variscan and the Late Mesozoic to Early Cenozoic Alpine orogenies, as well as the opening of the present Atlantic Ocean, have had a far-field effect within the shield area. However, to which degree these large-scale processes have affected the bedrock in the Oskarshamn region and the rest of southeastern Sweden, and especially which brittle structure belongs to which process is difficult to decipher. The main reason for this uncertainty is the great lack of time markers for relative dating, except for the sub-Cambrian peneplain and the Cambro-Ordovician cover rocks, and the difficulties to date brittle structures radiometrically. In the absence of exposed post-Cambrian markers it is also difficult to determine which fracture zones or faults that were formed or reactivated during the last 500 million years.

The first brittle faults in the region probably developed in connection with the emplacement of younger granites. During the subsequent geological evolution, faults and older ductile deformation zones have been reactivated repeatedly, due to the increasingly brittle behaviour of the bedrock. Brittle reactivation of ductile deformation zones is a general phenomenon, and is also the case in the Oskarshamn region. Both the Oskarshamn-Bockara, Oskarshamn-Fliseryd and Äspö shear zones display clear evidence of being reactivated in the brittle regime /see also e.g. Munier, 1995/. The alignments of dykes of fine-grained granite with the Äspö shear zone /Kornfält and Wikman, 1988/ indicate that either was faulting along the zone facilitated and possibly caused the formation and intrusion of the granites or else are the granites deformed along the zone after their formation (or both). Normally these granites are deformed, particularly in a brittle regime and their importance for the hydrology has been shown /e.g. Rhén and Forsmark, 2000/.

An inversion of the strike-slip component in the Äspö shear zone from sinistral during the older ductile deformation, to dextral during the younger brittle reactivation has been proposed by /e.g. Talbot and Munier, 1989 and Munier, 1995/.

The occurrence of ca 1000-900 Ma dolerites in southeastern Sweden testifies for a Sveconorwegian tectonic influence, since the intrusion of the parent magmas has been tectonically controlled. However, whether individual faults or fracture zones, which were not injected by mafic magma, were formed or reactivated during the Sveconorwegian orogeny, and if so which of them, is uncertain.

According to /Milnes and Gee, 1992 and Munier, 1995/, the Ordovician cover rocks along the northwestern coast of Öland are, except for displacements in cm-scale, tectonically undisturbed. This indicates that the E-W trending fracture zones/faults in the Oskarshamn-Bockara deformation zone, which can be seen in the magnetic anomaly maps to continue eastwards under Öland, do not affect the Cambro-Ordovician cover sequences on Öland. Thus, this indicates that these brittle deformation zones of regional character were not active in post-Cambrian time, but are related to the Precambrian tectonic evolution. Strictly post-Cambrian fracture zones/faults have, however, not been

recorded in the Oskarshamn region. On the northwestern part of Furö, a small island east of Oskarshamn, a fault contact between brecciated Cambrian sandstone and brecciated red granite has been observed /Bergman et al., 1998/. Furthermore, the occurrence of joints filled with Cambrian sandstone east of, but not west of, the N-S trending fault in the western part of the Göttemar granite, indicates that the eastern block has been down-faulted in relation to the western block in post-Cambrian time /Kresten and Chyssler, 1976 and Bergman et al., 1998/.

As mentioned above the sub-Cambrian peneplain is a potential marker to demonstrate post-Cambrian brittle tectonics. In general, all pronounced depressions and distinct differences of topographic level in the Sub-Cambrian peneplain constitute potential brittle deformation zones in a wide sense. /Tirén et al., 1987/ studied the relative movements of regional blocks in southeastern Sweden, which were bounded by fracture zones and ranging in size between 25 km² and 100 km². Differential vertical movements were interpreted to have occurred along existing faults both during periods of uplift and subsidence.

A general problem is to decipher the relation between the formation and subsequent reactivation of faults and fracture zones. The brittle deformation history of a region can be regarded as the combined effect of generation of new fractures or faults and reactivation of old fractures or faults. The ratio between generations of new structures and reactivation of older structures is presumed to decrease with time, since the orientation spectra of pre-existing structures increased with every new event of brittle deformation /Munier, 1995/. Relative age determinations of fractures, based on orientation and a succession of mineral filling with decreasing age, have been recorded on Äspö /Tullborg, 1997/, c.f. Table 6-9. It is reasonable to assume that these findings can be extrapolated to the surrounding parts of the Oskarshamn region. The oldest fractures are epidote- and quartz-bearing, and with decreasing age chlorite, zeolite and calcite appear as fracture filling. Since the mineralogy in individual fractures within fracture zones is essentially similar to fractures in the intervening blocks /Munier, 1995/, the fracture filling is a potential tool for relative age determination of movements (reactivations) of the former. Consequently, the calcite-bearing fracture zones/faults represent the youngest reactivation, but the absolute age is uncertain. Another problem is that several generation of the same fracture mineral occur (see also chapter 5.6.2). Based on data from Äspö, the orientation of the maximum compressive stress during the formation of the epidote- and quartz-bearing fracture zones was N-S/subhorizontal /Munier, 1989/, and had changed orientation to NE-SW when the chlorite-filled fracture zones/faults formed /Talbot and Munier, 1989/. The maximum compressive stress was still NE-SW when the fractures formed which is filled with Cambrian sandstone /Talbot and Munier, 1989/. The orientation of the maximum compressive stress during the subsequent tectonic evolution is presumed to be NW-SE, i.e. the same as the present stress regime. Consequently, a roughly NW-SE maximum compressive stress is inferred to have prevailed for a considerable period of time, i.e. possibly for hundreds of million of years.

Based on interpretations from remote sensing methods, /Nisca, 1987 and Tirén et al., 1987/ suggested that NE-SW trending structures are older than N-S and E-W trending systems. Furthermore, most of the N-S trending structures are presumed to be younger than the E-W trending.

Attempts have been made to use palaeomagnetic, electron spin resonance (ESR) and isotopic dating (K-Ar, Rb-Sr) techniques on some brittle structures at the Äspö site /Maddock et al., 1993/, in order to constrain the minimum age of the most recent movements. Characterisation of the sampled fault gouge material demonstrated that many fracture zones contain sequentially developed fault rocks and verifies that reactivation has occurred. The ages given by the various dating methods reflect both inherent differences in the techniques as well as differences related to the specimen or phenomenon that are being dated. The interpretation of the ESR dating was imprecise due to the resolution of the method, but yielded minimum ages of movements in the order of several hundred thousand to one million years. The results of the palaeomagnetic and K-Ar analyses strongly suggest that growth of the fracture infilling minerals took place at least 250 million years ago. The most recent fault movements are interpreted to have preceded this mineral growth. /Maddock et al., 1993/ concludes that any quaternary and holocene activity had little effect on the fracture zones they examined.

According to /Mörner, 1989/, a great number of supposed post-glacial faults occur on Äspö. However, none of the faults reported showed any positive evidence of kinematics /Bäckblom G (ed), 1990/. Some of the reported faults did not display any disturbance of Precambrian markers, others had their bases exposed by excavation and ice plucking could be positively demonstrated. /Talbot and Munier, 1989/ discuss post-glacial faults in connection with studied fault scarps, i.e. abrupt steps in the glacially polished bedrock surface on Äspö. According to /Munier, 1995/, post-glacial reactivation of individual fractures has most likely occurred, but despite searches no evidence of such features has been found on outcrops.

Ongoing tectonic activity caused by plate movements and land upheaval is manifested in seismic events and aseismic slip /Larsson and Tullborg, 1993/. According to /Slunga et al., 1984/, the so-called Protogine Zone of southern Sweden has been shown to be the border between a more seismic western Sweden and the more aseismic southeastern Sweden. The orientation of the maximum horizontal principle stress relaxed by the seismic events is ca NW-SE /Slunga et al., 1984/. This is in agreement with the results from rock stress measurements at depths more than 300m /Stephansson et al., 1987/, and also with the stress field generated by the plate movements (ridge push forces) in the North Atlantic Ocean /cf. Slunga, 1989/.

The relation between older ductile deformations and brittle fracturing of the rock is not fully revealed at Äspö, but many interesting observations have been made. On Äspö /Ericsson, 1988/ mapped ca 4500 fractures on outcrops. Ericsson separated the fractures into three areas; north of, south of and within the Äspö shear zone. It is evident that the fracture orientation is rather different in these three areas. Most obvious is the lack of fractures in the NE direction on the southern part of the island.

The distribution and orientation of fractures in the Geomod model domain is discussed in chapter 5.6. As can be seen in Figure 3-13, the fracture arrays at Äspö HRL is also present in a larger area, although the strong predominance of steep northwesterly striking fractures found at southern Äspö seems to be a local phenomena. At other localities in the region, the northeast direction of fractures seems to be equally or even more important. This is also the result from ongoing mapping at Simpevarp-Ävrö-Hälö /Wahlgren, pers.com., 2003/, but there are some localities where a similar pattern as that of southern Äspö also exists.

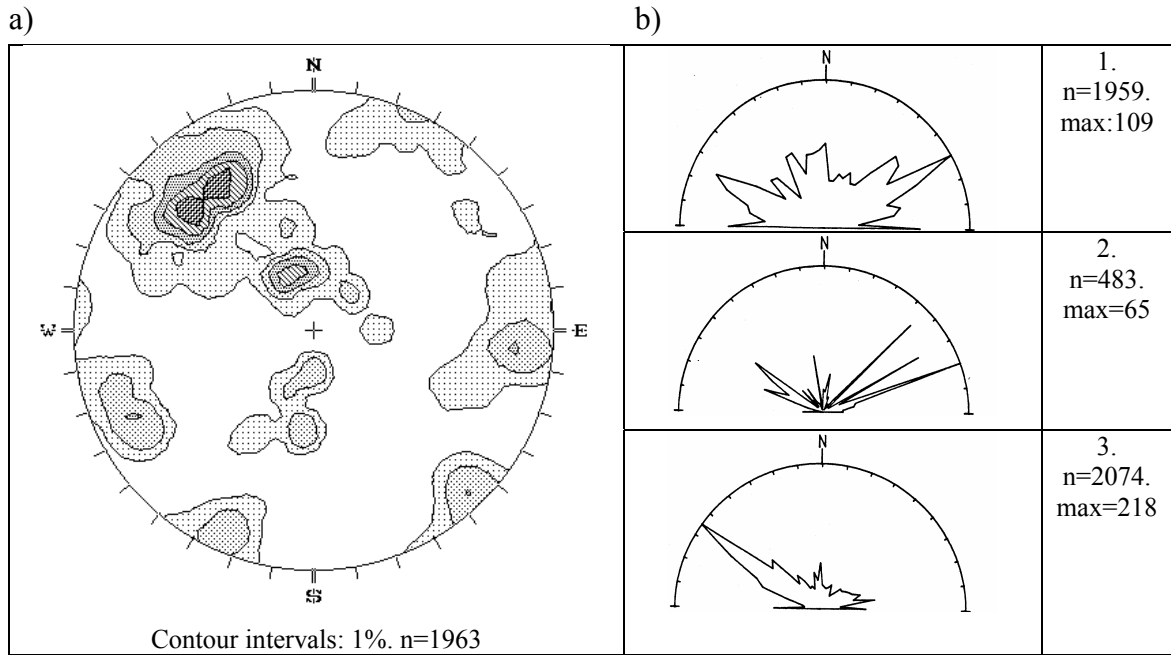


Figure 3-12. Fracture orientation from a) CLAB (Simpevarp) and b) Äspö /Ericsson, 1988/. The latter shows only the strike of fractures measured in 5° intervals (85% steep, i.e. 70-90 degrees), where 1 represent the area to the north of EW1, 2 the EW1 and 3 the area to the south of EW1.

The fractures in the bedrock outside deformation zones at Äspö HRL are plotted in Figure 3-13. It can be seen that although a few directions of fractures predominate, there is a scatter of orientation of fractures. The highest frequency per 1% area only reaches 5% of the measured population. Water bearing fractures have a stronger preference for the northwest direction.

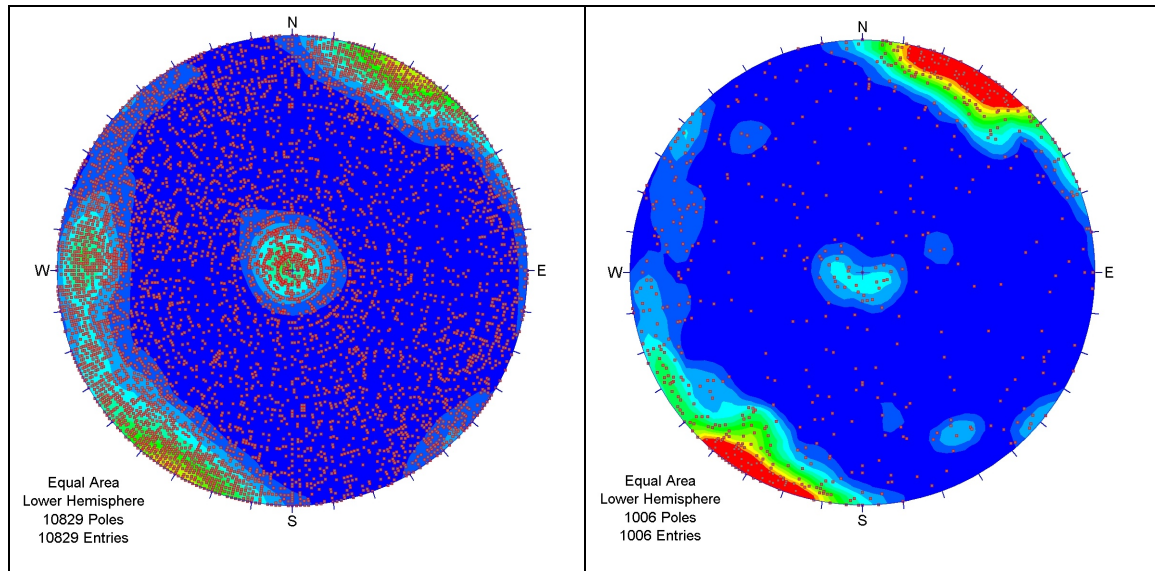


Figure 3-13. Fractures from the Äspö tunnel, within the Geomod model domain, except for those mapped in fracture zones. All fractures to the left (maximum ca 5% per 1% area) and water bearing fractures to the right (maximum ca 9%). Contour intervals at 1%. Each red dot represents a measured value, but note that there may be several measures having the same direction.

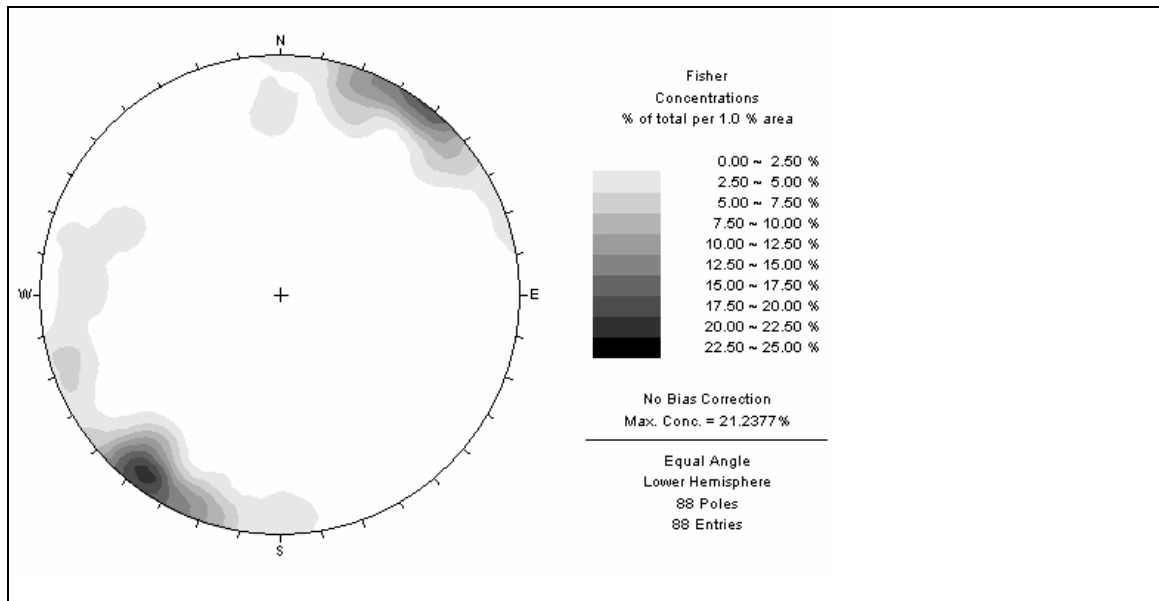


Figure 3-14. Poles to all water-conducting features (WCF) in the Äspö HRL /Mazurek et al., 1996/. These are faults traceable across the full tunnelsection.

Also the somewhat larger water conducting features of /Mazurek et al., 1996/ have a strong preference for this direction (Figure 3-13). Many of these (ca 30%) have ductile precursors. As can be seen in Figure 3-15, there is a systematic configuration of dextral and sinistral shear zones at Äspö. The similar direction of dextral mylonites and water bearing fractures and faults is noteworthy. However, the large-scale semiductile deformation zones in the area generally have a steep, northeasterly direction (Figure 3-10 and Figure 3-6). The mutual relationship and interconnection between the deformation zones in the area needs to be elucidated. The importance of these for the fracture systems, the rock mechanical situation and the geohydraulic systems at Äspö is probably very high.

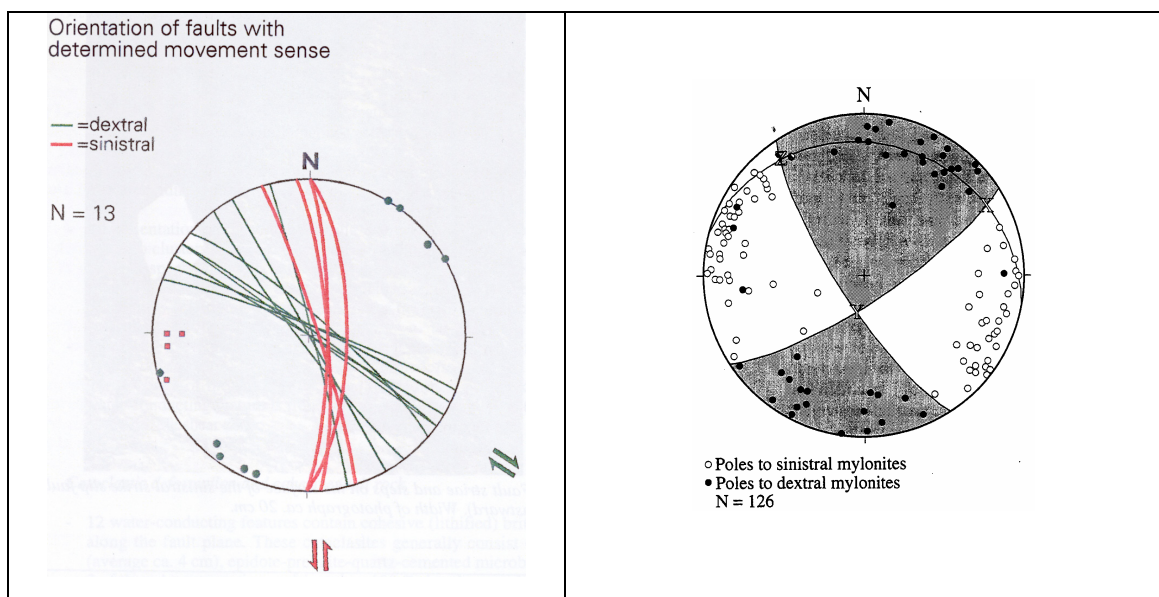


Figure 3-15. Poles to a) faults in the tunnel where sense of shear has been inferred /Mazurek et al., 1996/ and b) mylonites mapped at the surface of Äspö /Munier, 1995/.

4 Tree-dimensional site descriptive modelling, geology and geometries

4.1 Introduction

For the reader of the following description the best way to understand the RVS model is to have the model on a desktop computer, as two-dimensional figures may be difficult to comprehend.

In order to separate out sections of rocks in a borehole, a tunnel section or in an outcrop there have to be criteria and limits set up to decide what should be considered as zones and not. Such criteria could be geometrical and geological parameters length/width ratio of particular features, density or intensity of parameters, such as fractures, ductile deformation and alteration. It is not straight-forward to find the ultimate values for such boundaries and it requires that input data are consistent. However, once it has been done the selection procedure of zones can be made with higher transparency than without such boundaries. Such specified definitions has not been set up at the Äspö site, and consequently the modelling of Äspö02 has relied on existing description of zone characteristics and on characteristics that could be extracted from GIS-data, SICADA, TMS, BIPS images.

The definition of the term “Fracture Zone” at Äspö is zones having at least twice as high intensity of natural fractures as the surrounding rock and having “obvious tectonic/kinematic influence” /Rhén et al., 1997/. In the tunnel mapping system (TMS), the mapped sections were separated into a) normally fractured rock, b) “zones of increased fracturing” and c) fracture zones. The definition of “zones of increased fracturing” was more than 5 fractures per m, but with no “obvious tectonic/kinematic influence”. It should be noted that in a tunnel it may be difficult to see whether an excavated area of fractured rock actually extends in a zone-wise (high length/width ratio) manner or not, especially if the fracture sets are not parallel with the boundary. The fractured rock may at places correspond to irregular volumes of increased fracturing, rather than a zone.

The Geomod project does not involve any new field data. Considerations regarding if a specific section in a borehole or tunnel actually is part of a zone or not is made on the basis of information available in the database and in published reports. If no such information has been found, the geometrical and geological parameters of model object have been used to make judgement of probable interpolations and extrapolations. In this respect the geometrical data has been considered to be the most important if other, geological parameters do not prohibit the interpretation.

4.2 RVS

4.2.1 Introduction

The Rock Visualisation System (RVS) has been developed by SKB for use in visualizing geological and engineering data. It aims to assist in the interpretation of the geological environment by the construction of 3D structural geological models. It has been under development since 1994. The current version of RVS, version 3.4, is based on MicroStation V8[®] and the databasem/Access 97/2000[®]. The system is certified for Windows NT4 Workstation[®], Windows 2000 Professional[®] and Windows XP[®].

RVS has been designed to enable a close integration with SKB's investigation database SICADA. Since all raw data originating from the many investigation programs is carefully quality controlled before it enters SICADA, the close integration between the two systems ensures that this quality is maintained by automating data processing and transfer. This close integration ensures an acceptable level of data quality as well as ensuring a high level of traceability.

The other major data input source to RVS is from SKB's GIS database SDE (Spatial Data Engine). This type of data differs from SICADA data since it has already been processed and interpreted within a commercial GIS system and is therefore in a proprietary file format, which requires conversion before it can be imported and used by RVS.

4.2.2 Overview of the modelling process

This section of the report outlines a general modelling procedure following an imaginary investigation of a rock volume. The entire modelling process, to the creation of a block model with the assignment of parameters, has not been completed for the Geomod project. The graphics shown have been based on archive data from SKB's underground hard rock laboratory at Äspö and are not related to any active SKB project.

The RVS modelling process begins with the definition of the 3D model domain volume (Figure 4-1).

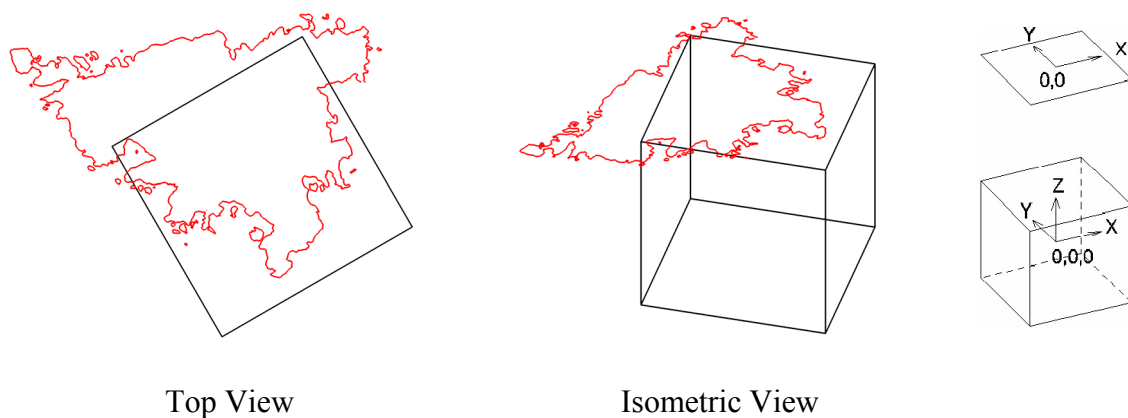


Figure 4-1. Definition of the model domain. The black cube represents the RVS model boundary.

A model may be built up initially from the results of the desk study and preliminary fieldwork. The desk study involves assembling all the relevant basic data available, such as topographic and geological maps, remote sensing data etc. The initial fieldwork may include basic geological mapping and ground control. Such key maps and data are input into a GIS system and then reprocessed and attached to the RVS model.

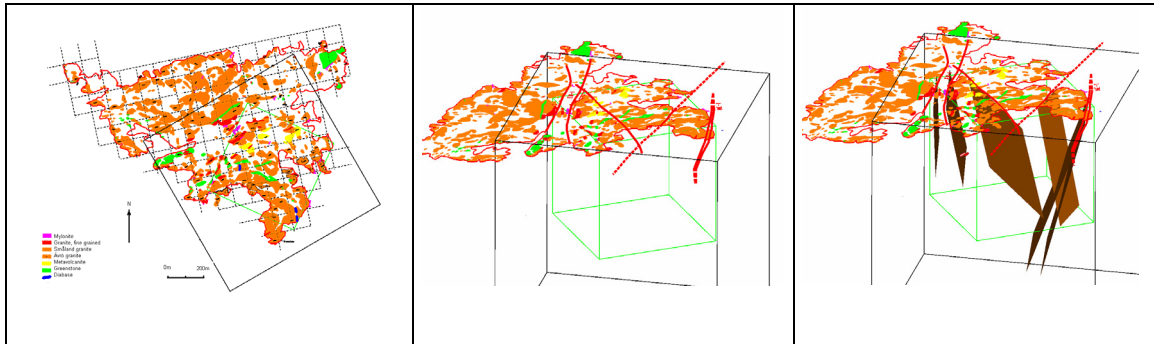


Figure 4-2. To the left is a top view of a model volume with an attached lithological outcrop map, based on field mapping. The results from lineament studies and geophysical mapping may be attached in the same way. The central figure show attached lineaments that may be extrapolated towards depth (to the right) if geological or other indications suggest so.

The interpretation of these data may lead to the proposal of number of surface traces (2D) representing various structural zones, the red lines shown in the figures below. Where evidence is available such surface traces may be given tentative orientations and visualized in 3D space. Such a zone can be visualized using the RVS *Model surface* tool where a surface trace can be drawn or fixed by specifying a strike and then given a value for dip. In addition a thickness can be specified so the zone appears as a 3D volume rather than a plane. Alternatively the coordinates of a number of known points can be input to a *Point table* and RVS can be asked to interpolate a *best-fit* plane for the data.

Direct physical evidence of the prevailing rock conditions at depth is obtained by drilling. The geometry of the boreholes, along with results from drill-core mapping and in situ testing, are assembled in the SICADA database and retrieved for modelling by RVS. RVS has various tools to aid working with borehole data.

Data is ordered from the SICADA database and imported into the local RVS database for modelling. As more information becomes available the geometry of the various interpreted structures may be modified with adjustments to their persistence, alignment and width; to better fit with the perceived reality.

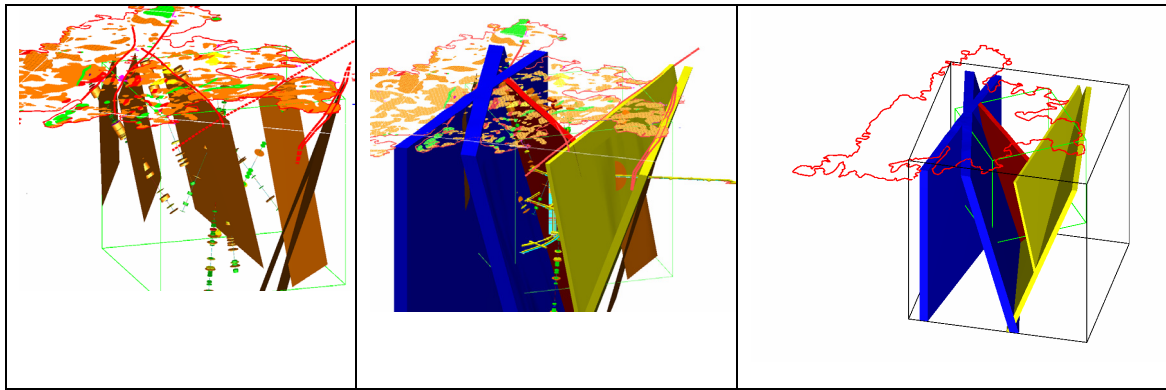


Figure 4-3. Geology in boreholes are visualized (left) and lead to modification in zone geometries (centre). To the right the model domain volume is being adjusted (green cube).

The model volume may be adjusted at some stage to focus on a smaller rock volume for more intensive study.

The network of inferred deformation zones defines a series of discrete blocks. Other interpreted features that may be used as demarcation of units are the interpreted rock type boundaries from the modelling of the lithology in 3D. Each block or unit is given its own identity within the model and assigned to a particular block group depending on type of boundary, e.g. deformation zone or rock unit boundary. All such groups and contained blocks are listed in the RVS *object manager*. From all the obtained investigation data and interpretations, each block group is characterized by assigning them characteristic values for the various parameters; rock-type, strength, permeability etc. In this way a description of the entire rock volume under study is generated.

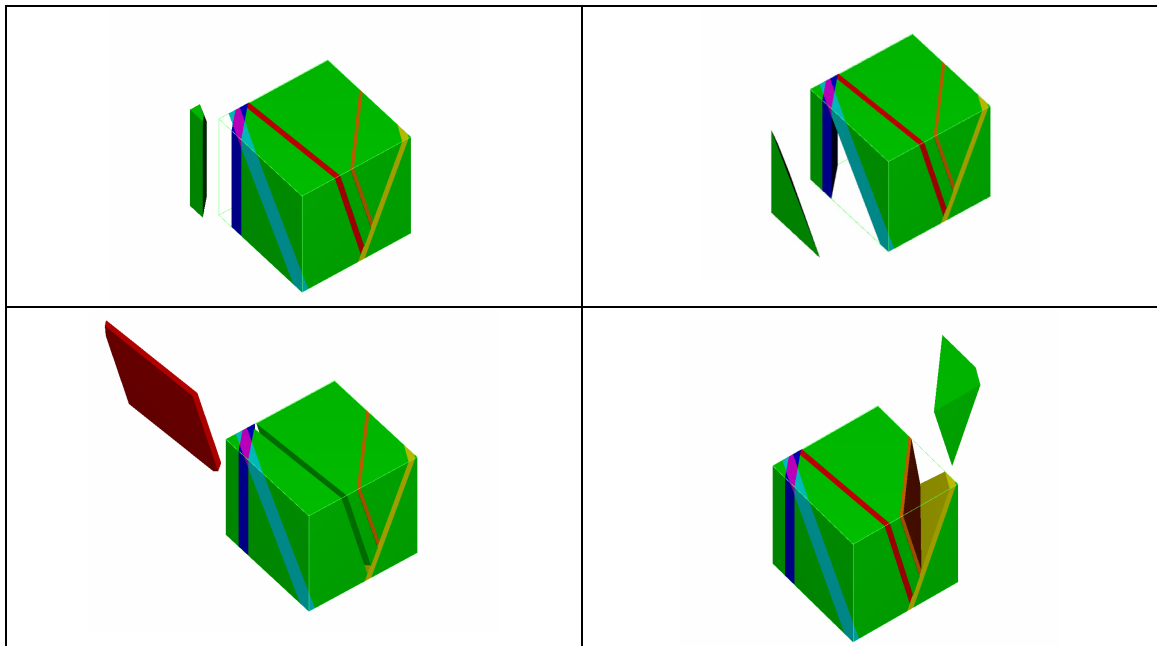


Figure 4-4. Example of how block symmetry can be visualized.

Even during the initial investigation stages of a project, any available preliminary design layout of a planned excavation can be attached to the model. In this way the design process can be dynamically interactive with the ongoing investigation and modelling work of the rock volume. By examining the block geometries, in situ stress and rock conditions, the overall siting and layout of any planned facility can be optimized and supply feedback for the planning of the ongoing investigations.

The visualisation and modelling work in RVS continues throughout the detailed design and construction phases (Figure 4-5). RVS is used in combination with other tools to visualise the detailed mapping of the excavations as well as the planning and visualisation of results from continued investigations.

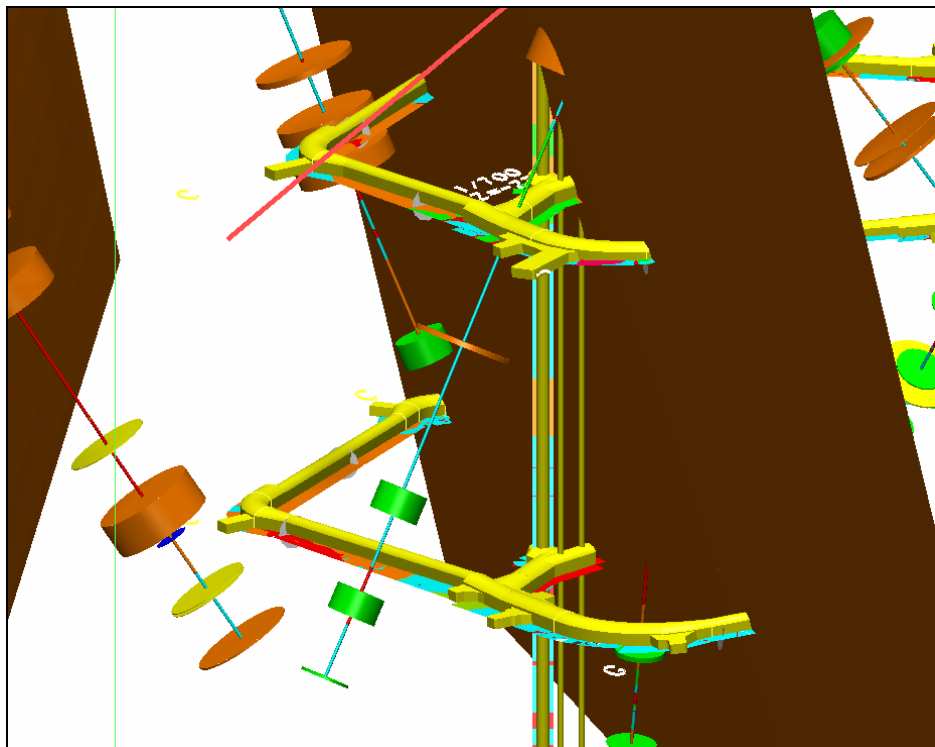


Figure 4-5. The figure shows a tunnel geometry, planar deformation zone surfaces, tunnel mapping and visualised borehole data.

4.2.3 Constructing and visualising surfaces

Point information from the visualized boreholes, for example an inferred crush zone, along with other point and trace geometries, can be used with the RVS modelling tools to generate surfaces, representing interpreted geological structures such as deformation zones. The created surfaces can be either planar or undulating.

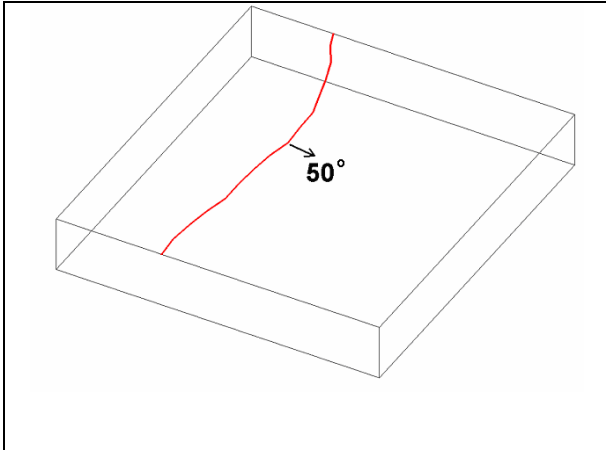


Figure 4-6. Example: Generation of an undulating surface in RVS, representing a deformation zone, from a topographic lineament trace combined with tentative dip information based on, for example, outcrop mapping or geophysical surveying.

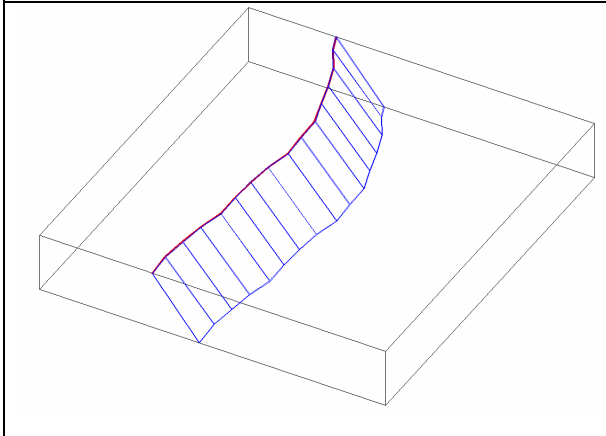


Figure 4-7. The user may vary the number of points, taken along the initial trace-profile line as considered appropriate.

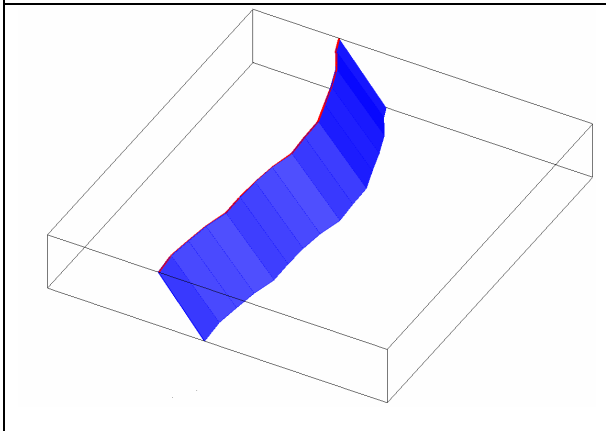


Figure 4-8. Final visualisation.

It is possible to calculate the best fit of a planar surface to a given point set. Restrictions on Strike, Dip and or location can also be given. It is also possible to create a triangulated undulating surface using a given set of points. The points can be irregularly spaced and sorted in any order.

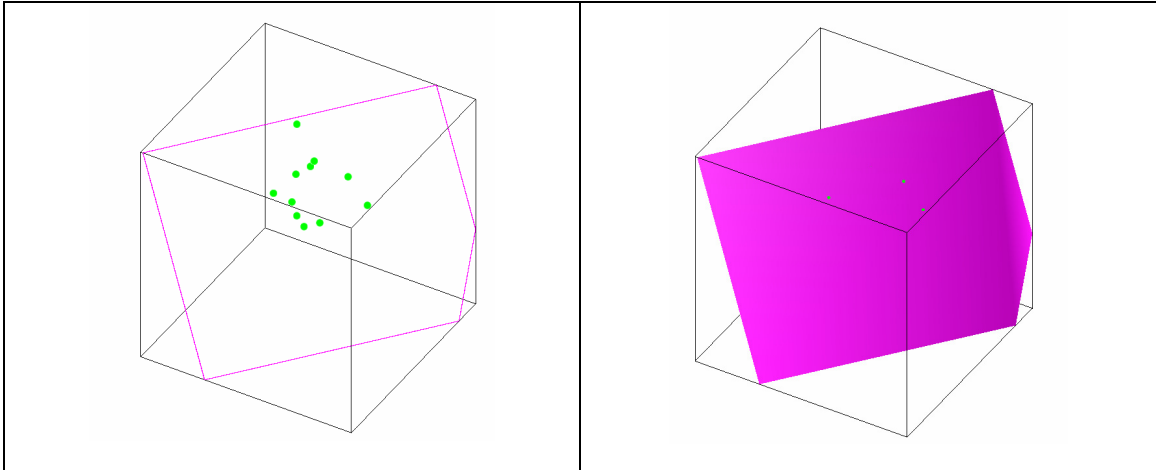


Figure 4-9. Example on the generation of a planar surface in RVS, representing for example a deformation zone. Green dots mark observed intersections.

Figure 4-9 illustrates how a planar surface may be generated in RVS, based on a series of point locations interpreted from mapping of drillcores, or tunnel mapping. Such point locations may, for example, represent sections of drillcore with low RQD-values and characteristically similar patterns of alteration, which may lead to an interpretation of them as belonging to the same tectonic structure. RVS has generated a "best-fit" mean planar surface assigned to the point cloud.

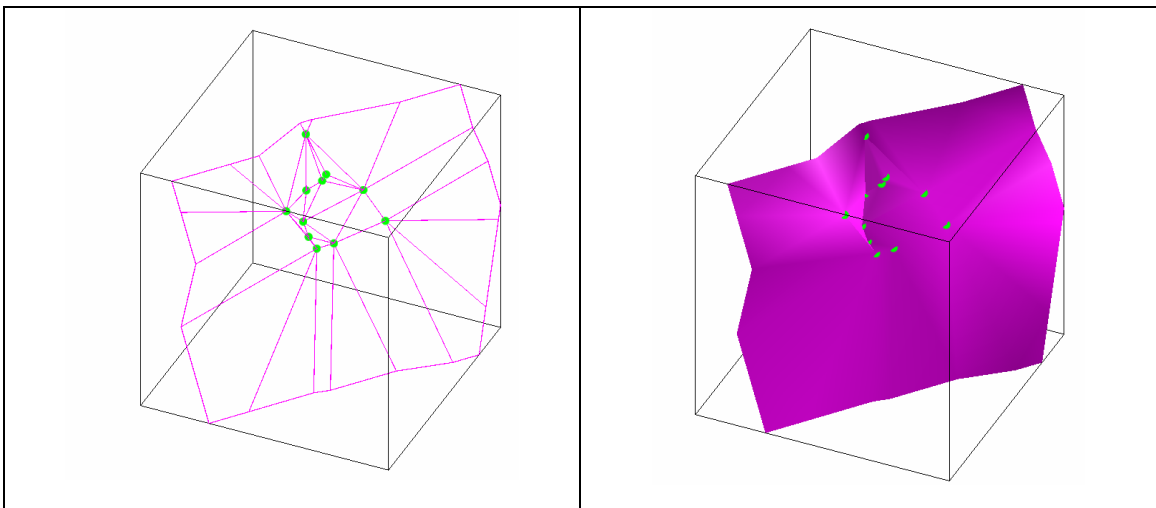


Figure 4-10. Generation of an undulating surface in RVS based on the same point data as used above. RVS has triangulated the points (see method description in text) and generated an undulating surface, which passes through all of the individual points.

RVS generates an undulating surface in the following manner:

- The point cloud is analyzed in order to determine the best projection onto a 2D plane.
- All the 3D points are then projected onto this 2D plane. The user can specify a *DTMXY tolerance*- a filter that filters out points that appear to be very close in a 2D projection of the point set, in order to avoid poor triangulation. The measure is the minimum distance allowed between two points, expressed in meters.
- Three new arbitrary points are added, forming an all-encompassing triangle, fencing the 2D point cloud.
- All the points are triangulated in 2D.
- Edges that are connected to the three fencing points are removed.
- True 3D vertices are restored.
- A triangular mesh surface is created and clipped to the Model Boundary. *Note:* the resulting mesh contains a collection of planar polygons, not necessarily limited to triangles.
- Adjacent polygons are further analyzed and whenever coplanar polygons are found, the connecting edges are removed.

The coordinates of the individual points, which form the basis for the interpretation of any surface are saved as a *point table* in RVS and are always available for review and editing, allowing further remodelling. The points may also be saved as a sub-object to the surface, appearing in the *Object Manager* tree.

Additional RVS tools exist to modify and further develop the modelled surfaces as more information from investigations becomes available. For example, an already created surface can be remodelled if point locations have been added or changed; surfaces that intersect can be trimmed against each other.

4.3 Modelling of deformation zones in GeoMod

4.3.1 Conceptual models

A conceptual understanding of the arrangement of fractures and fracture in the rock has been developed at Äspö. Much of the input to the “conceptual database” has successively been developed at Äspö in projects like “True Block Scale” /Andersson et al., 2002/, “Fracture Classification and Characterisation” /Bossart et al., 2001/ and “Tracer Retention Understanding Experiment” /Winberg et al., 2000/. The conceptual model is shown at different scales in Figure 4-11. For natural reasons the scales represented in a-d, i.e. is in the volume of rocks between larger conducting features and deformation zones, have been the major interest for most projects at Äspö. It is in these areas where canisters primarily will be disposed. The structures represented in Figure 4-11 e-f are less well constrained in three dimensions, partly because they are difficult to sample and measure.

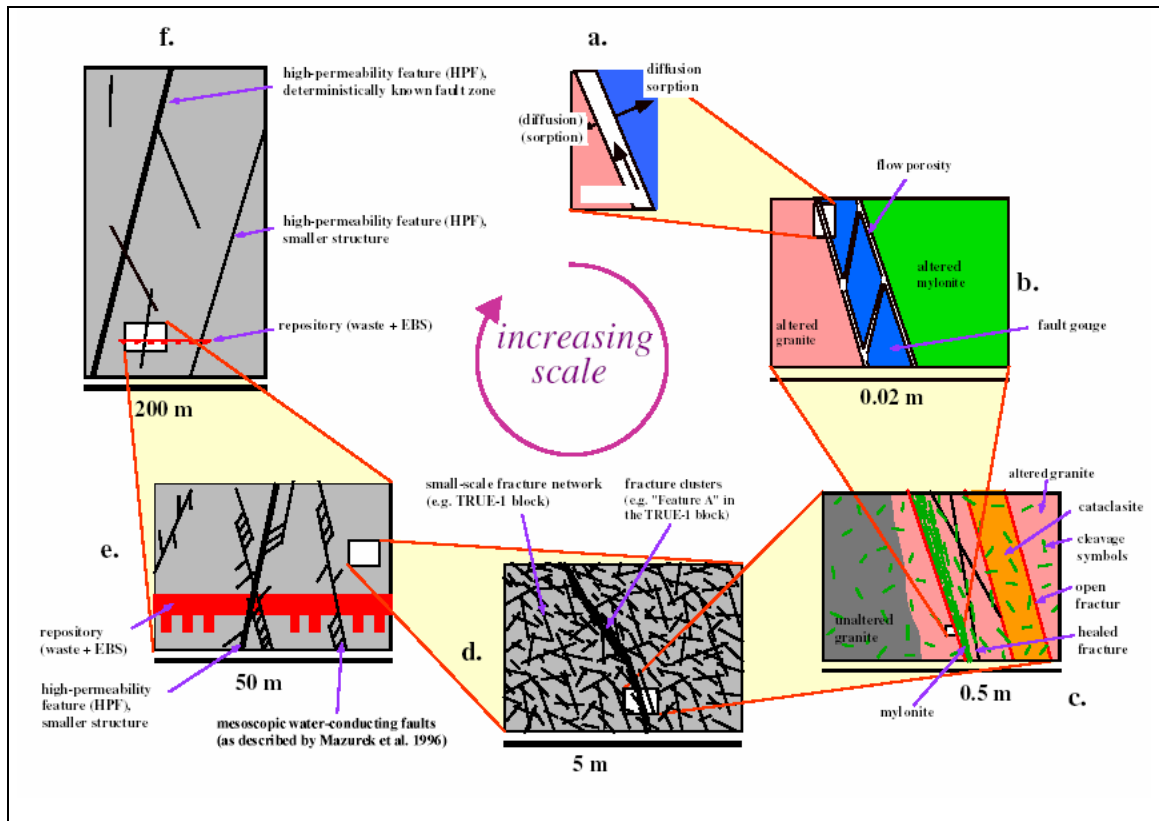


Figure 4-11. Conceptual models in different scales /from Bossart et al., 2001/.

4.3.2 General assumptions made

The following general assumptions have been made for the geology at Äspö, when considerations were made regarding which deformation zones were to be modelled and how.

Ductile zones are continuous over tens of metres along their strike. They are typically reactivated, possibly under ductile conditions, but generally at brittle conditions. Ductile zones generally also have a higher frequency of fractures related to them, as compared to the average rock mass. This is the case both within and in the close vicinity to the zone. Individual fractures and strict fracture zones are often discontinuous or irregular over longer distances along their strike.

4.3.3 Prerequisite for modelling zones

The strategy regarding zone size, geometry and extension, in relation to which zones that should be modelled, was discussed early in the Geomod project. The following requirements were set up.

A cut off for zone width at ca 1 m (average) was used, based on the individual observations that characterize the zone. The importance of a zone for the hydrogeological and/or rock mechanical conditions at the site also was, however, considered and has led to the inclusion of zones less than 1 m wide in the model. There is a certain degree of subjectivity in this.

In order to model a zone on a larger scale a certain amount of knowledge of the zone is required. One single observation of a zone is not enough. Several zones mapped in the tunnel system at Äspö have only been observed at a single location and do not seem to have a continuation along strike to other locations in the tunnel. Some of these locations are included in the RVS model as discs representing the zone boundary, but have not been extrapolated far outside the tunnel face. One of the following general criteria was set up as a guideline for the required amount of observations on modelled zones.

- number of separate, certain observations of the same zone : 1-2 or more
- number of separate, probable observations of the same zone: 2-3 or more
- number of separate, possible observations of the same zone: at least 3

Zones regarded as being of regional, or local major character in the Äspö tunnel would be modelled even if they were mapped at only one locality.

When the decision was made whether a zone should be modelled or not, also certain subjectivity had to be involved. Except for the general guidelines suggested above, a pragmatic judgement of properties and continuity, such as the degree and character of fracture sets and its relation to the lithology, has been made. The most important characteristics of the zones when modelled in 3D are, however, the mutual location and orientation of the observations.

4.3.4 Extent of modelled zones

The width of the zones in the geometrical Äspö02_v1 is 2 cm, which is the smallest width that can be assigned to a zone in RVS. This width has thus nothing to do with the actual width of the zone, but is a feature of the system involved in the model work. The length of the modelled zones is longer than the observed length. Below are a few guidelines that were used when extrapolation and interpolation was done.

Regional and local major zones was, as a first assumption, modelled with the same orientation and extent as was done in a model created for separate rock mechanical project /Andersson et al., 2002; Staub et al., 2002 and Hudson, 2002/.

When local minor zones were looked upon and modelled the guidelines in Table 4-1 was used. Ending of zones in the base model was against other zones or towards the model domain boundary.

Table 4-1. Guidelines for interpolation and extrapolation of local, minor zones.

Interpolation:	<p>If recognized as the same zone in the Fracture Zone Catalogue (Annertz, Appendix 2 in /Munier, 1995/, in model Äspö96, or in separate projects at Äspö HRL - IP between the observations.</p> <p>If zone characteristics are similar – several times the maximum observed length.</p> <p>If zone characteristics are dissimilar – less than ca 50 m.</p>
Extrapolation:	<p>Approximately 3 times observed length or 2 times the maximum interpolated length, if zone character does not suggest a different interpretation.</p>
Zone intersections:	<p>Relative size, information regarding kinematics and reactivation was looked for to model the most probable symmetry between intersecting zones. If no such information exists and if the size of the zones is similar, zones were modelled as continuous across intersections with no deflections.</p>

4.3.5 Characterisation

General

Previously named zones are renamed according to PLU convention (i.e. ZAS0001A1 etc) according to the following description. However, the old names have been used to get the report more readable. In the zone description (chapter 5.4) the old names are given within brackets.

Other zones were named as they first were recognized in the tunnel, borehole or report. The procedure is to first assign three letters (ZAS) denoting deformation zone (Z) and model (AS as in Äspö) and then to assign a specific number to each zone (0001 to nnnn). Finally the two last positions are used to separate between branches of one zone at different scales, such that A to Z denotes separate branches in a more regional scale and the last position, 1 to n denotes separate branches in a more local scale.

Initially a general characterisation procedure of potential zones to be modelled was performed, in this case with the so called “Fracture Zone Catalogue”, the TMS database, SICADA and project reports as a base for the judgement, with the prerequisites discussed above in mind. Observations of a deformation zone made at the surface, in the tunnel, or in a borehole are written down in protocols as a basic input when assigning properties to modelled zones. Below is a checklist of the information that should be looked for.

Table 4-2. General characterisation of zone.

Parameters	1	2	3	4	5
Size	Width/variability				
Character of the state of deformation	Brittle	Semi-ductile ductile	Ductile	Complex (combination of previous)	
Host rock	(Name)	Frequency (%)			
Deformation rock nomenclature	(Name)	Frequency (%)	Location (chainage or similar)		
Orientation (internal fabrics and boundaries)	Strike/dip				
Reactivations	Yes/no	Character			
Fractures	Number of sets	Frequency/set	Size	Strike/dip	
Mineralogy (Host rock, zone, fracture sets)	Mineral 1	Mineral 2	Mineral 3	Mineral 4	Mineral 5
Water	Yes/no	Flow location	transmissivity	Occurrence of grouting	
Alteration	Type	Frequency in zone (% of zone)	Amount (weak, partly, strong, complete)	Location in relation to zone	
Comment	Relation to other structures	Kinematic information	Other general comments		

If the decision was to model the zone, then a protocol was used (see appendix 2) to characterise the zone on the basis of available information in databases and reports from individual zone intersections. It turned out that much of the desired information in the general characterisation stage was unavailable. The primary source of information was the TMS database and SICADA.

4.3.6 Visualized parameters in RVS

Table 4-3. Visualized boreholes parameters imported from SICADA to RVS

Visualisation name	Parameter RVS source and mapping source	Method	Current LUT	Value	Meaning	colour	diameter
tecto_pc	rock	cylinder	Tecto	MTA	Mylonite	5	10
	pc_logging_new / rock (Petrocore data)			MT	Tectonites	3	10
				MTB	Tectonic breccia	6	10
				MTC	Tectonite	10	10
Tecto_bm	bm_rock	cylinder	Tecto	MTA	Mylonite	5	10
	Boremap / bm_rock (Boremap data)			MT	Tectonites	3	10
				MTB	Tectonic breccia	6	10
				MTC	Tectonite	10	10
pc_structure	structure	cylinder	pc_struc	104	Banded	0	0
	pc_logging_new /structure (Petrocore data)			105	Mylonitic	37	10
				106	Brecciated	6	10
				107	Layered	0	0
				108	Tectonized	10	10
bm_structure	Bm rock structure	cylinder	bm struc	Mylonitic		37	10
	Boremap / bm_rock_structure (Boremap data)			Schistose		28	10
				Brecciated		6	10
				Tectonized		10	10
				Oxidized		3	5
pc_alteration	alteration_type	cylinder	alt	700	Oxidized	3	5
	Petrocore / alteration_type (Petrocore data)			701	Chloritized	146	5
				702	Epidotized	82	5
				703	Weathered	40	5
				704	Tectonized	10	10
bm_alteration	Bm alteration_type	cylinder	bm_alt	Oxidized		3	5
	Boremap / bm_alteration_type (Boremap data)			Chloritized		146	5
				Epidotized		82	5
				Weathered		40	5
				Tectonized		10	10

Table 4-4. (continued) Visualized boreholes parameters imported from SICADA to RVS

Visualisation name	Parameter RVS source and mapping source	Method	Current LUT	Value	Meaning	colour	diameter
pe_crush	Pe_crush_variable Petrocore / pe_crush_variable (Petrocore data)	cylinder	crush	4	crush zone	15	12
RQD	rqd pc_logging_new / rqd (Petrocore data)	cylinder	RQD	0		1	10
				10		1	10
				20		103	8
				30		103	8
				40		120	6
				50		120	6
				60		120	4
				70		120	4
				80		120	2
				90		240	1
				100		240	1
				150		0	0

The parameters in Table 4-3 have been visualized with method, colour and size as stated in the table. There are also other visualisations in boreholes and tunnels included to the RVS model. To set up the full RVS-model, reference files included, please contact SKB/Äspö.

5 The Äspö02 site descriptive model

5.1 Base model

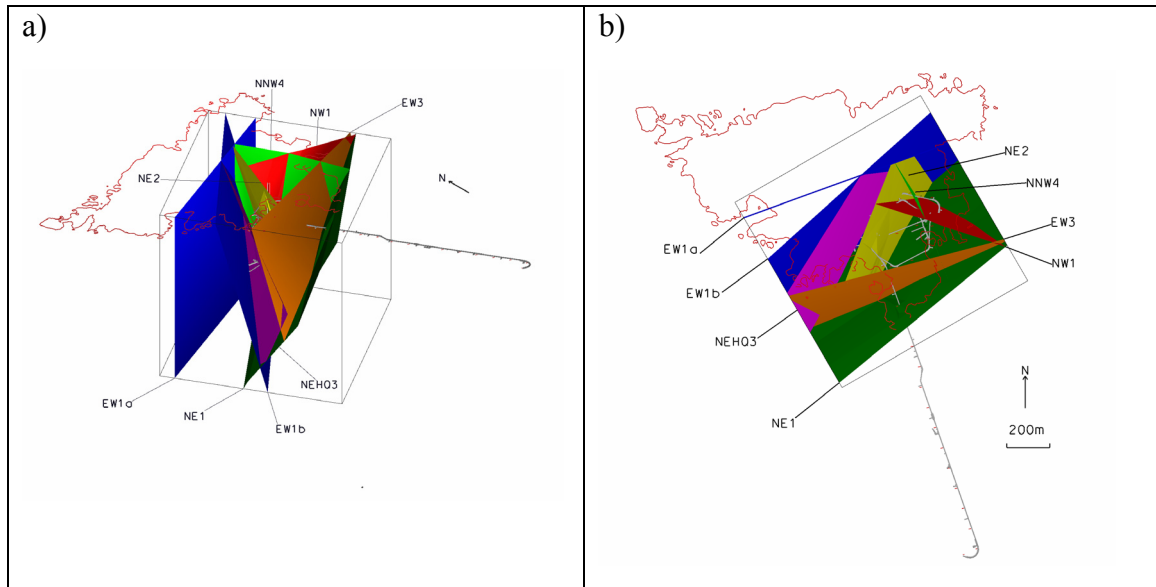


Figure 5-1. The base model, Äspö02_v1 in a) isometric view and b) top view.

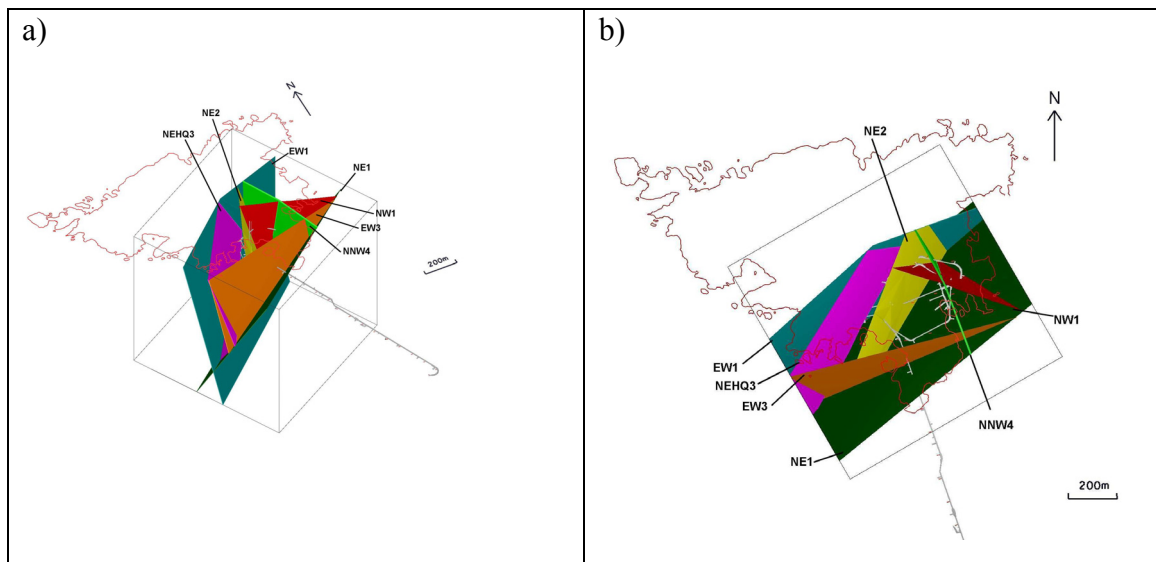


Figure 5-2. The base model, Äspö02_v2 in a) isometric view and b) top view.

The Base model of Äspö 02 is being presented in two versions; Äspö 02_v1 and Äspö 02_v2 (Figure 5-1 and Figure 5-2). The first version has been used as input for the modelling work in the three other geo-disciplines in GeoMod; Hydrogeology, Geochemistry and Rock mechanics. The major difference between the two versions is that v1 only has planar surfaces that represent the zones, whereas the surfaces in v2 are undulating. The undulation is created by RVS as a triangulated surface (see chapter 4.2.3 for details). Both models are present in RVS in the SKB model database SIMONE, from where the coordinates of geometries can be derived, for v1 and v2, respectively. One zone, NW2 (NW-3 in Äspö 96) was omitted in Äspö 02_v2 and NW1 was extended across NE1. Also slight adjustments have been made regarding intersections used in v2.

The geometry and geology of objects in the model are described in chapter 5.4 and 5.5 below. An atlas that gives a brief overview of each zone was part of the objectives of Geomod. Complete atlases remains to be put together for the zones, but the format and layout for zone NE2 is shown under the description of that zone in the following.

5.2 Sub-model

The sub-model has not been finalized and is therefore not presented in this report. The aim of the sub model is to characterise and visualise the zone in the central part of the laboratory in greater detail, where possible. The model volume is therefore smaller than for the Base model, concentrated around the tunnel spiral between 200 and 500 m depth below sea level. The aim with the model is also to present several alternative interpretations of zone geometries and to incorporate deformation zones that primarily show ductile deformation history in the model. These latter types of zones have not been visualized in the present or earlier models. The deformation history and developed structures at Äspö is strongly influenced by the activities along EW1 (Äspö shear zone). Minor ductile branches and other local ductile zones in the area may be of importance for the understanding of the geology at site, not only for the distribution of rock units, but especially for the distribution of structures, such as variations of intensity and orientation of the foliation and not least for the fracture arrays at Äspö.

5.3 Lithology

There is a lot of literature from the region in this subject that needs to be synthesised and presented along with a lithological model of the laboratory. The possibility to model the lithology at Äspö with high resolution and with a low level of uncertainty is at present judged as small, primarily depending on conflicting data and lack of high resolution lithological data. Thus, this report only gives a brief summary of the geology in the Simpevarp-Äspö region (chapter 3).

5.4 Zone description

The character of each zone is primarily derived from the tunnel intersections if such exists. The data from these intersections normally comes from the TMS-mapping and the connected TMS database if nothing else is stated. All the zones in the model except for EW1 cross the tunnel system at least once. In these tunnel sections as compared to cores from a borehole, there are unique opportunities to map and investigate the zones with respect to their geological character because the size of the intersection gives information regarding parameter variability. In the cores from boreholes the diameter from the zone never exceeds 76 mm and the orientation of the zone is only rarely documented in the mapping. The general character of a zone, both with respect to geometries and geology, measured as parameters therefore have higher level of certainty in a tunnel observation.

In the TMS, all deformation zones that were mapped are fracture zones, with the definition of having at least twice as high intensity of fractures as in the surrounding rock indications of shearing, faulting or clay alteration. Completely disintegrated and chemically altered rocks were included in the definition of a fracture zone. Primarily, ductile deformation zones are thus not included in the TMS database as zones. There is a remark column in the database that occasionally was used to document findings of ductile deformation, but not in a systematic way.

At ten locations the structural type code “mylonitized” (four mylonites) has been used, whereas “sheared” has not been used at all. The rock type “mylonite” appears at six localities. However, as a “fracture mineral” it appears rather frequent in the database. Mapping rock types as fracture minerals was used where the mylonite (or other rock type) occurred as a vein having a width of less than 10 cm.

The core mapping systems that have been used as a data source in this work, Petrocore and Boremap, have utilized different ways to document ductile deformation. Zones of brittle deformation is mapped as “crush zones” when it was impossible to restore the core along individual fracture planes. No fracture zones are mapped, but fracture frequency may help in this respect.

Two primary indications of ductile deformation are available in both Petrocore and Boremap. It is the rock type “mylonite” and structure type “mylonitic”, in the “rock type” and “rock occurrence” tables. In Boremap, however, has mylonite as a rock type only been used as a “rock occurrence”. The latter denotes sequences of rocks less than 1 m of core length. Its occurrence is restricted to five localities, all with less than 15 cm of core length. In a few localities in the Boremap system, the structure “brittle-ductile shear zone” has been assigned to a rock type (or “rock occurrence”), or as a structural feature. These localities are restricted to the True Block Scale and the Prototype project areas. In Petrocore “mylonite” has been used as a rock type rather frequent in the KAS boreholes (surface boreholes) and at a few localities in five other boreholes drilled from the tunnel. As structure it is also used frequently in Petrocores rock type table, primarily in the KAS boreholes but also in eight other boreholes.

Information regarding ductile deformation, except for what is mentioned in previous paragraph, comes from the Petrocore table “Structure”. Here all structures are presented with zero thickness and with Alpha/Beta angles only.

In Petrocore the SICADA parameter alteration give type of alteration as values between 700 and 706, of which 704 was “Tectonization”. The definition of this has not been found in documents, but it is probably related to brittle deformation.

In the geological description of the deformation zones in this chapter an effort has been made to find information regarding any ductile prehistory of the fracture zones.

The descriptions of both new zones in the model and partly or fully remodelled zones are included here, in order to give a complete description of the zones with references to the background data.

Most of the information regarding the geology of remodelled zones is derived from TR 97-06 and references therein. All locations for intersections have been taken from the SICADA and TMS database tables. For tunnel data the designfiles from the TMS have been used together with the underlying database. For boreholes visualisations of decisive parameters in RVS together with mapping data from Petrocore and Bormap have been used. For Bormap boreholes the BIPS-images has been checked for zones of ductile deformation. The geological character of each zone is derived from the database and from various reports as stated by references.

The level of uncertainty of given information and interpretations is labelled as “Certain”, “Probable” or “Possible”. The uncertainty of sampled values of parameters are estimated in the protocol for the intersections (appendix 2) and the uncertainty of that intersections actually belong to the zone in question is estimated in the point table for individual zones below. Finally the overall confidence of the modelled zone is discussed. This kind of uncertainty assessment is certainly not always straightforward. For modelled zones all intersections judged as certain or probable part of the zone in question has generally been used when the geometry was modelled in RVS.

Protocols from certain and probable intersections have been made up for the modelled zones and are included in appendix 2.

5.4.1 ZAS002A0 (NE1)

Introduction

There has been no new geological data published that can be positively associated with NE1 since the Äspö96 model. However, a possible location that may be related to the zone, or a splay to the zone, has been found in a section in the bottom of borehole KI0025F.

The NE1 is one of two zones of regional extent in the model domain. It can be regarded as a boundary to the laboratory in the south, in a similar manner as the EW3 can be considered as a boundary to the north. These two regional zones most probably have had an important role for the geometries of the fractures and deformation zones that formed in the block between them, e.g. in the Äspö HRL. This is concluded from the recognition of EW1 and NE1 as representing major zones of weakness (see chapter 3.4.2). Faulting along these zones forces the block between them to adjust in response to imposed stresses.

Geology

The geological character of the zone is primarily based on the character of the intersection in the tunnel. The reason is that it is only here the zone has been named NE1 and it is also here where fracture sets and width have been determined.

The description of NE1 in /Rhén et al., 1997/ gives the following information. The zone consists of three branches, which together are ca 60 m wide. It is, moreover, related to rock types described as Äspö diorite, fine-grained granite and greenstone. Two planar water-bearing branches were used to approximate the major part of the zone. The northern of these branches is the most intense part of the zone and is ca 28 m wide in the tunnel and was “highly water-bearing”. In this northern branch a ca 1 m wide central zone was found to be completely clay altered /c.f. SKB, 1992/. Outside the central zone a ca 5-8 m wide, partly clay-altered zone was found, including ca 1 cm wide fractures and cavities. Towards the boundaries of the 28 m branch the fracture frequency varies, with a distinct boundary to the surrounding rock. The observed fracture geometries in NE1 were found to be similar in the zone as the average geometries of the Äspö HRL, even though safety consideration during the construction did not permit a detail investigation. Only the northernmost branch of NE1 has been modelled in Äspö02.

Except for the general description of the zone in e.g. /Rhén et al., 1997/ above, there is also a mineralogical and chemical study of the zone made on three separate samples, a mylonite and two fault gouges /Stanfors et al., 1993/. The mylonite is quartzo-feldspatic with accessories of chlorite and corroded magnetite. The precursor to this rock could be either a fine-grained granite or a coarser granitoid. The mylonite is penetrated by fractures sealed with quartz and iron hydroxides, with some fluorite and pyrite. The gouge samples consist of angular fragments of tectonized rock, which are oxidized to a various degree. The fragments have first been deformed under ductile conditions, then oxidized and finally deformed under brittle condition that produced the fragmentation. Late overgrowth of calcite indicates that the zone has been reactivated also in a brittle state. Smaller fractions contain large portions of clay minerals, but lithic fragments only show weak signs of clay alteration. The clay mineralogy is dominated by mixed layer illite/smectite.

In the TMS database and from the design drawings the following can be concluded: The mylonitic, 1-2 m wide zone mapped as Z7, lies in the centre of a fine-grained granite, in the central part of NE1 and is strongly to completely clay altered. This is probably where the sample, described in previous paragraph, comes from. It has the same orientation as the major zone, mapped as Z6. NE1 is strongly water bearing and there are also fractures around the zone with various orientation, which are water bearing. About 10 m south of the zone there is also a fractured and water bearing fine-grained granite mapped as zone Z5, with the same strike as NE1.

The porosity in the tunnel intersection has been estimated to 0.3-1% /SKB, 1992/, an estimate with a high degree of uncertainty, because of the problems of investigating the rock mass unaffected by drilling, blasting and reinforcement.

The fracture orientation found in NE1 in the tunnel intersection in the TMS database, which is the only available information regarding the orientation of fractures in the zone, has been plotted in a stereogram (Figure 5-3).

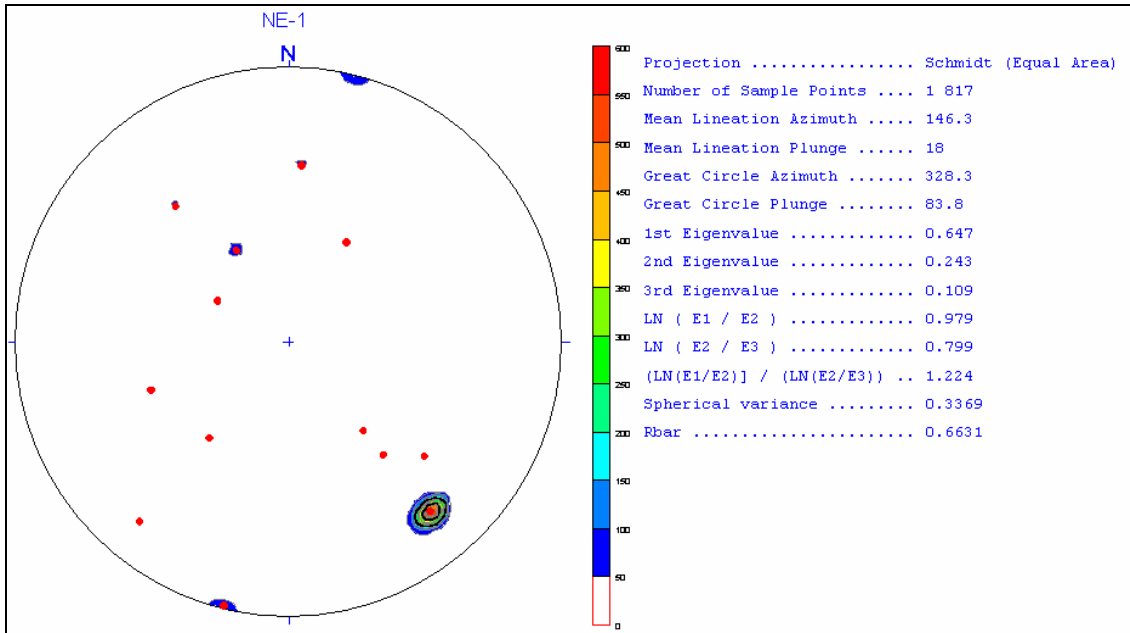


Figure 5-3. Orientation of fractures in NE1, tunnel intersection. Red dots represent measured orientations. Zone orientation in the tunnel coincides with the highest density area (230/70).

Model

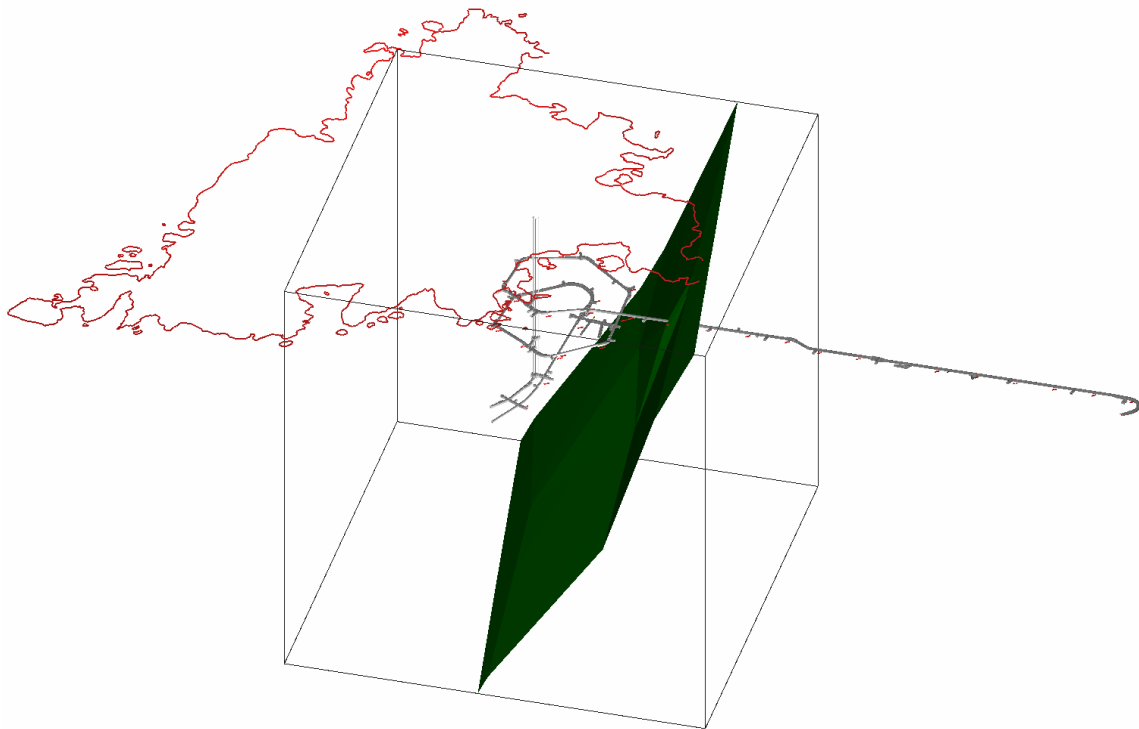


Figure 5-4. Isometric views of NE1. Tunnel symmetry is shown together with the model domain boundary.

The zone has been fully or partly penetrated by nine cored boreholes (Table 5-1). The configuration of these boreholes in relation to the zone can be understood from Figure 5-4. In Äspö 02 v1 the model plane representing NE1 three separate geometries for NE1 was considered as a first approximation:

- Alternative 1: A simple solution, using the average strike and dip of the zone boundary as it was mapped in the tunnel and extrapolating it through the model domain.
- Alternative 2: Also a simple solution, using the strike and dip value from the TMS database (230/70) and extrapolating it through the model domain.
- Alternative 3: Modelled as an average plane constructed in RVS with a central point in 7 most probable intersections.

The orientation of NE1 is 230-240°/70-75° according to the Äspö96 model. In alternative 1 and 3 above, the strike was 290° to 310°. The dip was to the north and they passed through many boreholes in the lower part of the laboratory where it has not been recognized. Alternative two above fits the probable intersections reasonably well but cross over the southern part of Äspö Island. For this reason the dip of alternative 2 was changed until the zone did not affect Äspö Island. The tunnel intersection was used as the point of rotation. In the adjusted alternative 2 the NE2 has the orientation 230/63 and is fairly close to the probable intersections. It is also close to a deformation zone found in the lower part of borehole KI0025F, but do not intersect this hole.

In Äspö02_v2 the NE1 has been partly remodelled. As for all zones in v2, NE1 is modelled to let the model zone pass through all certain and selected probable intersections (Table 5-1).

Three boreholes (KA1060, KA1131B and KBH02) do not fully penetrate the zone and the zone may therefore continue ahead of the bottom of these boreholes.

It is only the closest boreholes and KAS16 that are considered as probable intersections at the sections given (Table 5-1). Most of the boreholes with intersections that are judged as possible do, in fact, intersect the zone, but the difficulty is to state the exact sections with an acceptable high level of certainty. The reason for this is partly that the geological characterisation of the cores, as it can be understood from Petrocore data, does not discriminate between separate sections of possible intersections and the orientation and geometry of the zone is not certain enough from the observations in certain and probable intersections to disqualify one possible intersection from another.

The only new (but not used) intersection since the previous model (Äspö96), is found in KI0023F and is judged as possible. The borehole is part of the drilling program of True Block Scale and the project group considered the section of bad rock to be a minor branch of either NE1 or EW3. The structure was the single largest structure found in True Block Scale project /Hermansson and Doe, 2000/.

The complex geometry of NE1 as it appears from current knowledge does not permit modelling of the zone across the model domain without a high level of uncertainty. This is in spite of the size of the zone as well as its regional extent at the surface, as indicated in previous models and by its geophysical expression, suggesting that the zone most probably does penetrate the full model domain. Instead it was decided in the Geomod project group that a confidence volume, outside of which the zone is unlikely to appear, should be modelled, in order to try to visualise its northern boundaries. In order to do that a central point in the zone at each intersecting borehole (and tunnel) was identified. Only boreholes where the zone was judged to be with a level of uncertainty estimated as at least possible, was used. The created undulating surface has an orientation of 231° /64.5°

From these points an undulating surface was created in RVS, which was moved to the northern boundary of the zone to incorporate all part of the intersection in the boreholes (and tunnel). Finally a planar surface was applied on top of the undulating surface, representing a confidence boundary, north of which the zone probably does not exist.

The geometry of the southern boundary on the other hand is more difficult to model, due to the existence of sub-parallel branches and probable splays, or parallel zones as described in /Rhén et al., 1997/.

Confidence

The geological characteristics of the zone are not distinct and well known enough to discriminate between possible intersections in many boreholes. This in turn leads to a higher uncertainty for the geometry of the zone away from the tunnel.

KAS08 and KAS09 are the two boreholes that cross the NE1 zone closest to the top of the model boundary. The location, orientation and other characteristics of the zone at such locations predict how the zone should be extrapolated beyond these points. Other input in this matter is the observations and interpretations from regional studies in the form of borehole and geophysical investigations and other three dimensional models (Ävrö, Laxemar and Simpevarp_ver0).

The regional strike of the NE1 can be estimated from remote sensing, regional geophysical investigations and regional geological mapping. Nearby RVS-models (Simpevarp version 0, Ävrö and Laxemar) can also contribute to decide the location and orientation of the zone. As NE1 do not outcrop at or near Äspö the geophysical information becomes especially important. On the aeromagnetic map (Figure 3-6) NE1 appears as a ca 100 m wide low magnetic zone trending SW-NE from the SW towards the southern tip of Äspö. East of Äspö this signature is dispersed. There is also another magnetic lineament of similar magnitude that extends in an E-W direction immediately south of Äspö. This lineament corresponds to the strike of the alleged EW-5 zone, as indicated during the pre-investigations /Wikberg et al., 1991/.

Possible intersections in boreholes KAS07, KAS02 and KI0025F are situated far below the main part of the intersections in the point table (Table 5-1). Because they are regarded as only possible, it would lead to a higher level of uncertainty for the geometry of the zone, if these intersections were included in the geometrical modelling.

Table 5-1. Point table for deformation zone NE1.

	Type	Id	Precise location (borehole length, tunnel chainage or X;Y;Z)	Orientation	Source	Uncertainty (part of this zone)	Uncertainty (orientation)	Comment
1	Borehole	KA1061	198.32- 208.5	NA	Petrocore	P	NA	Does not penetrate the whole zone.
2	Borehole	KA1131B	172.97 - 203.1	NA	Petrocore	P	NA	Does not penetrate the whole zone.
3	Borehole	KAS07	497.14 - 602.11	NA	Petrocore	Po	NA	
4	Borehole	KAS08	536.84 - 601.49	NA	Petrocore	Po	NA	
5	Borehole	KAS09	50.02 – 11.68	NA	Petrocore	Po	NA	
6	Borehole	KAS11	155.71 - 219.98	NA	Petrocore	P	NA	
7	Borehole	KAS14	50.93- 90.67	NA	Petrocore	Po	NA	
8	Borehole	KBH02	666.94- 706.1.	NA	Petrocore	P	NA	Does not penetrate the whole zone.
9	Borehole	KAS02	806.07- 914.30.	NA	Petrocore	Po	NA	
10	Borehole	KI0025F	169.57- 200.	223/86 in mylonite	Boremap	Po	Po	Not used Does not penetrate the whole zone.
11	Borehole	KAS16	Ca 380- 430	NA	PR25-93-01	P	NA	Not found in SICADA
12	Tunnel	TASA129 0	1290 - 1325	230/70	TMS	C	P	

5.4.2 ZAS0003A0 (EW3)

Introduction

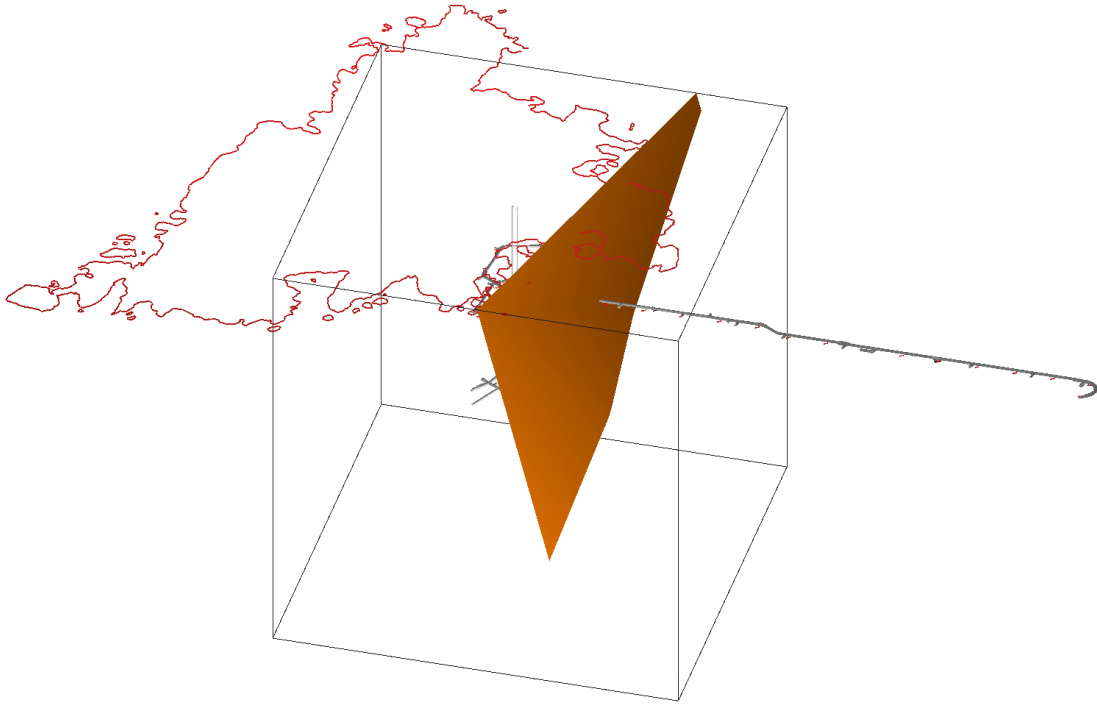


Figure 5-5. Isometric views of EW3. Tunnel symmetry is shown together with the model domain boundary.

No new data that concerns EW3 has been published since model Äspö 96.

The following information is found in /Rhén et al., 1997/. The tunnel and one borehole intersect the deformation zone EW3. In addition there is another possible intersection in borehole KAS07. This was not used, however, because the current interpretation with EW3 ending at NE1 is judged to be more probable. EW3 has also been mapped at the surface in an excavated trench.

Geology

The intersection in the tunnel is 12.1 m wide and has a central, 1.5-2 m wide central zone of clay alteration. In the rest of the zone the alteration is weak to medium and one of the five fracture sets have clay as fracture filling. The probable intersection in KAS06 show medium to strong tectonization with an average of ca 10 fractures/m as well as several sections of crushed core, where individual fracture were impossible to map. Clay was not mapped in the core, but may of course have been washed out during drilling. About 1 m core is mapped as mylonite or mylonitic. The intersection in the trench is a ca 1.5 m wide mylonite. Except for location and orientation of the mylonitic, there is no more information available.

In the tunnel the zone was strongly water bearing with seepage of ca 90 litres per minute. There are also many fractures close to the zone that are sub-parallel with it and are mapped as water bearing. It is evident from the stereograms from the bounding rock block to the south, that the primary water bearing fracture sets in the zone and in the block south of the zone are sub-parallel to the zone itself.

The observation protocols in appendix 2 gives further information on the character of the zone as it is documented in both the TMS database and SICADA.

The fracture orientation found in EW3 in the tunnel intersection in the TMS database, which is the only available information regarding the orientation of fractures in the zone, has been plotted in a stereogram (Figure 5-6).

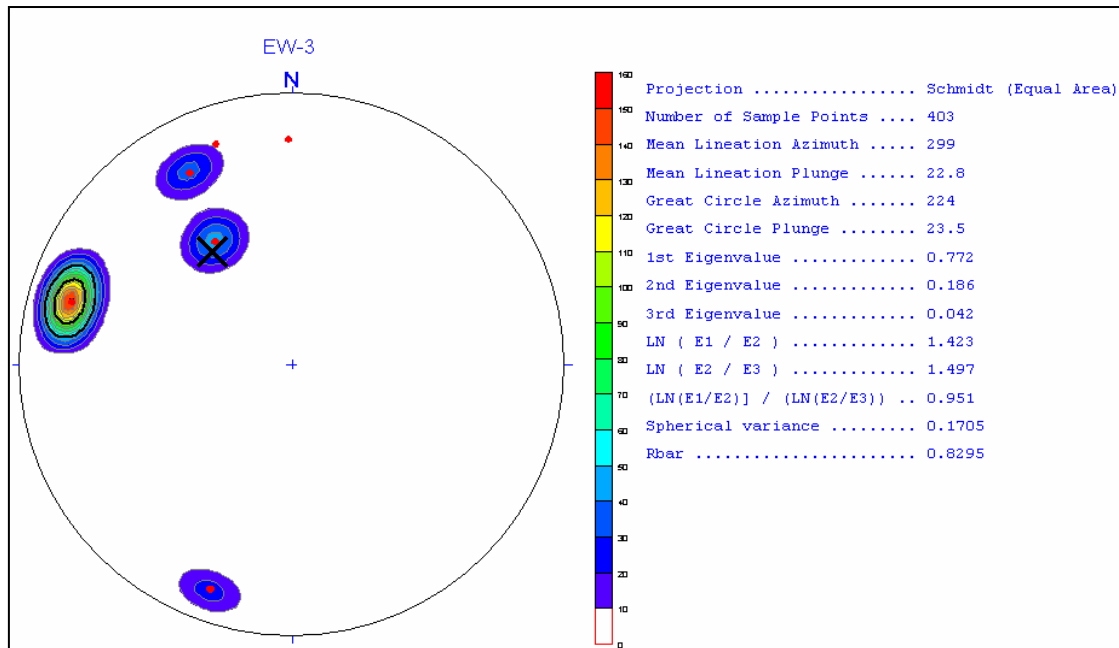


Figure 5-6. Orientation of fracture in EW3, tunnel intersection. Red dots represent measured orientations. Zone orientation is indicated by black cross.

Model

The modelling of EW3 was made quit simple, with only three intersecting points used. There is also a topographical lineament and a magnetic lineament that are aligned with the zone at the surface. These lineaments were the primary input data when modelling the zone during the pre-investigations. The orientation of lineaments of this kind and in the scale considered here (a few hundredm to one kilom) is not straight linear, but curvilinear and the exact position in relation to an underlying deformation zone is a matter of subjective decisions when not verified. For this reason no point from the lineaments where used in the modelling. Borehole KAS06 and KAS07 gave further input for the pre-investigation model. No point in KAS07 has, however been used for the modelling of EW3 in Äspö02. The reason for this is the judgement that possible intersection in KAS07 is uncertain with respect both to location and even to its existence. Instead the EW3 is modelled to end at NE1. The size of NE1 is much larger than EW3 and it is judged probable that faulting along NE1 have at least offset EW3. However, an alternative and possible model for EW3 would be that it continued below NE1 and thus to include the tectonized section in the lower part of KAS07 as an intersecting point for EW3 in the modelling. Such a model would only slightly change the orientation of the model zone and this was one of the alternative orientations tested before the final basemodel was created. The four alternatives were:

- Alternative 1: Using a central point in the zone with an average orientation from the two planes in TMS bounding the zone in the tunnel.
- Alternative 2: Using a central point in the zone and orientation 89°/73°, which are the values given for the zone in the TMS database.
- Alternative 3: Using a central point in the zone and orientation 71°/76°, which are the values given for the central clay-zone (Z0) in the TMS database.
- Alternative 4: Using a central point in the zone together with points from tectonized sections in KAS06, KAS07 and the mylonite in the surface trench at southern Äspö.

It turned out that an extrapolation of the orientation of the central clay-altered zone fitted exactly with the observed mylonite in the surface trench, which also has a similar orientation (70°/90°). It is also close to the centre of the tectonized section in KAS06. This was, thus, considered to be a probable location and orientation of the EW3, bearing in mind that these three locations is only about 250 m apart.

Confidence

The two certain observations of EW3 and the closeness between these points give a high confidence of the zone position and orientation in this area. The existence of the intersection considered as probable in borehole KAS06, in close proximity to where it was expected, further increase the confidence. The correlation between the zone and the topographic and magnetic lineaments give high confidence to the modelling of the zone laterally across the model domain. Also the length of the lineaments, together with the known depth (to the tunnel), gives high confidence in that the zone being modelled at least down to NE1. Whether there also should be an intersection in borehole KAS07 is less certain, but on the other hand should the confidence that the zone actually end at NE1 be considered as low.

Table 5-2. Point table for deformation zone EW3.

	Type	Id	Precise location (borehole length, tunnel chainage or X:Y:Z)	Orientation	Source	Uncertainty (part of this zone)	Uncertainty (orientation)	Comment
1	Borehole	KAS06	66.15	NA	Petrocore	P	P	
2	Borehole	KAS07	No point	NA	Petrocore	Po	NA	EW3 is not modelled below the NE1
3	Tunnel	TASA140 7	588.66	71/76 (Z0)	TMS	C	P	The orientation is measured in the central clay zone.
4	Surface	Trench	X:6367638. 1 Y:1551412. 4 Z:2.5	70/90	Geologi-cal map	C	P	

5.4.3 ZAS0004A0 (NE2)

Introduction

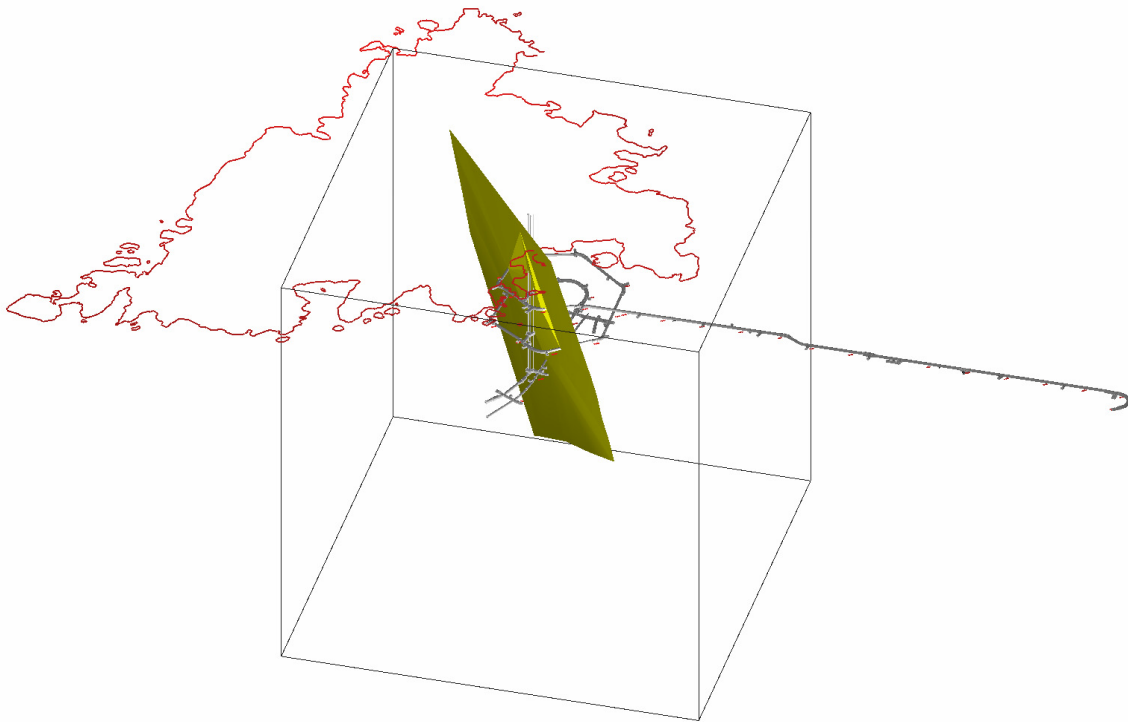


Figure 5-7. Isometric views of NE2. Tunnel symmetry is shown together with the model domain boundary.

The NE2 is modelled to cross the tunnel system in the laboratory at 6 localities, including the elevator shaft.

Geology

There are several intersections of zones in the tunnel system that show the same orientation as NE2, but these are located too far offside from certain intersections to be considered as possible intersections of the zone. However, the zone does undulate or splay significantly. It has not been possible to distinguish between undulations or splay geometry. The undulating character shown in the model is chosen because it is the simplest solution.

The width of the zone varies between ca 0.5 and 7m. If the interpreted intersections are correct the zone becomes narrower towards depth and north. The intersection in the tunnel at chainage 3337 is a ca 1 dm wide mylonite mapped as fracture and in tunnel section 2861 it is a narrow ductile zone, used as a possible (but most probable of the alternatives) location.

Four certain tunnel intersections and a certain surface location yielded data to characterise NE2. The surface location is located in one of the trenches that was excavated across Äspö and the tunnel intersections are all from the upper spiral and upper part of the elevator shaft. The NE2 a ductile deformation zone that has been brittle reactivated. It is often adjoined with dykes of fine-grained granite that normally is affected by the zone deformation. Clay is common as fracture filling in the upper intersections, but is not documented at lower levels.

The zone appears to be water bearing to a various degree. The intersection at chainage 1844 is especially water bearing and a seepage of 18 litres per minute has been registered here. Of the other intersections it is only in the elevator shaft at ca -150 masl that seepage other than drip has been recorded.

The observation protocols in appendix 2 give further information regarding the character of the zone as it is documented in the TMS database and SICADA.

The fracture orientation from the TMS database in the tunnel intersections, the only available information regarding the orientation of fractures in the zone, has been plotted in a stereogram (Figure 5-8).

The zone appears to vanish towards depth. The four intersections in the lower parts of the tunnel system are all judged as possible and the tunnel intersections here are very narrow (less than 0.5 m). There are no good alternative intersections here, but one alternative solution for the zone geometry would be that it ended already at a higher level.

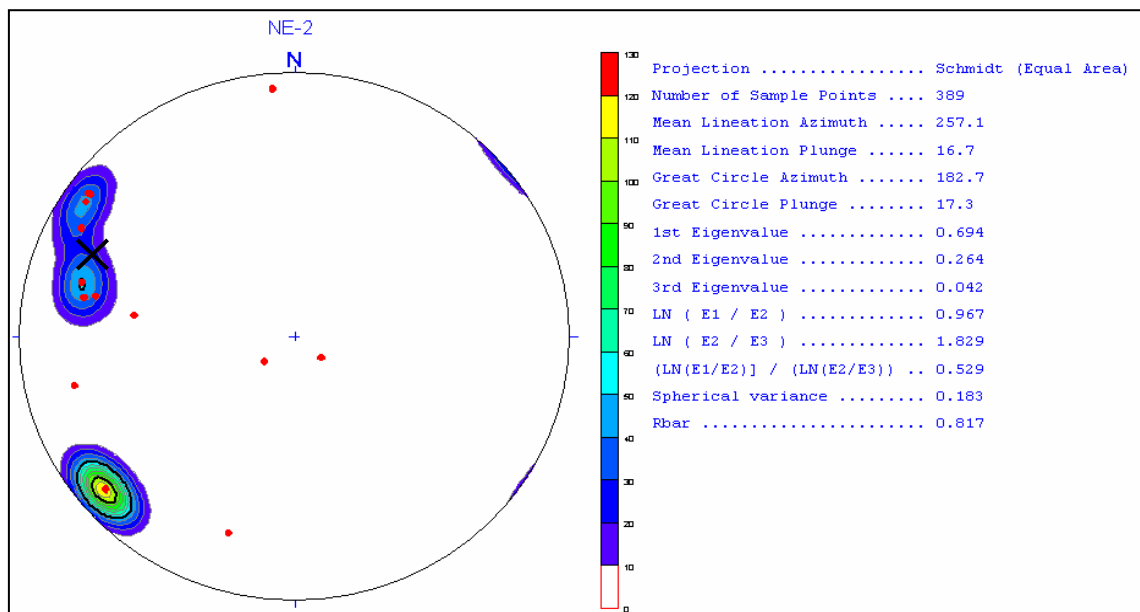


Figure 5-8. Orientation of fractures in NE2 in four certain tunnel intersections. Red dots represent measured orientations. Zone orientation is indicated by cross.

Model

The model zone for NE2 has the orientation 21°/77.5°, based on the intersection presented in Table 5-3. The orientation is the same for the undulating zone in Äspö02_v2.

KA2162: there is a long tectonized section where NE2 probably passes. The zone is, however, much less wide, and the exact location in the borehole cannot be deduced on the basis of available parameters in RVS. For this reason no point has been assigned here.

KA3191: The borehole is subparallel to the TBM tunnel. In the tunnel a thin epidote rich mylonite has been correlated with NE2, but in the borehole no mylonite has been mapped. There are a few fractures with epidote in the vicinity of the probable location of NE2, but no section has been specifically assigned to the zone in this borehole.

KA3385: the zone was identified as a foliated and tectonically affected granodiorite and fine-grained granite in the BIPS-image of the borehole wall. Both brittle and ductile deformation was recognized. The fine grained granite is strongly tectonized (brittle) and therefore the rock type is partly difficult to decide.

KAS05: the chosen intersection location is a tectonized section, in both granodiorite volcanite, pegmatite and fine-grained granite. The upper part of the section is altered (epidotized). An alternative intersection for NE2 in this borehole is further up, at 315-333 m length in the borehole, where a longer tectonized section occurs, including a mylonitic part. The choice of the lower intersection was based on the closer appearance of this section in relation to the average plane, and the associated fine-grained granite.

KAS13: A ca 16 m long section of altered (oxidized and tectonized) and crushed rock. It is hosted in granite. The lowermost part includes an 8 cm wide mylonite.

KAS02: there are a few thin crush zones in the vicinity of the supposed location of NE2, but otherwise no indications of deformation or alteration of the kind that characterise NE2. None of the crush zones have been assigned to NE2 since there are no evidences or indications of which of them that may be related to the zone. Fine-grained granite is normally related to NE2 and there is a section of such rock, with adjacent crush zones at the supposed location.

KC0045: This borehole seems to have been drilled sub-parallel with a dike of fine-grained granite. There are a few thin crush zones in the vicinity of the supposed location of NE2, but otherwise no indications of deformation or alteration of the kind characterising NE2 at nearest observation locations. None of the existing crush zones has been assigned to NE2, since there are no evidences or indications of which of them that may be related to the zone.

The tunnel intersections in the A-tunnel at TASA1602, TASA1844, TASA2476 and TASH150 are considered as certain. They were all assigned as part of the NE2 during the mapping of the tunnel. Intersections at lower levels must be considered to have a higher uncertainty that they actually belong to this zone simply for this reason.

Confidence

The character of the NE2 deformations zone as a local minor zone (possibly local major) with an undulating course, make the uncertainty of the location in particularly the boreholes high. In the upper part of the laboratory the confidence of the geometry and character of the zone is fairly high, because of the recognition of the zone as NE2 during mapping at five separate locations /see above and Rhén et al., 1997/.

Away from this area the confidence decreases. However, the alignment of a magnetic-low anomaly with the zone at the surface (Figure 3-6 and Figure 3-7) indicate that the length of the zone is at least as long as modelled (it seems possible that it may continue through EW3), but also that it may be a part of the shear zone system related to the EW1. If the latter is correct, the size of NE2 should extend across the model volume.

There are several indications of zones with similar orientation and size in the tunnel, especially in the lower parts of the tunnel system. Both NEHQ3 and two zone locations that not have been modelled at ca TASA3230 and TASA3600 are sub-parallel and have a primarily ductile character. The latter two indications were not modelled because it was not possible to extrapolate them to other intersecting tunnelsections or boreholes with an acceptable level of confidence. With these indications in mind, the confidence of the modelled location of NE2 at depth becomes lower, because they indicate that the zones in this direction actually do splay and interact.

Table 5-3. Point table for deformation zone NE2.

	Type	Id	Precise location (borehole length, tunnel chainage or X;Y;Z)	Orientation	Source	Uncertainty (part of this zone)	Uncertainty (orientation)	Comment
1	Borehole	KA2162B	No point	NA	Petrocore	P	NA	
2	Borehole	KA3191F	No point	NA	Petrocore	Po	NA	
3	Borehole	KA3385	24.7	NE-SW	BIPS	Po	C	Orientation based on geometric estimate
4	Borehole	KAS02	No point	NA	Petrocore	P	NA	
5	Borehole	KAS05	401.4	NA	Petrocore	Po	NA	
6	Borehole	KAS13	208.49	NA	Petrocore	Po	NA	
7	Borehole	KC0045F	No point	NA	Petrocore	P	NA	
8	Tunnel	TASA1602	1602	36/82	TMS	C	P	
9	Tunnel	TASA1844	1846	15/70, 11/68	TMS	C	P	
10	Tunnel	TAS2476	2480	32/65	TMS	C	P	
11	Tunnel	TASA2862	2861	8/50	TMS	Po	P	
12	Tunnel	TASA3336	3337	31/85	TMS	Po	P	
13	Shaft	TASH150	160	20/75	TMS	C	U	Elevator shaft TN 25-93-07i, strike/dip from TMS
14	Surface	Trench	X:6367778.8 Y:1551295.2 Z:6.2	35/80		C	NA	TN 25-93-07i

5.4.4 ZAS0007A0 (NW1)

Introduction

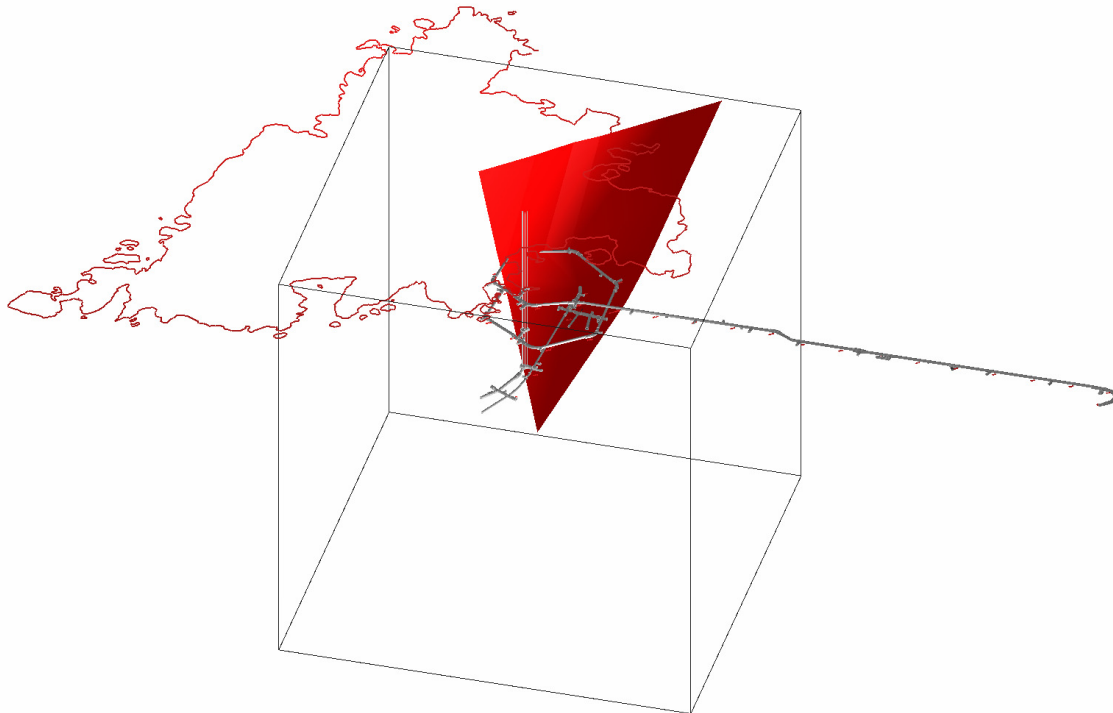


Figure 5-9. Isometric views of NW1. Tunnel symmetry is shown together with the model domain boundary.

There are six intersections that have been interpreted as possible parts of the deformation zone NW1. Four of these are probable or certain. The intersections in the tunnel were investigated during the tunnel mapping and are included in the Fracture Zone Catalogue /appendix 2 in Munier, 1995/, but no interconnecting zone has been modelled previously.

The major argument for modelling a zone here is the close distance and the similar character of the two intersections in the tunnel (number 4 and 5 in Table 5-4). The orientation is similar in the two intersections and when extrapolating their strikes and dips the fit is close to planar.

One probable intersection has been found during a short field check in the tunnel in mars 2003. It was located in a niche at chainage 2050 in tunnel A. The section here is mapped as a zone of “increased fracturing” in TMS, which is defined as a section with a fracture frequency of more than 5 fractures/m /Annertz K, 1994/. Hidden in this zone of increased fracturing is a deformation zone, with geometrical and size characteristics that would fit nicely to the characteristics shown in the two intersections mentioned above. However, since the intersection is not included in the TMS database it has not been used in the characterisation of the zone or in the modelling. The area should be remapped in order to include the new information in the database.

NW1 have not been observed at the surface, direct or indirect.

Geology

The three tunnel intersections in Table -5-4 give most of the information to constrain the geology of the zone. The borehole intersection in KA2050 gives no information, except for the fracture frequency. The strike of the zone in the two uppermost intersections, at TASA1876 and TASA1979 are very similar, 109°-112° and 290° with dips between 84° and 90°. These two intersections also have similar geology, with fracture sets primarily parallel with the zone and both water bearing. At both locations injection grout where mapped in some fractures.

The width of the zone varies between ca 0.2 and 1.5 m.

A fracture set parallel with the zone contains mylonite as “fracture mineral” at intersection TASA1979 and the intersection at TASA3083 is mapped as ductile.

The intersection at TASA1979 was mapped in detailed by /Mazurek et al., 1996, figure 4-8/, and was regarded as a typical example of a complex fault changing character along its course from one “master” fault to several master faults with interconnecting splays. The conclusion was here that the fault is dextral and that there were only weak signs of ductile precursors.

The zone is mapped as water bearing in all tunnel intersections. At location TASA1876 a seepage of 102 litre/minute was recorded.

The fracture orientation found in NW1 in the tunnel intersection in the TMS database, which is the only available information regarding the orientation of fractures in the zone, has been plotted in a stereogram (Figure 5-10).

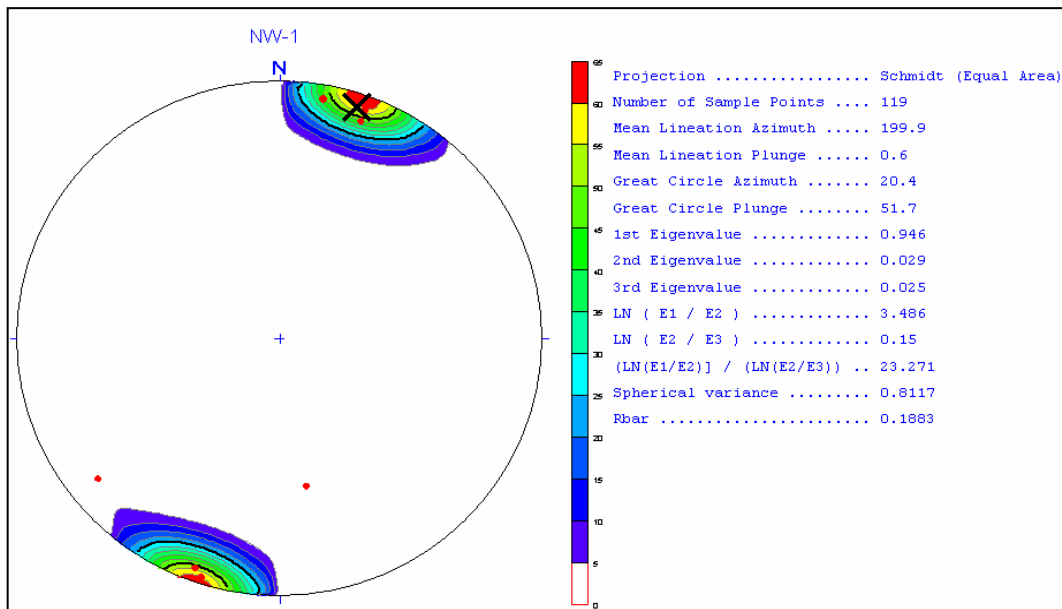


Figure 5-10. Orientation of fractures in NW1 tunnel intersections. Red dots represent measured orientations. Zone orientation is indicated by black cross.

The observation protocols in appendix 2 give further information on the character of the zone as it is documented in the TMS database and SICADA.

Model

The orientation of the NW1 in Äspö02_v2 is 288°/83.5° as compared to 104°/89° in version 1.

In Äspö 02_v1 the zone was modelled between NE2 and NNW4 using a best-fit plane between three points, 3 to 5 in Table 5-4. In Base model version 2 the zone is ended in the west towards NE2, but continues to the model domain boundary in the east and thus crosses NNW4. The interpretation that NW1 ends towards NE2 is based on the fact that no indication of the zone has been identified beyond that zone. The change from Base model version 1 and version 2 in the east was caused by new findings of possible continuation of the zone beyond NNW4 and by considerations regarding the orientation of NNW4. The most probable of these indications is unfortunately not fully documented in the TMS database. It is a section of bad rock (mapped as fracture zone code 2 = zone of increased fracturing) in the niche at chainage 2050 in tunnel A, where a strongly foliated and fractured section during a field check in Mars 2003 was found to align well with the orientation of intersections 4 and 5 in Table 5-4. Since the intersection does not exist in any database, it has not been used to model the zone. It is suggested that the database is updated with additional mapping in this niche and that the model then is updated.

The other intersection east of NNW4 is at chainage 3083 in tunnel A. It is estimated as possible, but show similar characteristics as the intersections above. The fracture sets are parallel to the zone and the zone is water bearing. The orientation is only slightly different from what could be expected from extrapolation of the certain intersections. The distance and the slightly different geometry make it possible, rather than probable.

The two possible intersections in boreholes KA3105 (oxidized crush zone) and KAS06 (tectonized section and high low RQD) do not really fit the geometry for the two certain intersections. No orientation of a possible zone is available in these borehole sections either. They are therefore not used in the modelling.

The borehole KA2050 has an interval with crush zone and low RQD between 6.3 and 8.2 m length. The intersection is very close to the observed zone intersection in the niche at chainage 2050 in the A-tunnel and is therefore judged as probable.

Confidence

The degree of confidence for the existence of NW1 between NE2 and NNW1 should be regarded as high. Once the niche at chainage 2050 has been mapped, the confidence that the zone continues towards EW3 will be high. The geological character of the zone as a narrow, dextral fault with some evidence of a ductile precursor is also high.

Table 5-4. Point table for deformation zone NW1.

	Type	Id	Precise location (borehole length, tunnel chainage or X;Y;Z)	Orientation	Source	Uncertainty (part of this zone)	Uncertainty (orientation)	Comment
1	Borehole	KA2050	7 m.	NA	Petrocore	P	NA	
2	Borehole	KA3105	No point	NA	Petrocore, BIPS	Po	NA	
3	Borehole	KAS06	No point	NA	Petrocore	Po	NA	
4	Tunnel	TASA1876	1876 (Z8)	110/80 and 110/84	TMS	C	P	
5	Tunnel	TASA1979	1979 (Z9)	288/88, 290/85, 109/88	TMS	C	P	
6	Tunnel	TASA3083	3083 (Z1)	302/75	TMS	Po	P	

5.4.5 ZAS0005A0 (NNW4)

Introduction

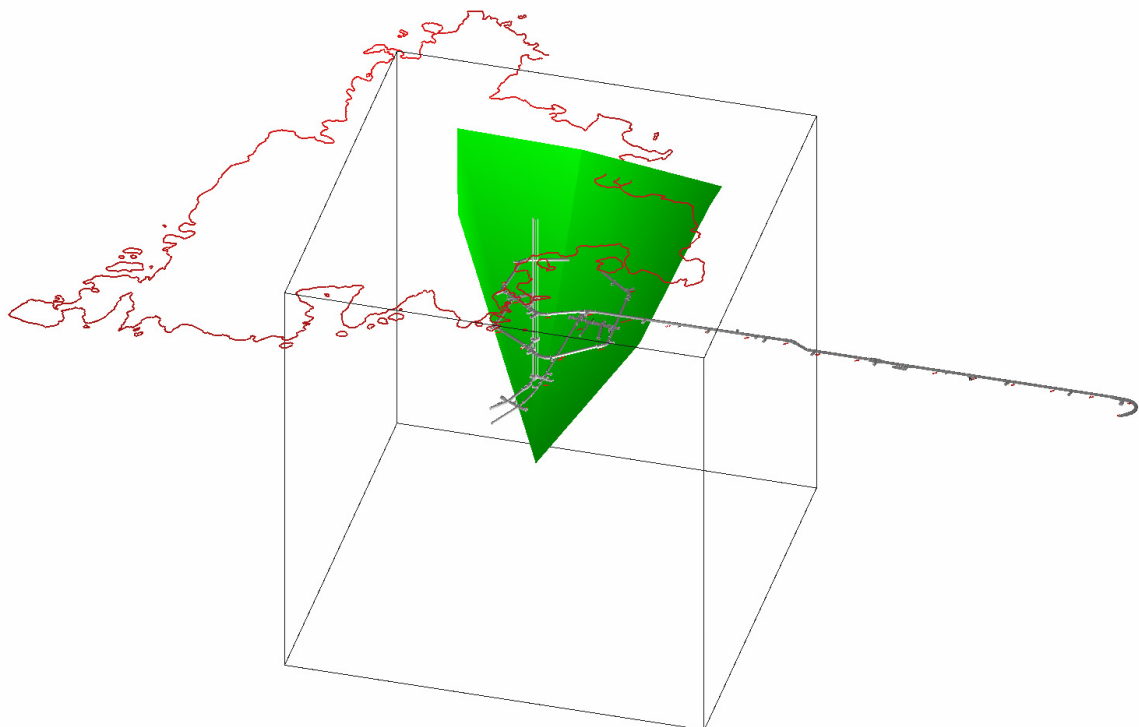


Figure 5-11. *Isometric views of NNW4. Tunnel symmetry is shown together with the model domain boundary.*

The NNW4 is one of several steep structures that, on a geohydraulic basis, was suggested in Äspö96 to be interconnected across the Äspö tunnel system with this orientation. The others (NNW1, NNW2 and NNW7) have not been possible to model, but see also chapter 5.6.1.

Geology

There are three tunnel intersections that were mapped as NNW4 in TMS. Two of these are south of NW1 in the upper spiral and one is north of NW1 in the lower spiral. Large values of seepage have been measured along this zone and especially in the south where water bearing fractures also surrounds the zone. Many of these are at high angle to the zone. Although the intersection at TASA2914 is strongly water bearing, the internal fracture sets is not mapped as such. Several point flows exist in the zone intersection. All three tunnel-intersections have been grouted.

The width of the zone varies between ca 0.5 and 8 m. The alteration is weak to medium. In the two southern tunnel intersections clay has been detected as fracture filling.

No remark regarding ductile deformation history has been found in the database, but abrupt ending of lithologies along the zone at intersection TASA2020 suggest significant faulting. At chainage 3130-3165 an expected intersection of NNW4 is located. Here no zone of this character has been found, but several water bearing fractures runs across the tunnel in approximately the same orientation as the zone. This seems to imply that the zone end or splay towards depth into several sub-parallel fractures. At least one of these fractures has mylonite as “fracture mineral” /c.f. Mazurek et al., 1996, figure 4-6/.

The probable borehole intersection in KA2048B at 27.91-45.69 m length has high fracture frequency (ca 8 fracture per m) and 5 intervals of crushed core (ca 1 m in total).

The observation protocols in appendix 2 gives further information on the character of the zone as it is documented in the TMS database and SICADA.

The fracture orientation in NWW4 from the tunnel intersections, as documented in the TMS database, which represents the available information regarding the orientation of fractures in the zone, has been plotted in a stereogram in Figure 5-12.

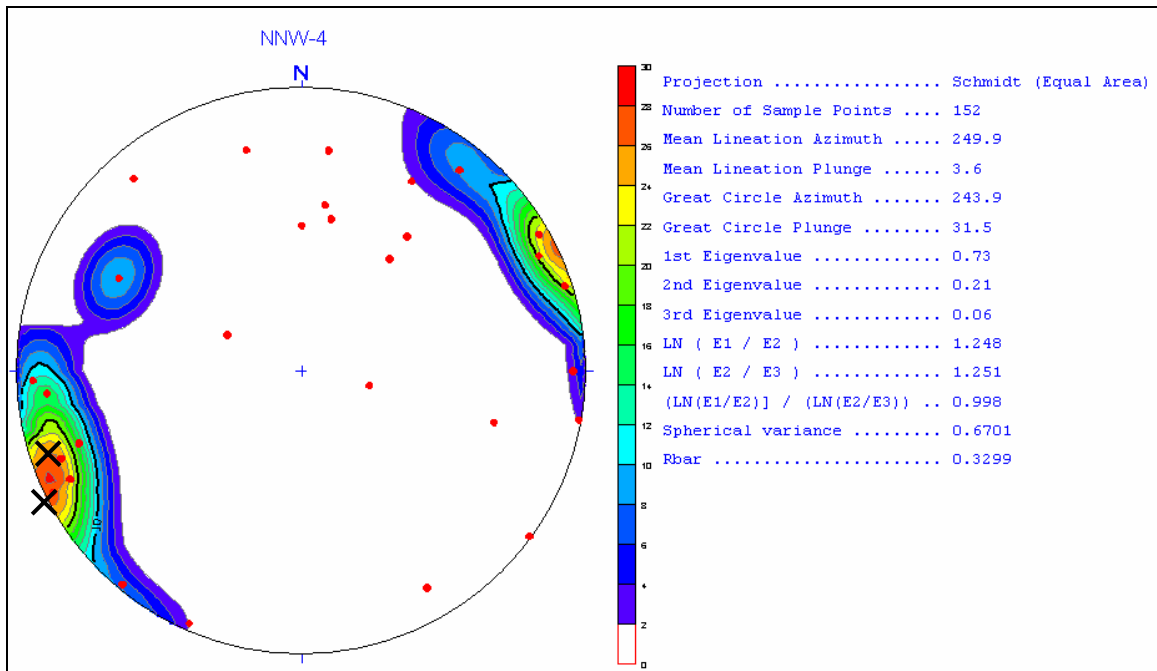


Figure 5-12. Orientation of fractures in NWW4 tunnel intersections. Red dots represent measured orientations. The zone orientations are indicated by crosses (the northernmost corresponding to the part north of NW1).

Model

The two intersections south of the zone are considered as certain and the northern one together with a borehole intersection at 35m length in KA2048B is considered as probable. The zone is modelled to end at NE1 and EW1.

In Äspö02_v1 these four intersections were used to model a best fit plane and the adjoining zone NW1 ended towards NNW4. The orientation and geometry of the two southern tunnel-intersections fit this plane fairly well, whereas the wide intersection at TASA2920 has a somewhat different orientation and is located approximately 25 m to the west of the plane.

In Äspö02_v2 NW1 continuous to the east of NNW4, which in turn is bent in the intersection with NW1 to better fit the geometry in the northern tunnel intersection. The southern part of NNW4 (“NNW4s”, south of NW1) is modelled with intersections 1, 3 and 4 (Table 5-5) locking the dip to 80°. This latter adjustment was necessary because the intersections are close to each other vertically and sensitive to small variations in location of chosen intersection point. In stead the most frequent measure of the dip from these intersections, 80°, was used.

The northern part of the zone was modelled by selecting two points in the intersection line between NNWs and NW1, one high up in the model domain and one in the lower part. These two points were then used together with intersection 5 to define the orientation of NNW4n.

Confidence

The NNW4 was the most obvious hydraulic conductor found in the tunnel spiral of Äspö laboratory. However, the surface expression is only defined by a rather vague electric signature /Nisca and Triumph, 1989/. The zone is not found at chainage TASA3130-3165, where it should appear, although it might be subdivided into discrete fractures here. The different orientation in the intersection to the north may indicate that the zone bends towards north or change direction in NW1 as modelled.

These data indicate that although the confidence of the zone locally is high, close to the two southern tunnel-intersections, it should be regarded as rather low away from this location. The zone ends or splays up towards depth.

Table 5-5. Point table for deformation zone NNW4

	Type	Id	Precise location (borehole length, tunnel chainage or X;Y;Z)	Orientation	Source	Uncertainty (part of this zone)	Uncertainty (orientation)	Comment
1	Borehole	KA2048B	35.	NA	Petrocore	P	NA	
2	Borehole	KC0045F	No point	NA	Petrocore	Po	NA	
3	Tunnel	TASA2020	Point at the centre of Z1.	335/80, 342/72, 154/83	TMS	C	P	
4	Tunnel	TASA2121	Point at the centre of Z3.	355/80, 345/80, 355/80, 350/88	TMS	C	P	
5	Tunnel	TASA2920	Point at the centre of Z9.	128/80	TMS	P	P	

5.4.6 ZAS008A0 (NW2)

The NW2 was modelled in Base model Äspö 02_v1 but was omitted in version 2. The reason for this was that the level of uncertainty became larger when one of the suspected intersection points (borehole KA2865A) in version 1 was examined closer in BIPS-images from the borehole. The orientation and location of the deformed section in question was located 3.3 m north of the modelled best fit plane and the orientation was almost at right angle to the modelled zone. When this point was omitted, there were only three possible and probable intersections left in the zone, of which two was only classified as possibly. The zone was for this reason omitted because of low confidence.

5.4.7 ZAS0006A0 (NEHQ3)

Introduction

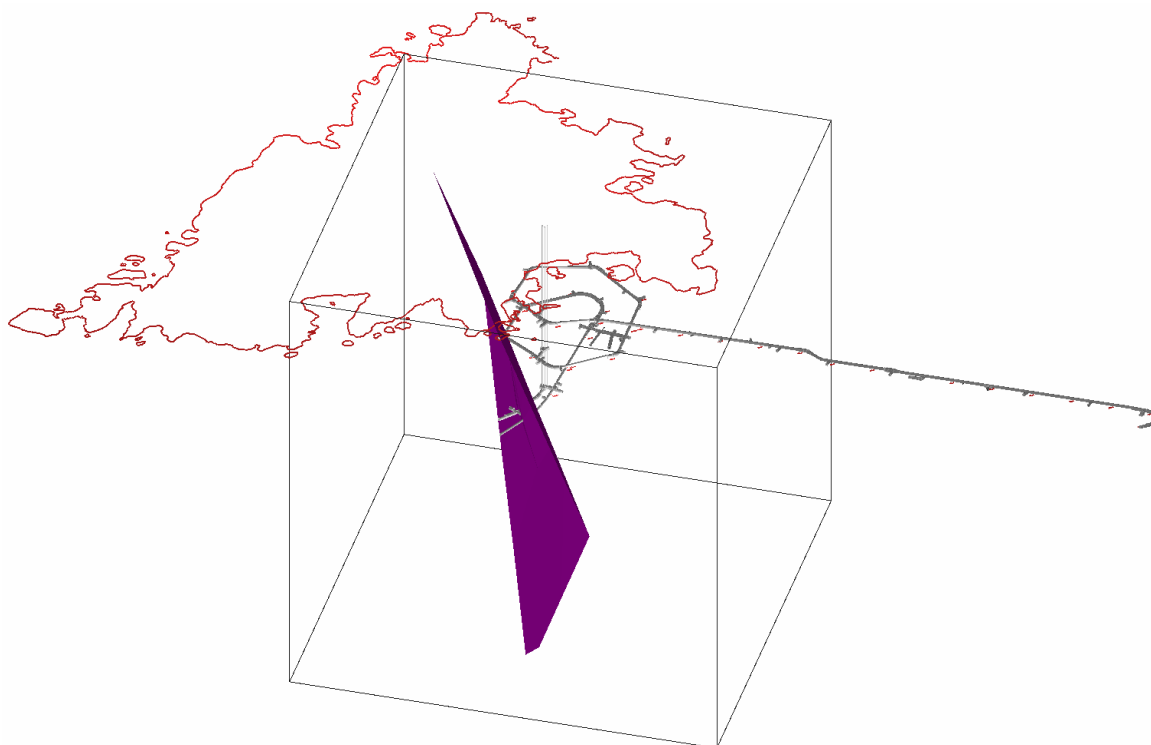


Figure 5-13. Isometric views of NEHQ3. Tunnel symmetry is shown together with the model domain boundary.

The NEHQ3 was not modelled in Äspö96. The zone crosses the NW part of the True Block Scale project area, representing structure 8 in that project.

Geology

The characteristic of the zone are primarily based on how it appears in the tunnel system (point 11-13 in Table 5-6). The three intersections in the tunnels A, F and N are close to each other and show fairly similar geometries and character. These are considered as certain intersections. The brittle deformation in the zone is not very obvious, but the ductile deformation history is clearly indicated by a ca 2 m wide mylonitic imprint with strong foliation sub-parallel to the zone boundary. In these tunnel intersections the zone is developed in a granodiorite. The closest intersections in boreholes are located in KA3510 and KA0044F, where a ca 2 m mylonitic section in a fine-grained granite and mylonitic granodiorite has been mapped, respectively. At both these locations a few open fractures appears, but their orientation is unknown. The alteration in the tunnel and probable borehole intersections is mapped as medium and in the borehole intersections the type of alteration is oxidization. The orientation of the zone in KA0044 has not been measured, but in KA3510 it is mapped as 232°/89° as compared to 216°/90° and 218°/88° in the tunnel. This seems to indicate a bend or undulation of the zone, although it partly may be related to data uncertainty.

The zone is mapped as dry in the tunnel, but there are a few water bearing fractures associated with the zone. All of these fractures end towards the zone or close to the zone boundary. No water bearing fractures crosscut the zone or is parallel to it according to the TMS mapping of the tunnel intersections.

The fracture orientations found in the TMS database for NEHQ3, which is the only available information regarding the orientation of fractures in the zone, has been plotted in a stereogram in Figure 5-14.

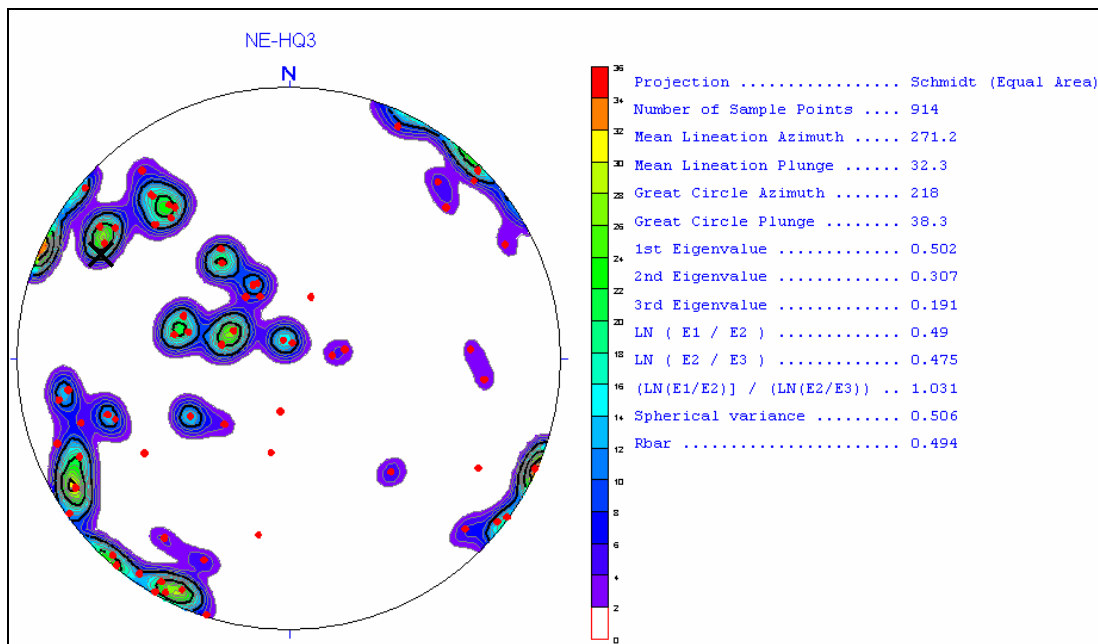


Figure 5-14. Orientation of fractures in NEHQ3 tunnel intersections. Red dots represent measured orientations. Zone orientation is indicated by black cross (bottom part of the zone).

The observation protocols in appendix 2 gives further information on the character of the zone as it is documented in the TMS database and SICADA.

Model

The concentration of three certain tunnel and two close probable intersections around the tunnel system at a depth of ca –450 masl give the basic input for the zone geometry. The orientation and characteristics of the zone here is extrapolated outside of the area to look for fitting geometries and geology elsewhere. To the south the zone is extrapolated through the borehole KA2563. Using the geometry at the tunnel intersections along the zone would appear in the lowermost parts of the core, but there is no good agreement with any structures found here. However, at ca 243 m depth in the borehole there is a ca 3 m wide mylonite with a mapped orientation of 35°/70°, i.e. similar strike, but dipping in the opposite direction. Because of the small diameter of a core, this may for example represent a local undulation. The location is east of where it was expected, but also the location in KA3510 indicated that the zone actually might bend in this direction. The intersection in KA2563 is judged as possible, but included in the modelling.

There are no further indications towards the south for NEHQ3, but the zone is modelled to end at NE1. To the north and beyond the tunnel intersections at this level (c. -450 masl) there is no more certain or probable intersection either. The zone is actually not very easy to extrapolate towards the north and upwards. A borehole of special interest to get an idea of whether the zone extends in this direction was KA2598. In this borehole (mapped in Petrocore) there is an altered section at the supposed location, but no mylonitic rock or any decrease in RQD.

In the tunnel section between ca TASA2660 to TASA2770 there is several fracture zones, both increased fracturing and strict fracture zones exist. The extrapolation of the geometries of NEHQ3 intersects the tunnel hereabout. Several of the fractures in this area contain mylonite as “fracture mineral” and zone “Z2” is mapped as ductile. The orientation of this zone is 32°/70°. This intersection is judged to be possible, and the location and orientation of Z2 is used to extrapolate the zone to the surface.

Although there is no surface observations made for NEHQ3 it aligns well with the lithology and magnetic pattern (Figure 3-1 and Figure 3-8).

In the boreholes KF0066 and KF0069 ductile shear zones, similar to the NEHQ3 in the tunnel sections at -450 m, have been recognized in BIPS images. These have been visualized as local parameters in RVS to see how they may relate to NEHQ3. Their location and approximate strike extrapolates towards the tunnel sections at -450 m. However, if these were included in the zone it would implicate that the zone bends rather dramatically to the east, which do not seem probable. Instead it is probable that this is a separate zone or a splay to the NEHQ3. There are also other boreholes further to the northeast exhibiting similar structures with similar orientation. Further work is necessary to incorporate these findings into the geological model.

Confidence

The confidence in the existence, geology and geometry of NEHQ3 close to the area where the certain and probable intersection is high. The size of the zone implicate that it should continue at least many tenth of m outside of this area. In the True Block Scale domain the zone (No. 8) has been modelled as NEHQ3, with approximately the same intersection points and only slightly different orientation to the A tunnel /Hermansson and Doe, 2000/. The interpretation in that report indicates that the zone may divide into several branches towards southwest. This in turn lower the confidence in that the zone continues towards NE1 as is modelled here.

Towards the north an upward the confidence in the zone geometry must be considered as low, since there are few intersections here. It is, moreover, not very likely that the zone has a sharp bend and then continues in another direction, though still possible. The magnetic low at the surface, do indicate that there are some zone of deformation or alteration. The current model was chosen as a possible, simple solution that fairly well fits the available data.

Table 5-6. Point table for deformation zone NEHQ3.

	Type	Id	Precise location (borehole length, tunnel chainage or X:Y:Z)	Orientation	Source	Uncertainty (part of this zone)	Uncertainty (orientation)	Comment
1	Borehole	KA2862	No point	Steep SW-NE	BIPS	Po	NA	Orienetation based on geometric estimate
2	Borehole	KA2858	No point	Steep SW-NE	BIPS	Po	NA	Orienetation based on geometric estimate
3	Borehole	KA3510	16 m	232/89	Petrocore BIPS	P	P	Orientation from Table 3-1 in IPR 00-34
4	Borehole	KA2563	243 m	35/70	Petrocore BIPS	Po	P	Orientation from BIP:s mapping
5	Borehole	KF0069	No point	47/85	BIPS	Po	Po	Orientation based on geometric estimate
6	Borehole	KF0066	No point	50/85	BIPS	Po	Po	Orientation based on geometric estimate
7	Borehole	KJ0044F	17.26 m	NA	Boremap	P	NA	
8	Tunnel	TASA2741	In the centre of zone Z2	32/70	TMS	Po	P	
9	Tunnel	TASA2826	No point	27/50	TMS	Po	Po	
10	Tunnel	TASA2690	No point	78/35	TMS	Po	P	
11	Tunnel	TASA3520	3520.	218/88	TMS	C	P	
12	Tunnel	TASF0010	7.5 m.	36/90	TMS	C	P	
13	Tunnel	TASN3506.9	19 m in Tunnel J.	24/90	TMS	C	P	
14	Borehole	KA2598	No point	NA	Petrocore	Po	NA	

5.4.8 ZAS0001A0 (EW1)

Introduction

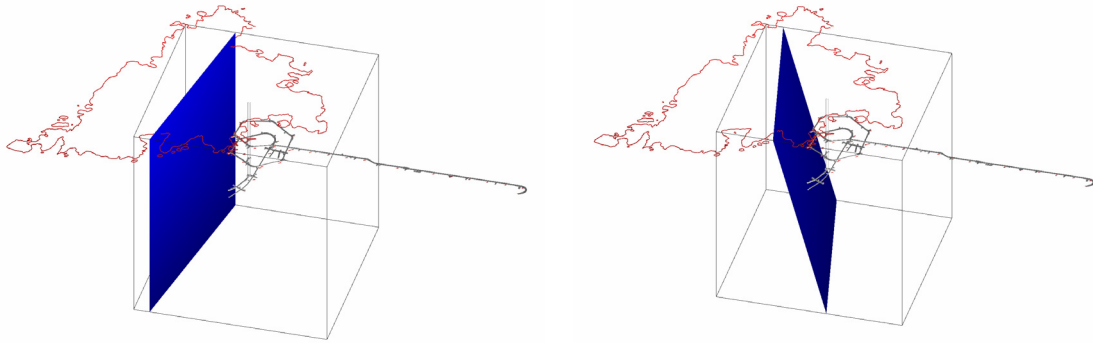


Figure 5-15. *Isometric views of EW1a and b respectively. Tunnel symmetry is shown together with the model domain boundary.*

The zone EW1 is more generally known as the Äspö shear zone. There are a few new boreholes in the vicinity of EW1 since 1996: KJ0052F01, KA3593G and KA3600F. However, none of these boreholes are inferred to penetrate the zone. There is thus no new geological data that concern the modelling of EW1 since the Äspö96 model was published. The previous model of EW1 in Äspö 96 was primarily based on a separate study published in /Stanfors et al., 1994 and c.f. figure 4-26 in Rhén et al., 1997/, which supported the interpretation that the zone forms two main branches. The orientation of these branches was further constrained by the existence of topographic lineaments and by hydraulic tests. In earlier models /e.g. Wikberg et al., 1991/ the zone has been viewed as one wider zone (ca 100 m), basically following the northern part of ground magnetic interpretation /Nisca and Triumph, 1989/ (see also Figure 3-8), which indicated that a deformation zone was the cause for the 300 m wide belt of magnetic low. EW1 was initially interpreted from the structures in magnetic surveys /Nisca, 1987; Nisca and Triumph, 1989/ and remote sensing on the topography /Tiren and Beckholmen, 1987/.

The interpretation in Äspö02v1 follows the one presented in Äspö96, with slight adjustments of the orientation of the E-W leg of the zone (EW1a) (see further below), and the conclusion in /Rhén et al., 1997/, that additional investigations are necessary to better constrain the geometry of EW1 is still valid.

Geology

EW1 is not outlined on the geological map over Äspö (Figure 3-1), but a major mylonite occurs in an excavated trench (Figure 5-16), which runs across the island. It was mapped in the central part of the island.

The partial alignment of lithological units along the zone, in particular the fine-grained granites, outline the zone on the map (Figure 3-1). In the boreholes KAS04 and KA1755A ca 30% of the core is in fact fine-grained granite. This may be compared with boreholes KAS 9 and KAS11-14 averaging at ca 15% /Sehlstedt et al., 1990/. An increased amount of fine-grained granites along EW1 may actually contribute to the magnetic low zone across Äspö, since these rocks normally have much lower magnetic susceptibility than the normal granitic and mafic rocks.

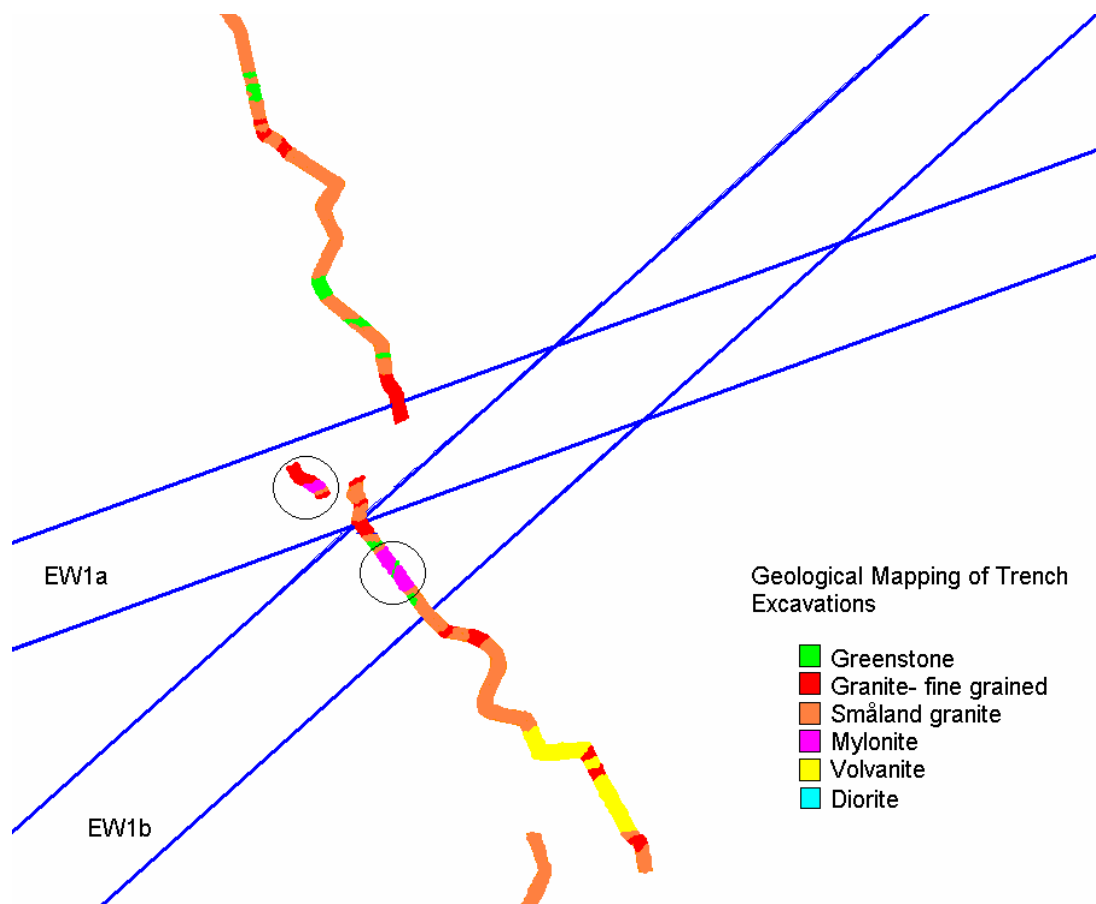


Figure 5-16. The two legs of EW1 and their relation to the mapped mylonites in excavated trenches. EW1 was in Äspö02_v1 modelled as two crossing planes with a zero width, centered in these mylonites.

The total width of EW1, including the fractured and altered boundaries, is at least 100 m in the central part of Äspö at the surface. An approximately 20 m wide mylonite has been found in a trench /Kornfält and Wikman, 1988/ in the central part of the island representing the SW-NE leg of EW1 (EW1b) (Figure 3-1). It was surrounded with a ca 30 m wide zone of strong foliation. There is also another outcrop further to the east on Äspö, with a narrow mylonite, that seems to indicate the location of EW1b. Less than 100m to the northwest, in EW1a, the corresponding values of mylonite and foliated rock are 5 and 10 m, respectively.

EW1b is the dominating leg of the zone. In its southwestern part it follows a topographic low and is observed in one of the trenches excavated across the island /Kornfält and Wikman, 1988/ Figure 3-1. EW1b coincides with the Äspö shear zone as it appears on regional tectonic and aeromagnetic maps (lineament ZSM0005A0, /SKB, 2002/). It has been traced from the Uthammar granite in the south, to ca 1 km northeast of Äspö. The deformation in this zone has been active both early in its evolution in a ductile regime and later been reactivated in a brittle regime, as documented both at Äspö /Munier, 1995; Mazurek et al., 1996/ and further to the southwest /Bergman et al., 2000/. The sense of shear has been interpreted as sinistral during the ductile development and dextral during brittle reactivation /Talbot and Munier, 1989; Munier, 1989; Mazurek et al., 1996 and Bergman et al., 2000/.

According to /Munier, 1995/ the zone comprises a fracture system that includes fractures striking ENE, NW and N. Figures 4-10 and 4-11 in /Mazurek et al., 1996/ illustrates the fractures in an outcrop along EW1b and their relationship to the older ductile deformation. The fractures were interpreted to have formed by dextral shear along the fault aligned with the ductile deformation.

In the northeast, the lineament along EW1b is not as prominent as it is further to the southwest and it curves slightly northwards (topography and magnetic, see Figure 3-6), which is opposite to what would be expected from the dip of the zone. There are few other indications of the zone in this area and the character of the zone here is basically not known.

The orientation of EW1a is not well constrained. A number of slightly different models, different from the geometry chosen here, would have been possible. Only one observation occurs at the surface (in a trench excavation) and only two cored boreholes penetrates the zone, both situated in the central part of the island.

The EW1 character, as described in /Rhén et al., 1997/:

“The fracture zone EW1 can be regarded as part of the about 300 m wide low magnetic zone (Äspö shear zone), trending NE, which divides Äspö into two main blocks. EW1 consists of at least two strands ...”, and “Initially the zone was formed by early ductile/semi-ductile deformation. Local development of mylonites and epidotic shear zones controlled the orientation of later brittle deformation in the form of increased fracturing and brecciation. Hydrothermal alteration and formation of different fracture filling minerals probably had an important sealing effect on the main part of the zone. The most conductive parts of EW1 seem to coincide with some narrow highly fractured sections or single open fractures which are probably not connected along the entire zone.”

The observation protocols in appendix 2 gives further information on the character of the zone as it is documented in the TMS database and SICADA for intersections regarded as certain and probable.

Model

The modelling of EW1 in RVS was done for a separate rock mechanical project /Andersson et al., 2002; Staub et al., 2002 and Hudson, 2002/ in the way described below.

The difference between Äspö02v1 and v2 is that in the latter only a confidence surface towards the south has been constructed. This decision was taken because the large uncertainties of the exact location of EW1 and its branches. This surface was constructed as the southern boundary of the combined EW1a and EW1b. Thus, all intersections judged as certain, probable and possible were located north of it.

The topographic lineaments and the mylonites in the excavated trench are the two primary input for the position and strike of EW1 in the Äspö02_v1. The width of EW1a is 25 m as given in Äspö96. The width was then adjusted to 45 m to incorporate probable locations of the zone in cored boreholes. The width of EW1b was first set to 50 m, with a strike of 48° and a dip of 75° towards the southeast. The width was constructed with the mylonite at the surface as centre point and then increased until it incorporated all probable and possible locations in boreholes.

Southern boundary of the EW1 that is modelled in Äspö 02_v2 is derived from intersections from both EW1a and EW1b.

The lack of data for large parts of the EW1 makes the interpretation of the strike of the zone difficult. The topography and the magnetic map help in this respect, though (Figure 3-8). The strike of the regional magnetic E-W lineament on western, central Äspö is used together with topographic depressions to extrapolate the strike of EW1a across the island. In the RVS-model EW1a has been slightly rotated around the central mylonite in order to achieve the best fit with topographic lows and creeks on either side of Äspö. The alignment with fine-grained granites (Figure 3-1) and seismic low-velocity section in the east is also used. EW1 is modelled as vertical, which gains some support from borehole information (Table 6-7) and partly from measured strike and dip in surface observations. The orientation in the Äspö02 is 70°/90°

The Äspö96 model was based primarily on E-W trending lineaments, which are prominent on a regional scale. Particularly for the eastern leg of EW1a in the existing model, this lineament is not very obvious on the local scale. The zone has been characterized from both surface outcrops and drillcores. It does, however, not affect any part of the tunnel system in HRL.

In /Stanfors et al., 1994 / an evaluation of EW1 with reference to the results from the boreholes KAS04, KA1755A, KA1754A and KA1751A, as well as available surface mapping, was presented. The report presents a vertical cross-section for EW1 in 2D that gives a summarized picture of the interpretation.

The bedrock map from /Kornfält and Wikman, 1988/ (Figure 3-1) shows the relationship between EW1 and fine-grained granites. Other rock types associated with the zone are Äspö diorite and “greenstones”.

In the cored boreholes the probable EW1-locations have characteristics as described in Table 5-7. The width of EW1 seems to decrease with depth, down to 785 m where a very high frequency of fracturing occurs over a wide interval. The mylonitic part of the zone definitely becomes thinner and possibly splits up into several splays. High fracture frequency is the most characteristic feature of the zone at depth, where the main information comes from borehole KA1755A.

Table 5-7. Borholes close to, or penetrating EW1. Indications of deformation.

Borehole	Approximate length. Depth of model zone, m (m.a.sl)	Description (quoted depths refer to down-borehole lengths)
KA1755A	-260 to -280(EW-1b)	At core length 95-140 m generally >10 fract./m, at nine sites >20 fract./m. This wide zone coincides geometrically with EW-1b. Most of the zone is developed in fine-grained granite and partly in granodiorite. Only a thin zone of true mylonite, with a medium tectonized area of 2-4m around it. RQD is less than 25 at several locations in the zone. At core length 203-213 m ca 10 fract/m except for a 1-2 m wide
	-300 to -317(EW-1a)	A crush zone, with enhanced fracture frequency. A thin breccia/mylonite and a ca 5-7 m wide zone of tectonization have been recorded. The area was interpreted as EW-1a in /Stanfors et al., 1994/.
KA1754A	-266 to -290	A crush zone and surrounding tectonization at ca 90-115 m fits geometrically with EW-1b. The area has a very high fracture frequency and the rock is fine-grained granite, granodiorite and "greenstone".
KA1751A	-247 to -250	Penetrates half the zone EW-1b. The rock is fine-grained granite, granodiorite and greenstone. No major indications of deformation in the database. However, in /Stanfors et al., 1994/ a section between core length 140 and 150 m coincides with EW-1b. The area in this report is mapped as a fracture zone and as tectonized. At approximately 110 m there is a crush zone and a tectonized area developed in fine-grained granite and "greenstone".
KAS04	-77 to -158(EW-1a)	Five thin mylonites at depths: 87, 140, 147, 153 and 158 m. Intense tectonization around the mylonite at 147 m.
	-225 to -358(EW-1b)	Two mylonites, one centrally in EW-1b and one in the southern part. Also four areas with weak to intermediate tectonization. The rock is granodiorite and fine-grained granite.
KA3510A		Does not penetrate the zone. No indication of tectonization.
KA3566G02		Does not penetrate the zone. Weak tectonization south of the zone.
KA3590G02	-461 to -469	Intermediate tectonization in the southern part of the zone. The rock is granodiorite. (The tectonization in this core supports the adjustment of the dip for EW-1b, from 78° to 75°)
KA3593G		Does not penetrate the zone. No indication of tectonization.
KA3600F		Does not penetrate the zone. No indication of tectonization.
KAS02	-785 to -913	Thin mylonite in the central part of the zone (at a depth of 854 m). Many areas of weak to strong tectonization along the borehole section that crosscuts the zone. Numerous sections with more than 50 fractures/m. The rock is fine-grained granite and granodiorite

Confidence

The orientation of the EW1 in Äspö 96 and Äspö 02_v1 is to a large extent determined by the orientation of the zone as measured at the surface and how it appears on topographical and geophysical maps. The geological field data is concentrated in the central part of the zone, where most outcrops appear. The confidence of the geometries and geology of the zone here is high.

Lineament studies and geophysical data require difficult interpretations regarding which anomalies that is related to different expressions of the zone, e.g. ductile deformation, brittle deformation, alteration or lithology.

Most of the observations from cored boreholes are situated in this central part of the island, whereas for other parts of the EW1 in the model, only lineament studies, geophysical indications and a few percussion drilled boreholes are available to substantiate the model.

Table 5-8. Point table for deformation zone EW1.

	Type	Id	Precise location (borehole length, tunnel chainage or X;Y;Z)	Orientation	Source	Uncertainty (part of this zone)	Uncertainty (orientation)	Comment
1	Borehole	KAS12	42.15	NA	Petrocore	Po	NA	
2	Borehole	KAS04	362.62	NA	Petrocore	P	NA	
3	Borehole	KA1751	133.2	NA	Petrocore	Po	NA	
4	Borehole	KA1755	95.39	NA	Petrocore	P	NA	
5	Borehole	KA2598	No point	NA	Petrocore	NA	NA	
6	Surface	Trench	X:1551229.2 Y:6368009.4 Z:6.1	NA	Dgn-file from IM; Geological mapping	C		
7	Surface	Lineament	X:1551000 Y:6367790 Z:0	082/NA	Dgn-file from IM	C		
8	Surface	Seismic refraction	X:1551466.1 Y:6368160.0 Z:1.9	NA	Dgn-file from IM	P		

5.4.9 Atlas of Deformation Zone

This is an outline of the intended design of the atlases of deformation zones suggested to be used as a brief summary for each zone.

SKB's primary data, stored in SICADA and RVS, are not easily accessible to all readers. To improve the understanding of the primary data used and with what uncertainties the zones have been modelled, an Atlas has been developed. The completion of the atlases remains, however (i.e. filled with data).

The use of an Atlas is meant to improve the tracability of primary data, but also in a simple manner show where a lack of primary data exist and illustrate the interpretations made. Furthermore, the Atlas is meant to be used in the integration process between the geoscientific disciplines.

The Atlas corresponds to the digital model. All information of one zone is assembled in an Excel-file folder. Figure 5-17 show the layout of the Atlas in Excel.

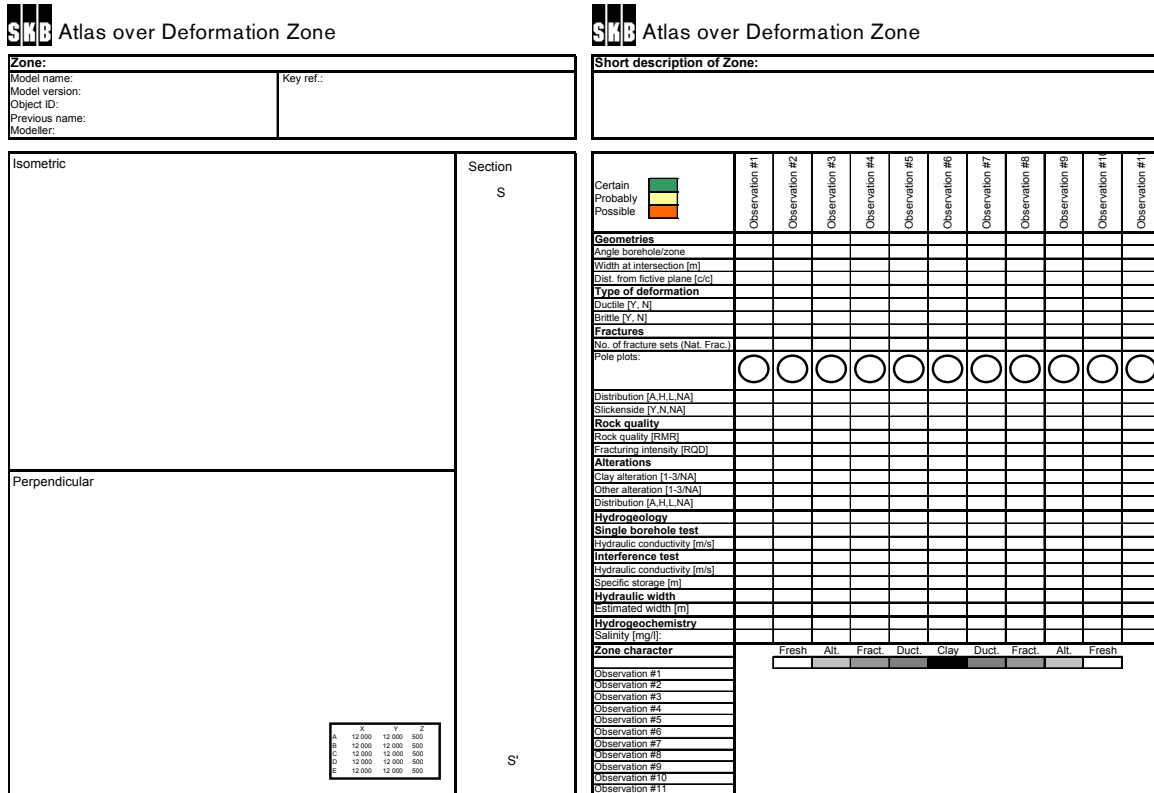


Figure 5-17. Atlas of Deformation Zone, see below for details.

The Atlas is composed of four fields:

1. General model information in the upper left corner in Figure 5-17.
2. Short description of zone at the upper right corner in Figure 5-17.
3. Isometric, perpendicular and section views of the zone in the major part of the left side in Figure 5-17.
4. Zone properties, major part of the right side in Figure 5-17.

The field “Model information” describes the basic information of the modelled zone such as; model name, model version, object id (RVS), previous name, modeller and key references.

In the field “Short description” it is possible to explain the zone in words and e.g. other possible interpretations of zone extent within the model.

Next field; “Isometric, perpendicular and section views” illustrate the zone visually. The isometric view shall give the reader a conception of zone position within the model. In the perpendicular view all observations (trenches, tunnel and borholes) are shown, parts of the zone with divergent properties are hatched and a co-ordinate list for zone extent is inserted. In the section view a cross-section of the zone is illustrated.

The remaining field “Zone properties” (Figure 5-18) show a number of selected parameters, measured at the observations in the zone.

Measure of confidence that observation belong to zone and confidence in parameter value.















Certain  Probably  Possible 	Observation #1	Observation #2	Observation #3	Observation #4	Observation #5	Observation #6	Observation #7	Observation #8	Observation #9	Observation #10	Observation #11																		
	Observations																												
Geometries																													
Angle borehole/zone																													
Width at intersection [m]																													
Dist. from fictive plane [c/c]																													
Type of deformation																													
Ductile [Y, N]																													
Brittle [Y, N]																													
Fractures																													
No. of fracture sets (Nat. Frac.)																													
Pole plots:																													
																													
Distribution [A,H,L,NA]																													
Slickenside [Y,N,NA]																													
Rock quality																													
Rock quality [RMR]																													
Fracturing intensity [RQD]																													
Alterations																													
Clay alteration [1-3/NA]																													
Other alteration [1-3/NA]																													
Distribution [A,H,L,NA]																													
Hydrogeology																													
Single borehole test																													
Hydraulic conductivity [m/s]																													
Interference test																													
Hydraulic conductivity [m/s]																													
Specific storage [m]																													
Hydraulic width																													
Estimated width [m]																													
Hydrogeochemistry																													
Salinity [mg/l]:																													
<table border="1" style="width: 100%; text-align: center;"> <tr> <td>Fresh</td> <td>Alt.</td> <td>Fract.</td> <td>Duct.</td> <td>Clay</td> <td>Duct.</td> <td>Fract.</td> <td>Alt.</td> <td>Fresh</td> </tr> <tr> <td></td> <td></td> <td></td> <td></td> <td></td> <td></td> <td></td> <td></td> <td></td> </tr> </table>												Fresh	Alt.	Fract.	Duct.	Clay	Duct.	Fract.	Alt.	Fresh									
Fresh	Alt.	Fract.	Duct.	Clay	Duct.	Fract.	Alt.	Fresh																					
Zone character																													
Observation #1																													
Observation #2																													
Observation #3																													
Observation #4																													
Observation #5																													
Observation #6																													
Observation #7																													
Observation #8																													
Observation #9																													
Observation #10																													
Observation #11																													
General zone character																													

Figure 5-18. The field “Zone properties” in the Atlas.

A number of geological, hydrogeological and hydrogeochemical parameters are inserted in the Atlas. The character of each zone is also averaged to a general view in the bottom part of Figure 5-18.

The observations are named as the related protocols (see chapter 4.3.5) that make the information in the Atlas traceable back to the primary data.

All observations are classified as being: certain, probably or possible (marked with colour in the table) part of the zone in question. Each parameter is classified in the same manner, regarding the measures level of uncertainty.

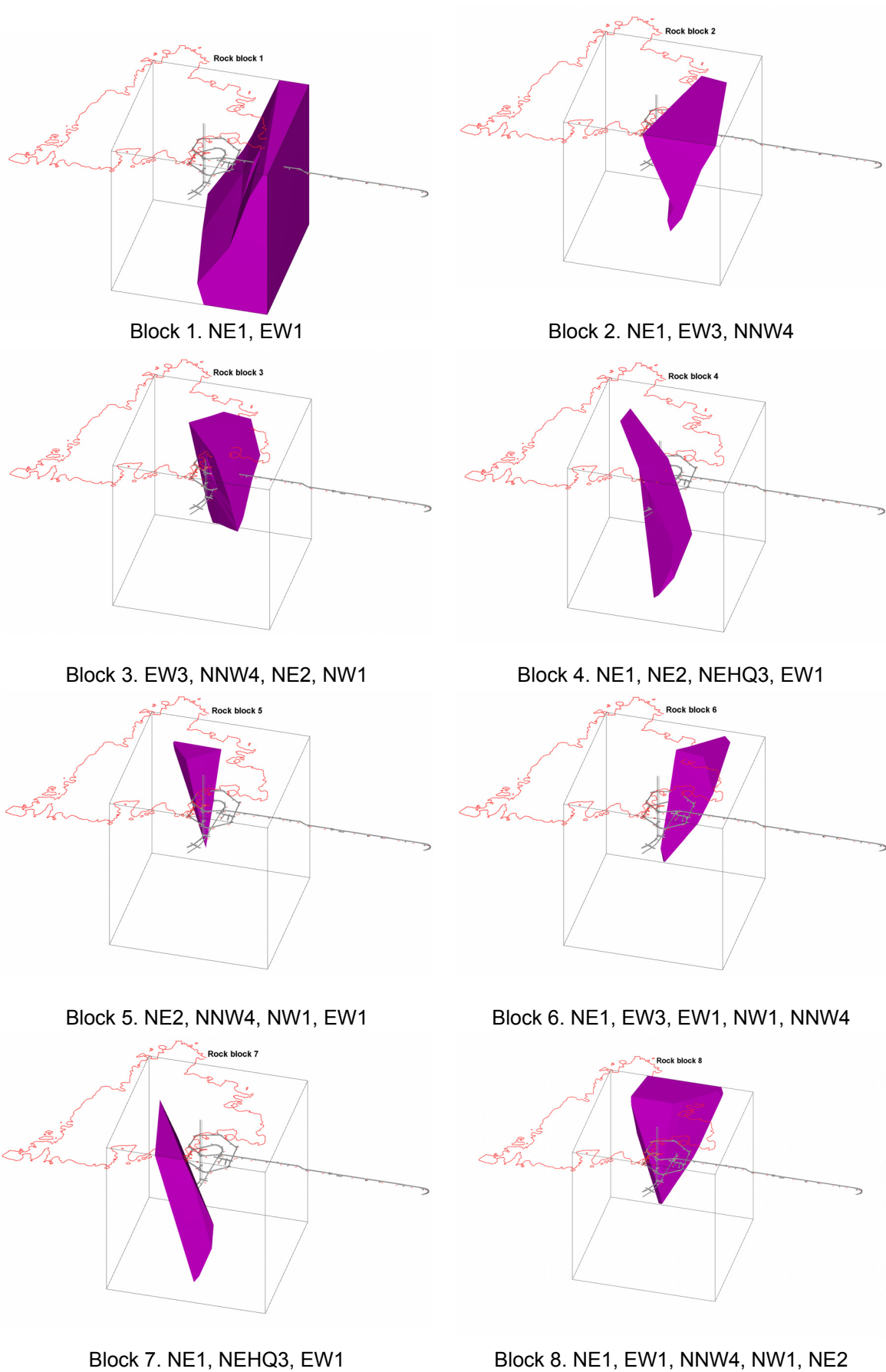


Figure 5-18. The eight rock blocks within the model volume

5.5 Rock blocks

In the Figures 5-18 below are the blocks defined by the separating modelled zones. Only those considered in the statistical section (chapter 5.6.3) are shown. A further subdivision of the model domain, into rock domains and units, on the basis of the characteristics derived from any of the geodisciplines is needed for a more complete model description. The eight blocks below are the ones where enough data was available to make a statistical analysis meaningful. The bounding deformation zones are named below the respective block.

5.6 Fractures

5.6.1 High Permeability Features

An update of the hydrogeological model at Äspö has been presented by Vidstrand et al. in the Geomod project /Vidstrand, in press/. It is concluded in the report that there is a discrepancy between the geological zone description and the hydrogeological conductor description, regarding position and width, as compiled from /Rhén et al., 1997/, and that an updated consistent description would require a complete re-work on the data. As an attempt to provide geological structures that transport the flow of water corresponding to the observed hydraulic responses at Äspö with, several studies have been initiated /e.g. FCC project; Hermansson, 1995; Rhén and Forsmark, 2000; Winberg and Hermansson, 1996 and Hermansson et al., 1996/.

In the Geomod project visualisation of water-bearing fractures longer than the tunnel width or 5 meter has been done as narrow discs oriented with the strike and dip given in the TMS database. These were used as input together with structures in the database of /Mazurek et al., 1996/ (see below), to make a geometrical evaluation of possible interpolation between separate tunnel locations.

Together with the geohydrological discipline in Geomod an attempt has also been made to correlate different types of flow log results in a few boreholes with fractures, some of which are oriented. This is not straightforward for several reasons. Some flow-logs are difficult to interpret in a simple manner and it is also difficult to pin point in exactly what fracture the flow occurs in relation to the observed log signal. Other logs may be fairly distinct in this respect, but comparison with the fracture locations was ambiguous at many locations. For a more thorough description regarding different flow logging methods, see /Vidstrand, in press/ and references therein. Fractures that could be correlated with a level of confidence regarded as high and with a water flow judged as certain are presented in (appendix 1) and visualized in RVS.

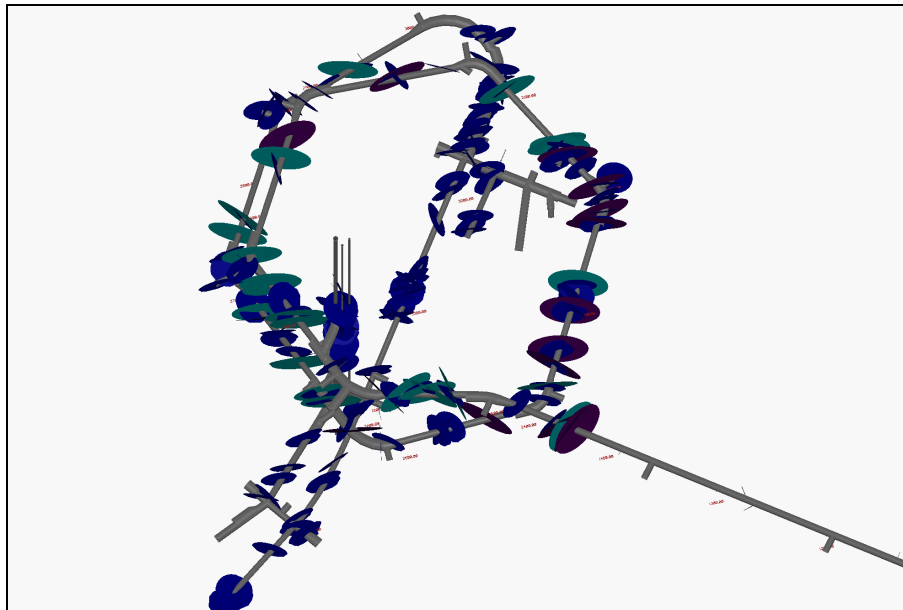


Figure 5-19. View looking steeply down towards the northeast. Visualized water bearing fractures longer than 5 m (small, navy blue), water-conducting features from FCC database (larger, light blue) and ditto with ductile precursor (purple).

In addition to the large-scale structures considered in the model described earlier in the chapter, a number of medium-scale structures from the Fracture Classification and Characterisation project (FCC) have been visualized in RVS as isolated discs along the tunnel spiral in Äspö HRL Figure 5-19. Information on water-conducting features was extracted from the database in /Mazurek et al., 1996/.

The FCC database comprises information on 88 water-conducting features (WCF) between tunnel meters 600 and 2935, i.e. in the deep part of the access ramp and in the spiral loops of the Äspö HRL. Only water-conducting features having a trace that cross-cut the entire tunnel cross-section was considered for mapping and characterization (i.e. fracture trace lengths of at least ca 7 m).

Within the interval considered for mapping, hundreds of water-conducting features have been observed and mapped during the construction phase, and data have been recorded in the Äspö Tunnel Mapping System (TMS) database and in SICADA (previously GEOTAB). In total 113 features in the TMS database cross-cut the whole tunnel diameter in the interval between 600 and 3050 m. Out of these 27 features are classified as fracture zones and 86 are classified as single open fractures /see Fig. 5-1 in Mazurek et al., 1996/.

Only 15 of the fracture zones and 29 of the single open fractures extracted from TMS were considered during the FCC mapping campaign. There were basically three reasons for excluding structures from the TMS database. Firstly, a large number of water-conducting features were completely or partly concealed under shotcrete reinforcements. Secondly, at some locations with severe and complex brittle fracturing it was not possible to map individual water-bearing fractures. These were often associated with poor outcrop quality and severe water inflow and were not considered further. Finally, some fractures extracted from the TMS database were at the time of investigation dry or were regarded as structurally and hydraulically insignificant.

On the other hand, about 44 additional water-conducting features were identified during the detailed mapping campaign and were included in the investigations (see Mazurek et al. 1996 for detailed description of the selection procedure). Most of these “new” features could be identified in the TMS design files, with geological information in the related database, as a number of shorter water-conducting features or fractures. These segments could be combined (generally by splay fractures) because they were interpreted as genetically related as part of a larger water-conducting feature.

A one-day reconnaissance inspection of all WCF in the FCC database, from about chainage 1300 and downward, was conducted in the spring, 2003, within the Geomod project. It could be confirmed that most structures were fairly well defined (possible to map out) and decided that the most hydraulically open ($T > 10E-6$ m²/s) structures should be visualized in RVS.

All water-conducting features in the FCC database are interpreted as being faults, composed of interconnected systems of shear fractures (master faults) by tensile fractures (splay cracks). The water-conducting features have variable internal structure with a continuous spectrum from *simple* structures, basically composed of only one master fault, to *complex* structures with two or more master faults and a number of splay fractures. For this reason the anatomy of the WCF is taken as the prime classification criterion. On the basis of the geometric arrangement of master faults and splay cracks, five subtypes are distinguished /type 1 to type 5 in Figure 6-1 in Mazurek et al., 1996/.

All water-conducting features included in the FCC database are less than 4 m wide. This implies that no major fracture zones are incorporated in the database (i.e. only local minor fracture zones and single fractures according to Table 8-4 in Geomod project description).

The database contain, for example, information on host rock lithology of the WCF, ductile deformation and alteration in wall-rock adjacent to the WCF, features and structures related to brittle deformation, fracture filling, rock support and grouting, geometric parameters of the WCF, and transmissivity as well as water discharge from probing holes interpreted to intersect the WCF.

Data from the spiral loops, i.e. from tunnel meters ca1550, where considered in the present analysis. It includes in total 56 structures; 36 structures are from the upper spiral (1536 to 2450 m) and the remaining 20 structures are in the lower spiral (2476 to 2935 m). As a consequence of the construction work in the Assembly Hall at that time and time restrictions the mapping stopped at about tunnel meter 3000.

Location and simplified geometry (taken from the sketch maps in the field notes) of the 56 water-conducting features are shown on Figure 1 and 2. Simple structures with one master fault are thus illustrated as one single line. In the more complex structures the numbers of master faults are also indicated. More prominent splay fractures are shown as well. The strikes of water-conducting features are shown with correct orientation. Because of the scale of the figure, however, the width of narrow structures is not at scale. A few additional water-conducting features, not in the FCC database are included in the first and second loop, respectively. These WCF were more or less completely covered by shotcrete and thus not possible to map and characterise in detail. However, orientation and width of the structure was available in the field notes.

High Permeability Features (HPF), as defined by /Rhén and Forsmark, 2000/, are water-conducting features with an inflow rate (data collected in probe holes while drilling or flow logging of during the preinvestigation phase) higher than 100 l/min or alternatively having transmissivities T of $\geq 1E-5$ m²/s. The evaluation of the Äspö database contains 79 such features. A preliminary correlation with the FCC database indicate that most of the of HPF:s in probe holes can be identified in the FCC database.

/Munier and Hermansson, 1994/ defined a special type of fracture zones, “fracture swarms”. These were zones with a relatively high fracture frequency, but not as high as a ‘fracture zone’ proper and with fracture orientations essentially parallel to the orientation of the zone boundary. A number of water-conducting features, especially type 2 and type 5 structures /Mazurek et al., 1996/, in the FCC database can be correlated to the modlled fracture swarm intersections with the spiral in Äspö structural model. The orientation of the individual FCC structures are, however, more westerly (WNW).

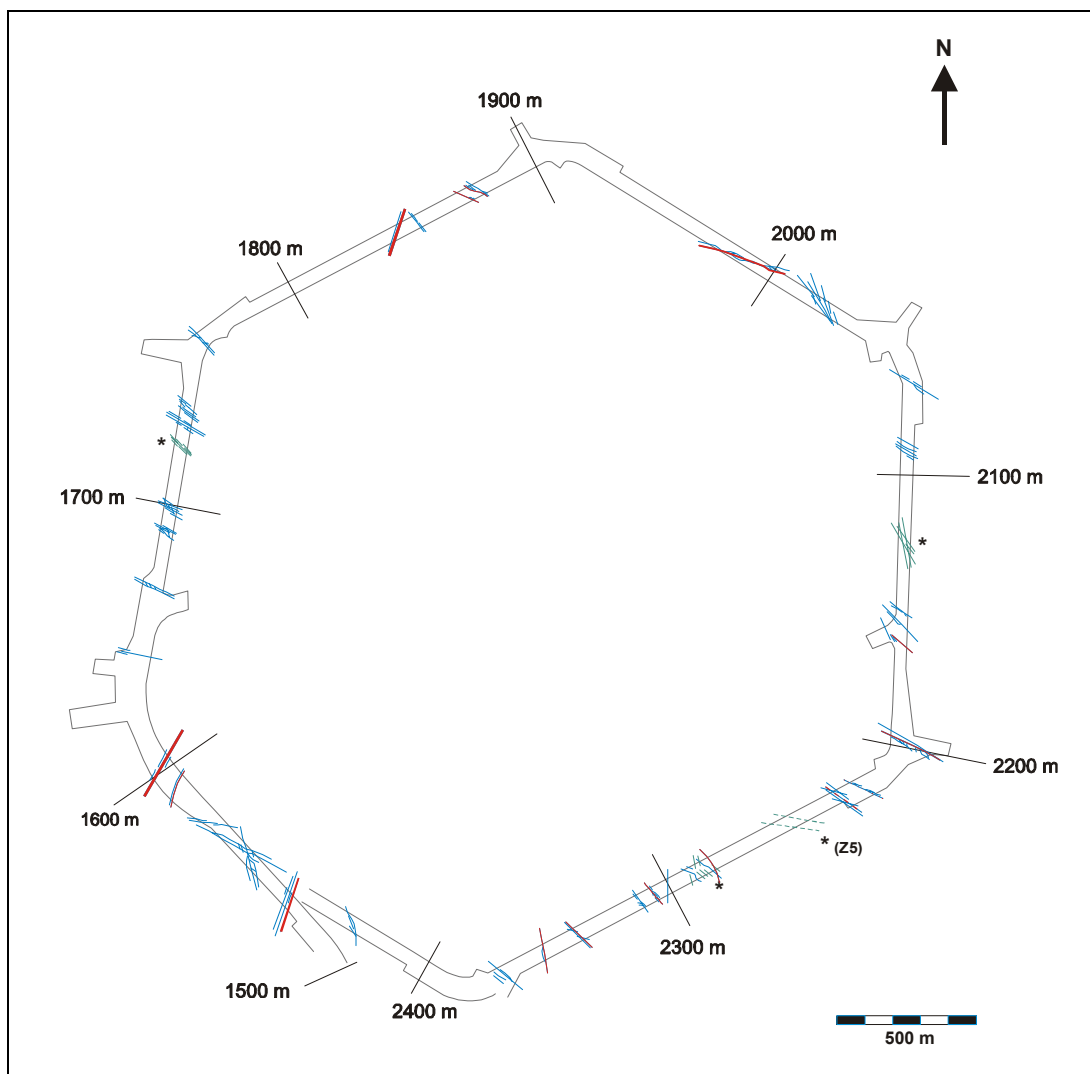


Figure 5-20. Water-conducting features in the tunnel section 1500 to 2450 (FCC database). Fault planes with ductile deformation in wall rock adjacent to the WCF are coloured red. Top view of Äspö HRL. * = WCF (shown with green colour) not in FCC database, only reconnaissance investigation (see text for explanation).

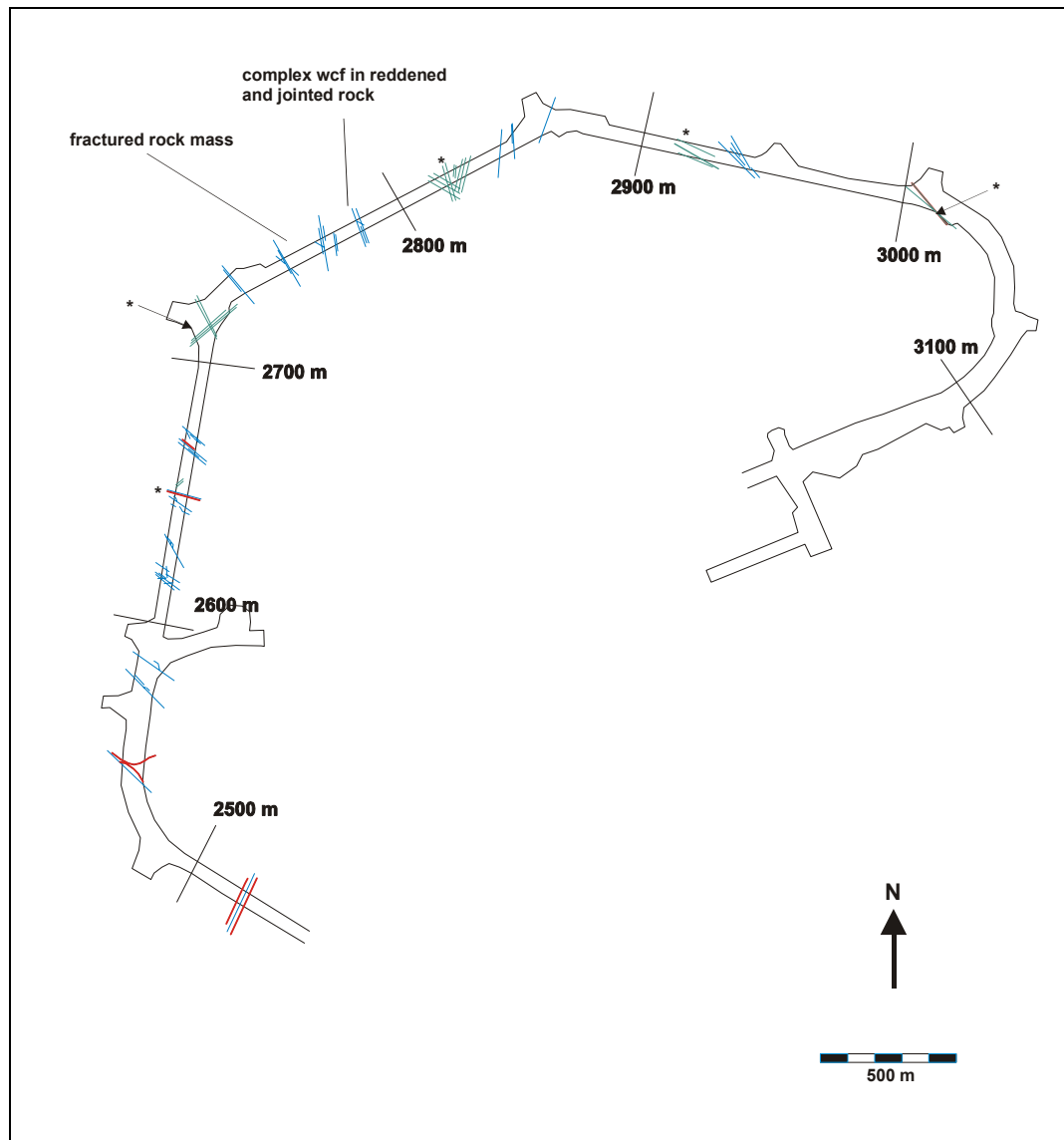


Figure 5-21. Water-conducting features in the tunnel section 2476 to 2935 m (FCC database). Fault planes with ductile deformation in wall rock adjacent to the WCF are red coloured. Top view of Äspö HRL. * = WCF (shown with green colour) not in FCC database, only reconnaissance investigation (see text for explanation).

Transmissivity data exist from 64 water-conducting features. T values were derived by extrapolating fault orientations outside the tunnel intersections towards probing boreholes drilled prior to the excavation. In several cases, the transmissivity value refers to two or more neighbouring water-conducting features that were all penetrated by the same borehole. Furthermore, many structures are penetrated by more than one borehole. A simple correction procedure was applied to obtained weighted transmissivity values and is documented in /Mazurek et al., 1996/. Average bulk transmissivity ($\text{m}^2/\text{s} \times 10\text{E}-7$) are highest for Type 2 and Type 2 structures /Figure 6-9 in Mazurek et al., 1996/.

Some of the FCC structures in Äspö HRL tunnel system can tentatively be extrapolated between two or three tunnel intersections Figure 5-22. However, it should be noted that a much more comprehensive analysis (considering for example information from boreholes) is necessary to increase the confidence in such a modelling.

In an initial assessment the roughly vertical water-conducting structures at tunnel meters 1690, 1730, and 1740 can probably be extrapolated downwards some 100 m to the lower spiral. Furthermore, the WCF at 1872 and 1876 m can be connected with the WCF at 1990 (the NW-1 structure). NNW-4W and NE-2 can also be identified among the FCC structures.

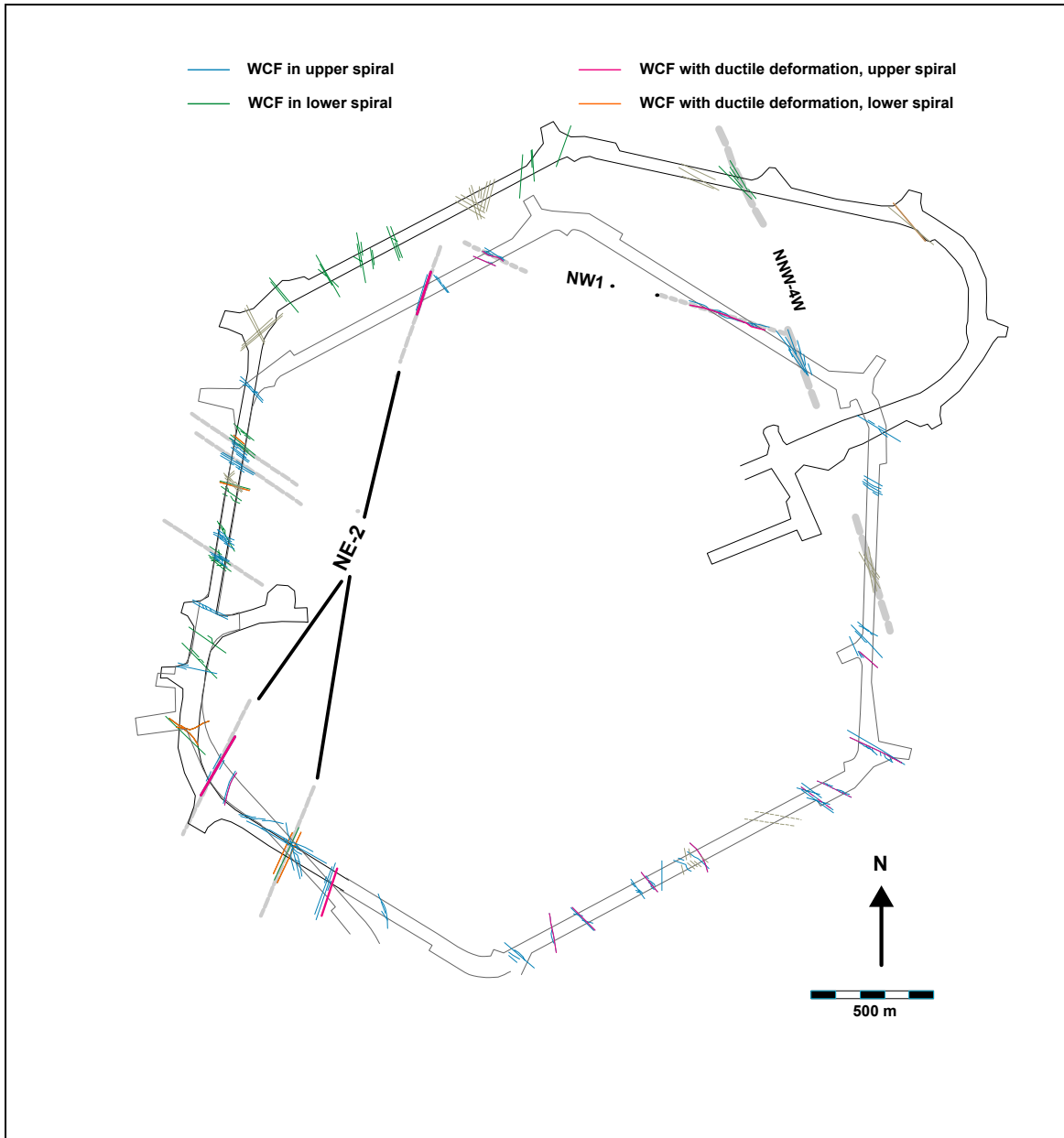


Figure 5-22. Water-conducting features in the tunnel section 1500 to 2450 (FCC database). Top view of Äspö HRL. Fault planes with ductile deformation in wall rock adjacent to the WCF are highlighted with different colour. WCF not in the FCC database are shown with grey lines (see text for explanation). Grey hatched lines denote structures tentatively possible to connect.

5.6.2 Fracture mineralogy

The fracture mineralogy in the Äspö area has been studied in numerous drillcores. The most common fracture minerals in the area are chlorite, epidote, quartz, calcite, prehnite, laumontite, low-temperature K-feldspar (adularia), clay minerals, hematite and pyrite. A sequence of mineralization has been established going from fillings of epidote over to prehnite and laumontite and down to more low-temperature fillings as clay minerals and calcite. These investigations were carried out up to 1995, and the results are included for example in the compilation by /Stanfors et al., 1999/.

It is obvious that many fractures have ductile precursors and reactivated mylonites are commonly observed. Other fractures show significant hydrothermal alteration along the fracture walls but tectonic imprint may be manifested only as higher frequency of micro-fractures. A minor set of fractures lack hydrothermal or ductile precursors. It has not been possible to tie fractures with different origins to any specific set of orientation.

Relative ages of the fracture mineralization events (episodes) have been determined based on textural relationships, which suggest the sequence of events given in Table 5-9 /Tullborg, 1997/.

Table 5-9. Sequence of tectonic and fracture mineralization events

	Event	Time before present
	Formation of the Småland granitoids	ca 1800 Ma (a)
1	Regional deformation resulting in E-W to ENE-WSW foliation	
2	Mylonitization; formation of fine-grained epidote, muscovite and recrystallization of quartz	> 1400 Ma (b)
3	Reactivation of mylonites and formation of idiomorphic epidote and fluorite	
4	Growth of idiomorphic quartz, hematite, fluorite, muscovite, calcite and spherulitic chlorite due to post magmatic circulation related to the Götemar granite	
5	Development of prehnite, laumontite, calcite, chlorite and fluorite	900-800 Ma (c)
6	Illite dominated mixed-layer clay, calcite, (chlorite) (fluorite)	c. 300 Ma (d)
7	Growth of calcite, Fe-oxyhydroxide, (clay minerals)	Recent

(a) Wikman and Kornfält, 1995, (b) Åberg et al., 1984; Smellie and Stuckless, 1985, (c) Tullborg et al., 1996, (d) Maddock et al., 1993; Tullborg et al., 1995.

Fracture calcites have been formed, dissolved or recrystallized more or less continuously during the time when the fractures have been water conducting. As a result of this, calcite is, and have been used to trace palaeohydrological conditions at Äspö /Tullborg, 1997; Wallin and Peterman, 1999 and Bath et al., 2000/.

The interpretations of the fracture mineralogy carried out up to 1997 were based on conventionally drilled cored boreholes. This means that loose and soft material present in the fractures have been flushed away. Fracture material sampled from the HRL tunnel /Banwart, 1995 and Puigdomenech et al., 1999/ have shown that clay minerals are underrepresented in the core mapping. However, the total amounts of clay minerals in the fractures are very low, >10%. On the other hand, ion exchange processes with clay minerals are rapid processes and will certainly influence the water chemistry of exchangeable elements /cf. Banwart, 1995 and Laaksoharju et al., 1999/.

New drillings using triple tube, mainly carried out within the different Tracer Retention Understanding Experiments, TRUE), together with the use of BIPS-logging have in a considerable way added information about the composition of the water conducting zones and fractures, especially concerning the presence of fault breccia and fault gouge and the compositions of the clay minerals present.

The definitions employed in the TRUE Block Scale analytical work for the identified unconsolidated materials are given below in Table 6-10. These definitions were based on size, ocular identification in BIPS log, chemical composition and to a lesser extent on genetic aspects of structure formation.

Table 5-10. Definition of Fault Breccia and Fault Gouge employed in the TRUE Block Scale Project /Andersson et al., 2002/.

Material type	Characteristic descriptors
Fault Breccia (FB)	Centimetre (> 2 mm) to m sized pieces of altered wall rock/cataclasite and/or mylonite. The chemical and mineralogical composition is usually similar to that of wall rock. Observable in the BIPS-log.
Fault Gouge (G)	Fragments and mineral grains ($\leq 2\text{mm}$) of wall rock and secondary minerals (clay minerals and calcite) The smaller fractions (< 0.125 mm) are to a variable degree enriched in clay minerals, calcite, pyrite and FeOOH. Not possible to identify from BIPS-log.

The gouge material is usually composed of altered wall rock fragments (\pm mylonite fragments) and in the smaller fractions, single grains of quartz, feldspars, epidote, chlorite, illite \pm other clay minerals. Calcite, sulphides and occasionally FeOOH are observed as mineral phases that have grown on the various fractions of the fault breccia and fault gouge.

Below is given an example of the mineralogical composition of the fine-grained (>0.125 mm) fraction of gouge material from four different hydraulic structures (fracture zones) in the TRUE Block Scale volume at ca 450m depth in the Äspö HRL. It is obvious that the most prominent clay mineral phases, besides chlorite, are illite and mixed-layer clay, usually with a high illite component.

Table 5-11. Estimated mineralogical composition of fine-grained (<0.125 mm) fault gouge samples from Structures #6, #19, #20 and #22 in the TRUE Block Scale volume at the ÄSPÖ HRL based on XRD and chemical analyses. Values should be regarded as rough estimates. The percentage of the < 0.125 mm fraction which is <0.002 mm and the associated mineral assembly is also shown, (from /Andersson et al., 2002/).

Mineral	Structure #6 KA2563A L=154 m	Structure #19 KI0025F02 L=133m	Structure #20 KI0023B L=69.9m	Structure #22 KI0025F02 L=66.7m
Chlorite	10	30	20	40
Illite	20	7	20	-
Mica	20	5	-	3
Mixed layer clay	-	3	2	25
Smectite	-	15	-	-
Calcite	3	-	25	5
Quartz	30	10	10	15
K-feldspar	5	5	10	5
Plagioclase	12	20	10	6
Sulphides	-	-	3	1
Epidot	-	5	-	-
Weight% <0.002mm (clay fraction)	15	21	28	42
Mineral comp. of <0.002 mm fraction	Illite Chl, Plag (minor; Qz, Kfsp and calcite)	Chl and smectite (minor; illite ,mixed-layer clay, Kfsp and Plag)	Chl, (minor; illite and calcite)	Chl and mixed layer clay

Conclusion

The major achievements during the last eight years have thus been the study of the outermost cover of fracture minerals, i.e. the latest generation of fracture minerals that usually show euhedral crystals and the identification of the loose and fine material found in fracture zones. This has been possible by the combination of triple tube drilling and BIPS logging. The identification of the mineralogical composition of different gouge materials has had large importance for the understanding and the modelling of the tracer tests e.g. in being able to select transport parameters (e.g Kd). The possibility to study calcite (and pyrite) grown on the fracture surfaces has contributed to the palaeohydrogeological understanding of the site (this is discussed in /Laaksoharju and Gurban, in press/).

5.6.3 Fracture statistics

Introduction

Several studies have been undertaken to describe fracture network geometry at Äspö site with the aim to provide stochastic models representing the observed fracture statistics with their probabilistic estimates.

/LaPointe et al., 1995/ used discrete network analysis for estimation of effective block conductivities. He and his co-workers used older data including outcrop mapping data, HRL tunnel drift maps, fracture mapping from HRL based on data from the database GEOTAB (now in SIACADA), borehole data at Äspö and Laxemar as well as data from HRL access tunnel and drifts. The main conclusion from their work was that conductive fractures are not geologically different from non-conductive fractures. They considered factors as mineral infilling, rock host type, openness, roughness, shape and orientation. To evaluate first-order relations among the data two-way contingency tables were used. The contingency tables showed no statistically significant correspondence between different states of a factor and fracture conductance status. In addition, three distinct orientation sets were identified and the analysis of orientation data suggested that the orientation of conductive fractures is indistinguishable from the non-conductive fractures. Each set was estimated by Fisher's probability density plot with the mean pole for each cluster, its dispersion and goodness-of-fit statistics (Set 1: mean pole trend 286° , mean pole plunge 6.7° ; Set 2: mean pole trend 204° , mean pole plunge 4° ; Set 3: mean pole trend 310° , mean pole plunge 83°). The study also included fracture size and density (volumetric intensity) analysis. Both size and density results were derived by means of iterative stochastic fracture network modeling involving defining prime assumptions on size and density distribution, network modeling, synthetic sampling in the modeled network, and comparing statistics of observed and synthetic data.

/Munier, 1995/ who based on more or less the same background data as La Pointe and co-workers distinguished four fractures set (three steep sets striking WNW, NNW and NNE, and one subhorizontal). Munier's work involved also a study on variation in frequency of the most common fracture fillings along the Äspö tunnel and fracture trace length distribution (found to be lognormal with mean 3.46m). The variation in mean fracture trace length along the tunnel showed no obvious correlation to fracture zones or sections of increased fracturing. It was observed though that trace length varies with strike. Contrary to /LaPointe et al., 1995/, the analysis based on contingency tables and Chi-2 statistics showed that mineral coatings on hydraulically active fractures differ slightly from coatings on hydraulically inactive fractures. Munier analyzed fracture orientations by testing similarities between stereograms including fractures mapped within subparallel tunnel sections and found that they were dissimilar, however, under an assumption that fracture arrays are constant with depth.

In another study /Stigsson et al., 2001/ present a concept of stochastic discrete fracture network geometry built upon fracture mapping of the TBM tunnel and 36 bore -and exploratory holes drilled from the TBM tunnel drift. In this study three distinct orientation sets are proposed and estimated with Fisher's probability function; Set 1: strike 219° , dip 83.7° , Set 2: strike 127° , dip 84.2° , Set 3: strike 20.6° , dip 6° . The set separation performed separately on all fractures and natural fractures (potentially water-bearing) showed similar result, the major difference was that the Set 2 had a larger proportion of natural fractures than the other two sets. The fracture size estimate was obtained through exploration simulation following principles presented by /LaPointe et

al., 1995 and some simulation results from /Follin and Hermansson, 1996/ were utilized. For all identified fracture sets size was approximated by lognormal probability density function with the mean 2, 8 and 5m for Set 1, 2 and 3, respectively. Fracture frequency analysis included study on one-dimensional density (along boreholes) as well as two-dimensional intensity measure and estimation of volumetric intensity through stochastic network modeling and synthetic sampling. Also a fracture spatial model was derived by analyzing pattern of fracturing on the trace maps from the tunnel's walls and floor.

Fracture orientations

Objectives with statistical tests

The purpose with the statistical analysis of fracture orientations was to study if any differences observed among the different blocks and zones (according to earlier definition of those features) could be attributed to systematic processes or simply are a product of coincidence. A formalized test procedure based on contingency tables and followed by *Chi-2* test was invoked. The principles of contingency tables and *Chi-2* tests are found e.g. in /Cochran, 1954; Baker and Lee, 1975 and Davis, 1986/. For applications in fracture orientation statistics see /Miller, 1983; Kulatilake et al., 1990 and Munier, 1995/. In short, the method goes on dividing lower hemisphere Schmidt plot of poles to fractures into equal surface area patches. Polar nets are used as opposed to meridian nets, normally used when illustrating structures. In Figure 3-13, all fractures in the SICADA database, within the Geomod model domain has been plotted. Each patch is considered as a cell in the contingency table and its entry in the table is the number of fracture poles that occur in that patch. The number of patches is decided based upon the total number of fractures that are included in tested sample populations. Figure 5-23 illustrates an example where lower hemisphere projection is divided into 34 equal area patches. Assuming that two sample populations are tested, a cell grid like the one in Figure 5-23 below is consecutively placed on Schmidt plots describing each population and subsequently, a number of observed fracture poles in each cell are compared with a number of poles expected in each cell.

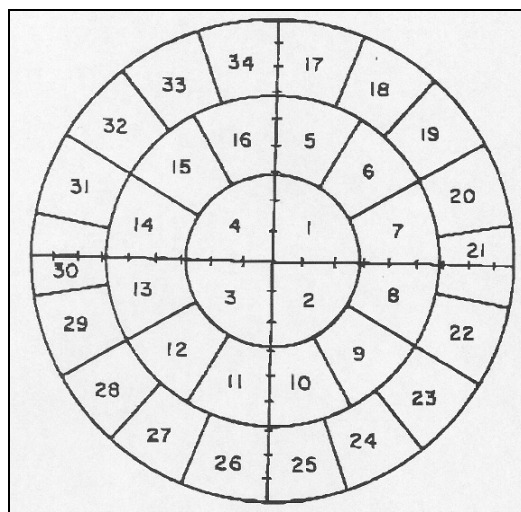


Figure 5-23. General principles for division of lower hemisphere Schmidt plot (polar net) in an array of equal area patches for construction contingency tables and following computation of *Chi-2* statistics /the figure adapted from Miller, 1983/.

The expected number of events (poles to fractures in this study) is computed on the assumption that the two tested sample populations in fact come from the same parent population /for details on computing expected events see e.g. Ryan and Joiner, 2001/. The compiled *Chi-2* statistics:

$$Chi - 2 = \sum [(Observed - Expected)^2 / Expected]$$

If *Chi-2* statistics is large the significance of the statistical test (expressed usually as *p-value*) is low. That means that the difference between tested sample populations (Schmidt plots in this case) is large and the null hypothesis on no difference between plots is rejected. The rejection, however, does not automatically imply the acceptance of the alternative hypothesis, i.e. a hypothesis that states that fracture orientations on tested Schmidt plots come from the separate populations.

Following null hypothesis have been tested in this study:

1. On tunnel surveying data:
 - a. No difference in fracture orientations between blocks (all fracture in database). Paired blocks comparison.
 - b. No difference in water-bearing fracture orientations between blocks (database subset). Paired blocks comparison.
 - c. No difference in non water-bearing fracture orientations between blocks (database subset). Paired blocks comparison.
 - d. No difference in non water-bearing fracture orientations between blocks (database subset). Multi block comparison.
 - e. No difference in fracture orientations between different depths/tunnel sections (database subset). Paired sections comparison.
2. On borehole surveying data:
 - a. No difference in fracture orientations between blocks (Boremap and Petrocore data). Paired blocks comparison.
 - b. No differences in fracture density between blocks (Boremap data) Paired blocks comparison.

Statistical tests on tunnel data

Schmidt plots with contoured densities of poles to fractures for all identified blocks are presented in Figure 5-24 - Figure 5-31. Schmidt plots for deformation zones are presented in chapter 5.4.1 - 5.4.8, in the zone descriptions. Figure 5-24 - Figure 5-31 depicts both water-bearing and non water-bearing fractures.

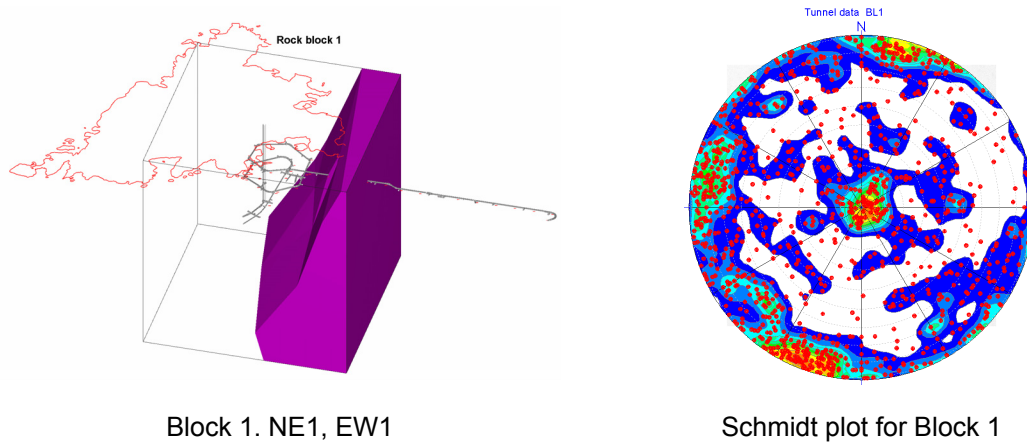


Figure 5-24. Lower hemisphere Schmidt plot (polar net) of poles to fractures mapped in Äspö tunnel block 1.

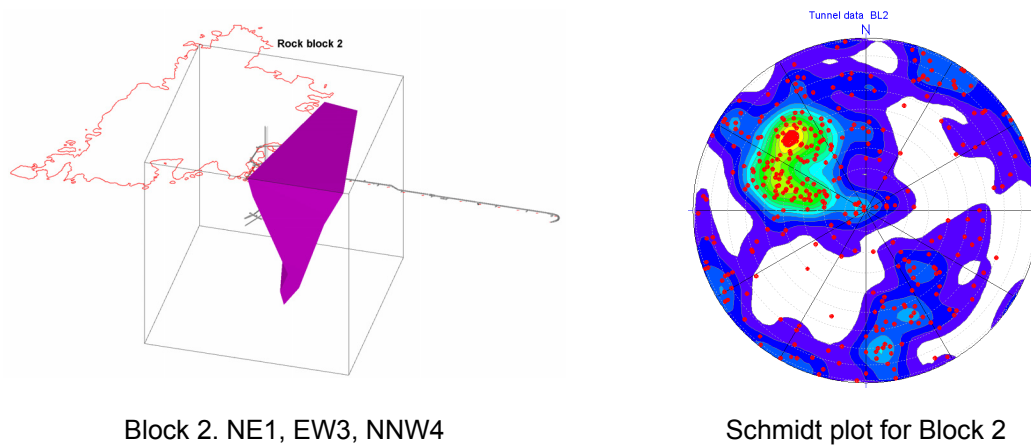


Figure 5-25. Lower hemisphere Schmidt plot (polar net) of poles to fractures mapped in Äspö tunnel block 2.

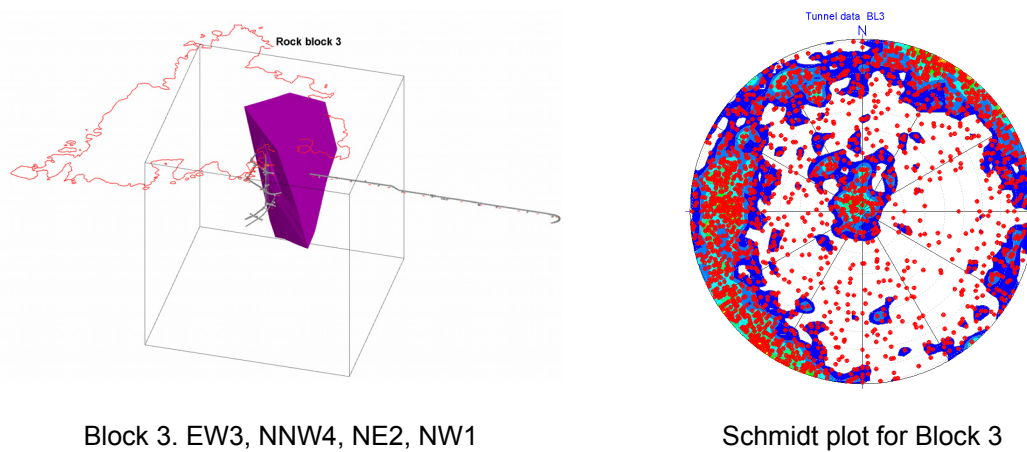
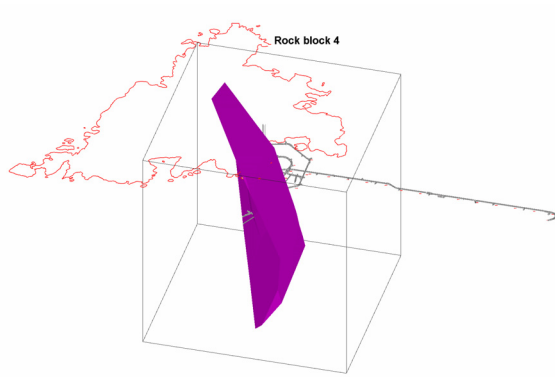
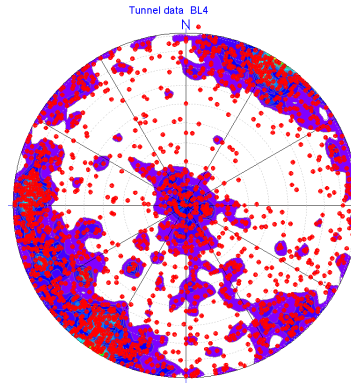


Figure 5-26. Lower hemisphere Schmidt plot (polar net) of poles to fractures mapped in Äspö tunnel block 3.

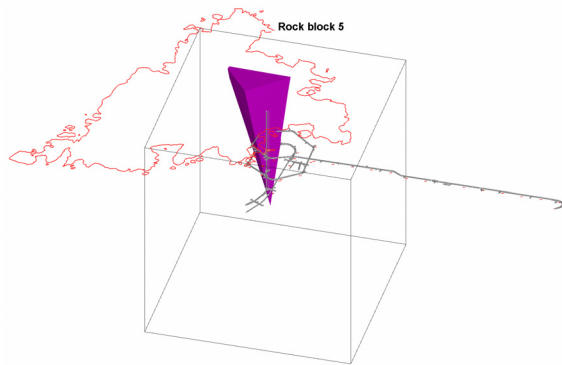


Block 4. NE1, NE2, NEHQ3, EW1

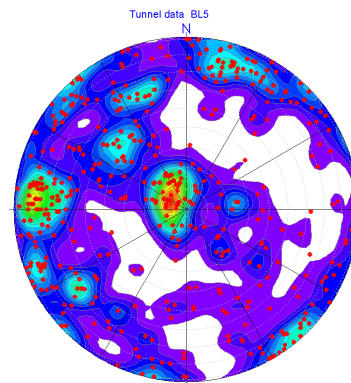


Schmidt plot for Block 4

Figure 5-27. Lower hemisphere Schmidt plot (polar net) of poles to fractures mapped in Äspö tunnel block 4.

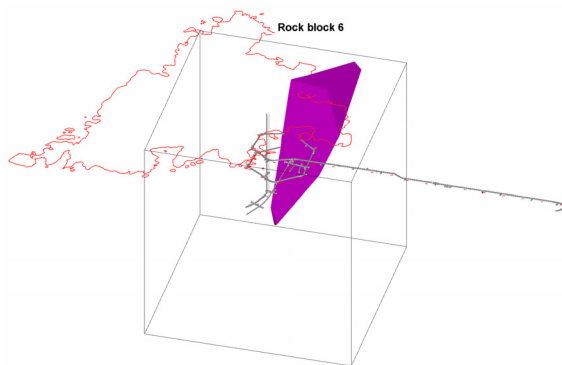


Block 5. NE2, NNW4, NW1, EW1

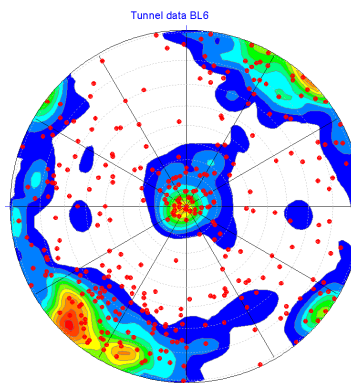


Schmidt plot for Block 5

Figure 5-28. Lower hemisphere Schmidt plot (polar net) of poles to fractures mapped in Äspö tunnel block 5.

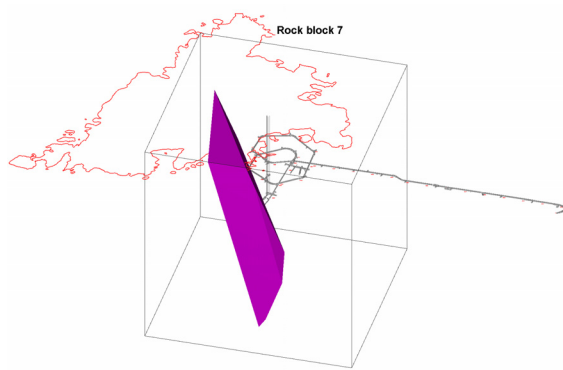


Block 6. NE1, EW3, EW1, NW1

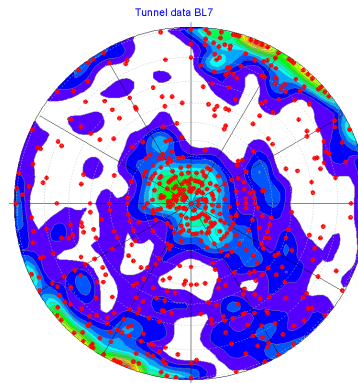


Schmidt plot for Block 6

Figure 5-29. Lower hemisphere Schmidt plot (polar net) of poles to fractures mapped in Äspö tunnel block 6.

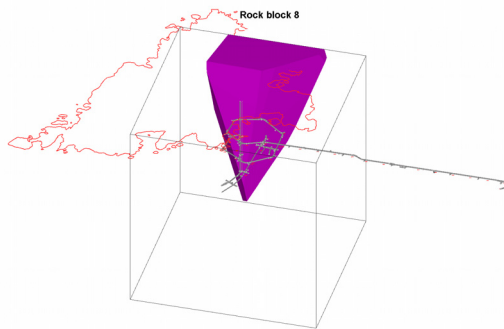


Block 7. NE1, NEHQ3, EW1

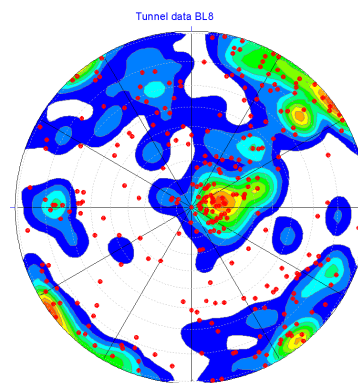


Schmidt plot for Block 7

Figure 5-30. Lower hemisphere Schmidt plot (polar net) of poles to fractures mapped in Äspö tunnel block 7.



Block 8. NE1, EW1, NNW4, NW1, NE2



Schmidt plot for Block 8

Figure 5-31. Lower hemisphere Schmidt plot (polar net) of poles to fractures mapped in Äspö tunnel block 8.

Table 5-12 presents number of observed fractures that belong to each block. For the block definition see chapter 5.5.

Table 5-12. The amount of fractures mapped in each block.

Block name	Number of non water-bearing fractures	Number of water-bearing fractures
BL1	1159	174
BL2	348	47
BL3	2949	262
BL4	3054	346
BL5	558	43
BL6	491	82
BL7	802	61
BL8	462	27

Contingency tables for two sample populations (two blocks tested at a time) were calculated and, consequently, *Chi-2* statistics for each test was derived. Initially, contingency tables were built upon a 34-patch network; however no signs of any similarity in terms of fracture orientations could be seen between tested Schmidt plots. For all tests the null hypothesis on same proportions of poles to fractures between two sample populations could be rejected at 1% significance level. Even though, according to theoretical assumptions on contingency tables, the division even in more than 34 patches would be justified /Miller, 1983/ another test was performed for 16 patches in order to minimize an impact on *Chi-2* statistics from differences between only few cells belonging to two tested grids. This made the test less sensitive to potential differences in fracture orientations between tested sample populations. As this 16 patch-test still resulted in significant differences among tested sample populations, the grid was then divided into only 10 patches. Even for this test array no similarities among blocks could be observed based on *Chi-2* statistics. Table 5-13 summarizes all tests performed for 10 patch-networks and for sample populations that included both water bearing and non water-bearing fractures treated as one lumped data set. Selection of the test groups i.e. choice of blocks tested together was based on their spatial proximity (two blocks separated by a deformation zone were expected to exhibit more comparable orientation sets than, for example, two blocks separated by deformation zones and another block) and also on visual inspection of the Schmidt plots.

Table 5-13. Summary of the null hypotheses test on no difference in fracture orientation between blocks. The test is based on *Chi-2* statistics for 10 patch-network draped on lower hemisphere Schmidt plots. Water-bearing and non water-bearing fractures lumped together.

Compared blocks	Calculated Chi-2 statistics	Critical Chi-2 statistics for 9 degrees of freedom and 1% significance level
BL1 vs. BL2	108	22
BL1 vs. BL3	142	22
BL3 vs. BL5	100	22
BL1 vs. BL4	110	22
BL2 vs. BL3	162	22
BL1 vs. BL5	61	22
BL2 vs. BL5	51	22
BL3 vs. BL4	166	22
BL6 vs. BL8	98	22
BL3 vs. BL6	100	22
BL5 vs. BL6	115	22
BL4 vs. BL7	168	22
BL5 vs. BL8	88	22
BL4 vs. BL5	138	22

For each different division into patches, i.e. 34, 16 and 10 patches the patch network was rotated through 180 degrees by 10 degrees increment. Thus, each pair of Schmidt plots was analyzed 18 times and *Chi-2* statistics was then averaged. This was done to minimize the subjective nature of the patch orientations. For some pairs of Schmidt plots the number of poles found in the network patches was lower than required and *Chi-2* statistics could not be computed /see Miller, 1983/.

Although the visual interpretation of the Schmidt plots in Figure 5-24 - Figure 5-31 may lead to a conclusion that some blocks consists of the same orientation sets (e.g. BL4 and BL6 seem to manifest roughly the same fracture sets), the *Chi-2* statistics does not provide any formalized evidence that such a statement is correct. As the test statistics was calculated for 1% significance level we are willing to risk rejecting the hypothesis when it is correct once out of 100 trials. In other words, a probability of rejecting true hypothesis (= the same fracture orientations in both tested blocks) is only 1%.

The same *Chi-2* statistics as for all fractures (presented previously) and for 10 patch-network was computed separately for non water-bearing and water-bearing fractures (see Table 5-14).

Table 5-14. Summary of the null hypotheses test on no difference in fracture orientation between blocks. The test is based on *Chi-2* statistics for 10 patch-network draped on lower hemisphere Schmidt plots. The analysis was done separately for water-bearing and non water-bearing fractures.

Compared blocks	Type of fractures	Calculated <i>Chi-2</i> statistics	Critical <i>Chi-2</i> statistics for 9 degrees of freedom and 1% significance level
BL1 vs. BL2	non water-bearing	102	22
BL1 vs. BL3	non water-bearing	114	22
BL3 vs. BL4	non water-bearing	155	22
BL3 vs. BL5	non water-bearing	84	22
BL1 vs. BL5	non water-bearing	57	22
BL1 vs. BL4	non water-bearing	94	22
BL2 vs. BL5	non water-bearing	42	22
BL2 vs. BL3	non water-bearing	140	22
BL3 vs. BL6	non water-bearing	99	22
BL4 vs. BL7	non water-bearing	157	22
BL4 vs. BL5	non water-bearing	117	22
BL3 vs. BL4	water-bearing	26	22
BL1 vs. BL2	water-bearing	21	22
BL1 vs. BL3	water-bearing	56	22
BL2 vs. BL3	water-bearing	55	22
BL1 vs. BL4	water-bearing	58	22
BL4 vs. BL7	water-bearing	22	22

On the whole, the similarity in orientation sets between water-bearing fractures was higher than between non water-bearing fractures. This is what the calculated *Chi-2* statistics points out in Table 5-14. For example, for water-bearing fractures at 1% significance level BL1 is not significantly different from BL2; the same applies to blocks BL4 and BL7. Also *Chi-2* statistics for BL3 vs. BL4 does not exceed much the critical level of *Chi-2* whereas *Chi-2* for blocks with non water-bearing fractures only is much larger. However, neither for water-bearing or sealed fractures the results indicates any strong set-similarity between different blocks; see explanation in the chapter “Confidence” below.

As a complement to pair comparison, a set of contingency tables and following *Chi-2* statistics was computed for arrays where more than two blocks were tested together for fracture set similarities. This was done since in some situations homogeneity/similarity in orientation sets on larger scale is not necessarily in compliance with homogeneity on smaller scales. Since the non water-bearing fractures in blocks showed large differences in previously described pair comparisons (Table 5-14) and we did not expected any similarities even on larger scale, this fracture category was not considered for further analysis and only the water-bearing fracture in blocks were subjected to complementary tests. At first BL1, BL2, BL3 and BL4 were tested; for this array the computed *Chi-2* was found to be 147 while the critical *Chi-2* for 1% significance and 27 degrees of freedom was 46. For the test array including BL3, BL4 and BL7 the computed *Chi-2* was 53 and the corresponding critical *Chi-2* (at 1% significance and 18 degrees of freedom) was 35. Thus, for both test arrays the null hypothesis on similarity in fracture sets among the tested blocks was rejected.

Statistical tests (tunnel data depth-dependence)

The between-blocks tests did not reveal any significant similarities in terms of fracture orientations. However, the variability of fracture orientations does not need to be spatially stationary. For example, variation in a vertical direction may be different from the lateral variation. The blocks embrace quite a volume of rock that extends over a sizeable depth interval and fracture orientations may be more stationary in vertical direction than horizontally, since the block-separating steep deformation zones have redistributed stresses in the geological past. To study if any evidence could substantiate this statement, contingency tables and *Chi-2* statistics was compiled for sections in the tunnel exhibiting the same orientation but located at different depths. The tunnel was divided in three main groups termed in this report as Green, Red and Blue. Green and Blue consisted of three and Red of four sub-parallel tunnel sections (see Table 5-15).

By testing if there is any similarity in fracture orientations among sections within each group one could conclude if fracture orientation is depth dependent or not. It ought to be stressed that for those tests no division in distinct structural blocks was done contrary to previous tests.

Table 5-15. Intervals and section depths for the three major tunnel segments (Green, Blue, Red) where all sections within each segment exhibit roughly the same tunnel orientation.

Section name	Section interval (m)	Section depth interval (m)
Green 1.1	1610-1760	228-248
Green 1.2	2065-2200	287-304
Green 1.3	2545-2715	348-370
Blue 1.1	1920-2055	268-285
Blue 1.2	2390-2510	328-344
Blue 1.3	2875-3015	390-408
Red 1.1	1770-1900	249-266
Red 1.2	2215-2345	306-323
Red 1.3	2730-2860	372-388
Red 1.4	3110-3599	420-447

The contingency table was based on a 10 patch-network. The *Chi-2* statistics resulted in rejecting the null hypothesis on the same fracture orientations among tunnel sections at different depths (see Table 5-16).

Table 5-16. Summary of the null hypotheses test on no difference in fracture orientation between tunnel sections. The test was done separately for each segment (Green, Blue, and Red) and is based on *Chi-2* statistics for 10 patch-network draped on lower hemisphere Schmidt plots. In the analysis water-bearing and non water-bearing fractures were lumped together.

Compared sections	Calculated <i>Chi-2</i> statistics	Critical <i>Chi-2</i> statistics for 9 degrees of freedom and 1% significance level
Green 1.1 vs. 1.2	57	22
1.1 vs. 1.3	60	22
1.3 vs. 1.3	59	22
Blue 1.1 vs. 1.2	38	22
1.1 vs. 1.3	52	22
1.2 vs. 1.3	55	22
Red 1.1 vs. 1.2	85	22
1.1 vs. 1.3	132	22
1.2 vs. 1.3	72	22
1.3 vs. 1.4	220	22

For visual inspection of fracture orientations as a function of depth see Figure 5-32, Figure 5-33 and Figure 5-34.

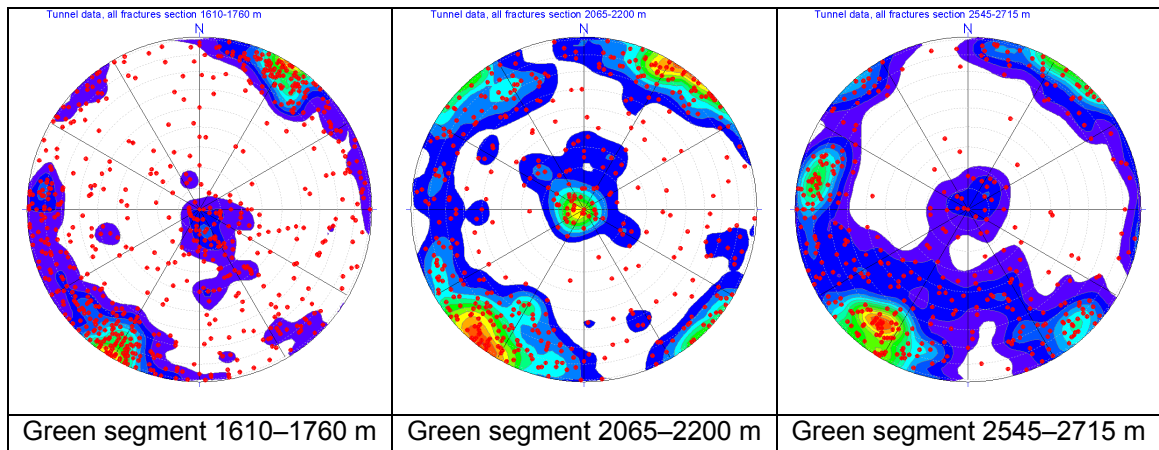


Figure 5-32. Lower hemisphere Schmidt plot (polar net) of fracture poles for three tunnel sections in Green-segment.

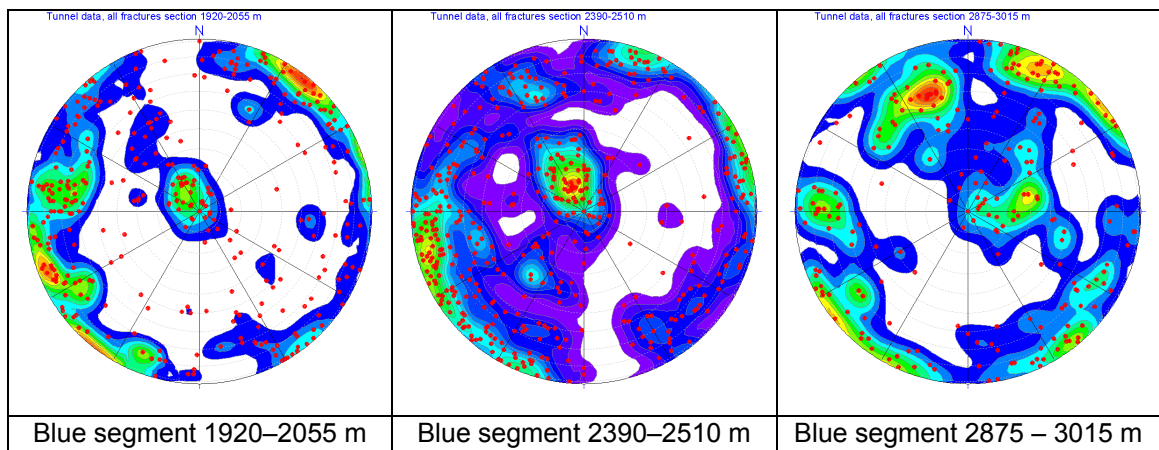


Figure 5-33. Lower hemisphere Schmidt plot (polar net) of fracture poles for three tunnel sections in Blue-segment.

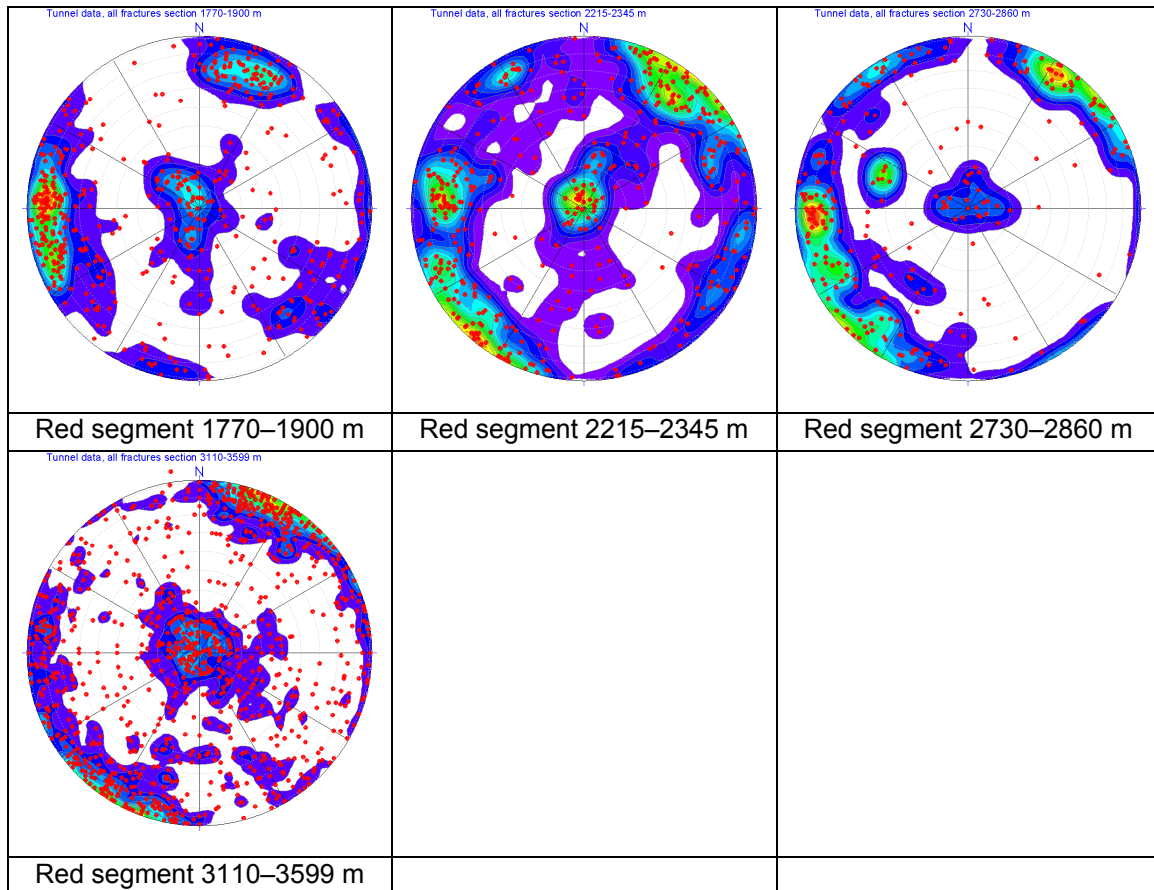


Figure 5-34. Lower hemisphere Schmidt plot (polar net) of fracture poles for four tunnel sections in Red-segment.

Confidence, data quality, uncertainties

All *Chi-2* tests presented in previous chapters were performed for a given significance level. This level was conservatively chosen by the test maker and simply corresponded to a lower bound probability of rejecting true hypothesis. For those tests for which the calculated *Chi-2* statistics exceeded the critical level at 1% significance one certainly would claim that at least from a statistical point of view the evidence pointing at no similarity between (and among) blocks is very strong. In such case the term confidence is expressed as a quantity determined through a formalized procedure. As for these cases the real level of significance is expected to be lower than 1% the opposite hypothesis e.g. blocks contained the same fracture orientation distribution has an extremely low probability to be true. Obviously in some situations coherence between statistical and physical significance may be weak and such discrepancy may imply risk for misinterpretations. However, in cases where rejection of null hypothesis is done at very low significance level (1% in this study) there is little rationale to argue any contradictory conclusions.

For these tests where the null hypotheses could not be rejected at 1% significance (see blocks BL1 vs. BL2 and BL4 vs. BL7 for water-bearing fractures in Table 5-14) the interpretation of the results may appear a bit ambiguous. This ambiguity is due to subjectivity in perception of statistical significance level in relation to its physical implications. The answer on whether water-bearing fractures exhibit the same orientation in BL1 and BL2, and in BL4 and BL7 upon performed *Chi-2* test at 1% significance or not should be put in a context of a potential “severity” the non-rejection of null hypotheses might have on defining blocks as different units. In the authors’ opinion in this particular case the non-rejection of the null hypotheses should be considered if the level of significance is at least 5%. It should be kept in mind that even if non-rejection could be done at let’s say 5% level of significance, from formal point of view it does not automatically entail the acceptance of the opposite hypothesis. Since the computed *Chi-2* statistics for the tests on all fractures was considerably larger for water-bearing fractures (Table 5-14) one could state that there is strong evidence that water-bearing fractures for blocks BL1 vs. BL2 and BL4 vs. BL7 demonstrate more similarity in fracture orientation than non water-bearing fractures.

It is believed that one of the main sources of the uncertainties in the interpretation of the fracture orientation between (and among) the blocks were the orientation sampling bias. No Terzhagi correction was applied on fracture orientations since the position (orientation) of individual fractures in relation to sampling plane was only available in a graphical format and the manual preprocessing of the data was not realistic within the available timeframe for this study.

The validity of the *Chi-2* statistics for testing variability in fracture orientation as a function of depth was believed to be stronger than *Chi-2* statistics for blocks’ testing in view of the fact that the populations tested belonged to tunnel sections manifesting nearly the same tunnel orientation in space and as such were equivalently exposed to orientation sampling bias.

Some could argue that contingency table and *Chi-2* statistics might be in some circumstances not a sufficient method to infer differences/similarities between sample populations with orientation data. As an alternative (or a complement) a cluster analysis might be considered, however clustering principles are by far more complex and results are more sensitive to uncertainty related to conceptualization of fracture sets that constitute each sample population.

Borehole data

Statistical tests

Two major groups of borehole data were analyzed: Boremap and Petrocore data. These two groups were pooled and treated as one lumped group of data. The statistical analysis of fracture orientation followed the same approach as for the tunnel data, i.e. contingency tables and *Chi-2* statistics. The analyzed fractures were made on natural fractures (potentially water-bearing) only. Table 5-17 and Table 5-18 depict those boreholes along with corresponding blocks or zones that were used for fracture orientation analysis. Note that some boreholes penetrate several different blocks.

Table 5-17. Borehole orientations and block/zone-intersections for Petrocore data.

Petrocore boreholes	Block/Zone	hole azimuth	hole inclination
KA2511A	4	234.75	-33.79
KA2598A	4	292.60	-32.15
KA2598A	7	292.60	-32.15
KA3191F	3	259.87	-8.28
KA3191F	3	259.87	-8.28
KAS02	3	330.12	-84.00
KAS02	3	330.12	-84.00
KAS03	Out of bounds (North)	338.12	-82.90
KAS04	11north	140.12	-59.90
KAS04	EW1a-b	140.12	-59.90
KAS04	EW1b	140.12	-59.90
KAS04	7	140.12	-59.90
KAS05	3	163.12	-84.90
KAS05	NE2	163.12	-84.90
KAS05	4	163.12	-84.90
KAS06	3	7.12	-59.60

Table 5-18. Borehole orientations and block-intersections for Boremap data.

Boremap boreholes	Block	hole azimuth	hole inclination
KA2377A01	3	229.60	-5.00
KG0048A01	3	221.70	14.93
KK0045G01	3	135.00	-89.80
KA2599G01	4	310.40	-80.10
KA3376B01	4	45.54	-0.90
KA3386A01	4	219.93	-1.95
KF0066A01	4	16.00	0.50
KI0023B	4	214.43	-20.71
KI0025F02	4	199.63	-25.62
KI0025F03	4	206.89	-29.80
KA3539G	7	0.00	-90.00
KA3542G01	7	188.70	-44.95
KA3542G02	7	6.25	-44.21
KA3548A01	7	188.40	-3.10
KA3554G02	7	8.18	-44.99
KA3557G	7	271.16	-81.49
KA3566G01	7	188.78	-44.87
KA3566G02	7	7.72	-43.80
KA3573A	7	188.41	-2.07
KA3590G01	7	186.66	-44.40
KA3590G02	7	7.94	-43.82
KA3600F	7	248.24	-1.83
KJ0050F01	7	52.20	-4.80
KA3065A02	8	59.91	-4.95
KXTT5	8	47.66	-14.91

Figure 5-35 illustrates density plots of fracture poles for all blocks and deformation zones that could be extracted from available database. It should be pointed out that not all blocks present in previous analysis (tunnel data) could be identified in the borehole data. Prior to statistical analysis fractures were corrected for orientation sampling bias following Terzhagi procedure with a maximum correction factor equal 7 /Dershowitz et al., 1998/.

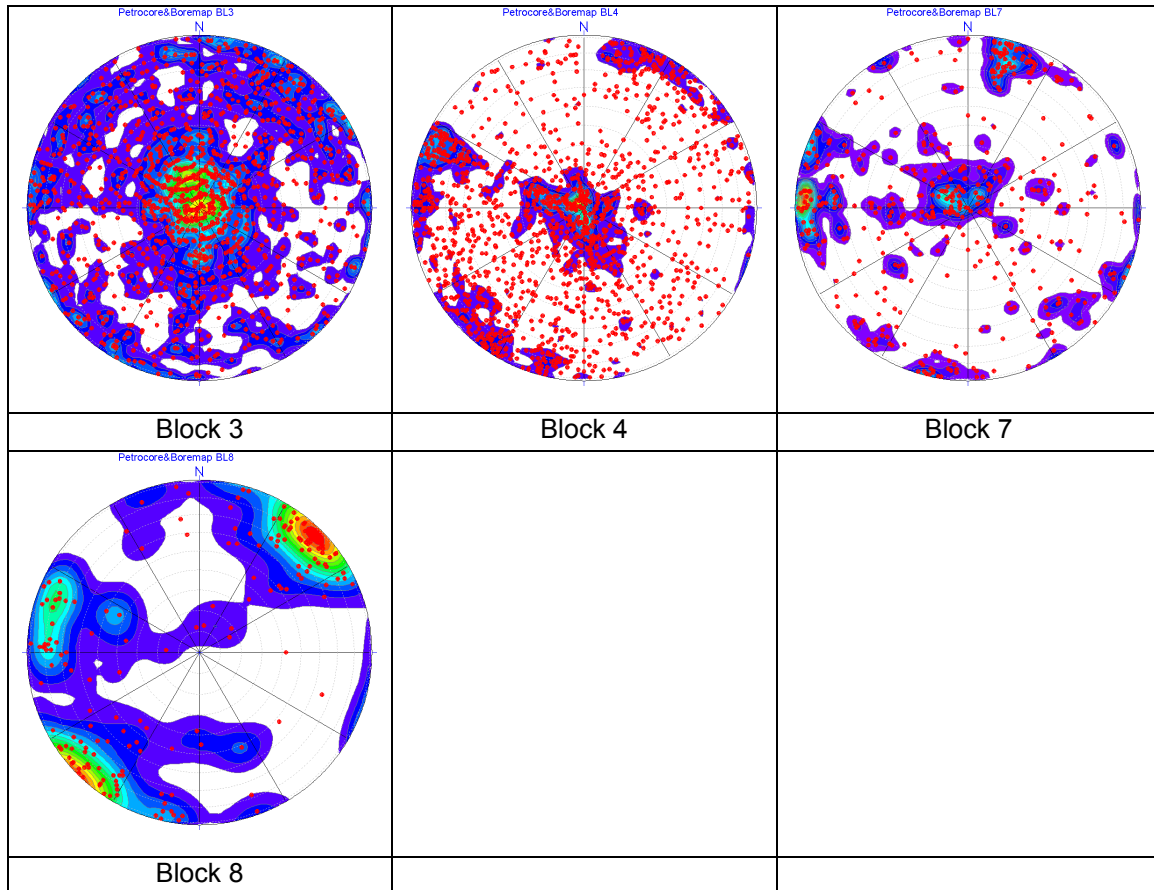


Figure 5-35. Lower hemisphere Schmidt plots (polar net) of poles to natural fractures (potentially water-bearing) mapped within different blocks/zones. Petrocore and Boremap data lumped together.

The results from *Chi-2* statistics based on contingency tables for 10 patch-network are summarized in Table 5-19.

Table 5-19. Summary of the null hypotheses test on no difference in fracture orientation between blocks. The test was done for natural fractures (potentially water-bearing) and for Petrocore and Boremap data lumped together.

Compared blocks	Calculated Chi-2 statistics for 9 degrees of freedom and 1% significance level.
BL3 vs. BL4	194
BL3 vs. BL7	180
BL4 vs. BL7	171
BL7 vs. BL8	107

Because the critical *Chi-2* statistics for 9 degrees of freedom and 1% significance level was much lower than any of the computed *Chi-2* statistics in Table 5-19 (critical *Chi-2* = 22), the null hypothesis on the same orientation sets between blocks was rejected. This points towards a statement that fracture orientations between blocks are rather different; this confirms previous results from the analysis of fracture tunnel data.

Confidence, data quality, uncertainties

The analysis of fracture orientation sets for borehole data was severely constrained by the fact that a substantial number of fractures detected during logging (Boremap data) and core mapping (Petrocore data) did not contain orientation records at all (no strike and dip data). In addition, many remaining fracture orientations were recorded with large, yet not known errors. Also lack in borehole orientation data (azimuth and inclination) for those boreholes where complete and correct fracture orientation records existed made impossible to correct a large portion of fractures for orientation sampling bias and, consequently even being registered those fractures could not be included in the statistical analysis.

It was assumed that the occurrence of fractures with no orientation records as well as fractures with record errors along depth interval in the boreholes had a random character. If this assumption was valid it would be expected that the non- and error-records did not have any serious impact on the statistical analysis as the analyzed population could be simply considered as a random sub-sample from a parent population and as such it should exhibit nearly the same statistical distribution as the parent one. If however, the occurrence of non- and error-records were depth-dependent (and consequently be non-random) there would be a risk that some important information on fracture orientations, which may be characteristic to specific depth intervals could be overlooked. To recap, approximately half of registered fracture population had to be excluded from the analysis due to poor data quality.

Pooling Boremap and Petrocore orientation data and treating them as one lumped data set may also affect statistical analysis. Data spread for the Petrocore seem to be larger than for the Boremap as more distinct clusters were found on Schmidt plots for Boremap data than for Petrocore (Figure 5-36). If both the Boremap data and Petrocore mapping errors are assumed to be non-systematic the orientation features (clusters) present in two or more blocks should be substantiated through *Chi-2* statistics irrespective of fracture detection method. As the *Chi-2* turned to be much higher than the critical rejection level we believed the dissimilarities between blocks were due to the existing differences in fracture sets and not due to discrepancies between measurement/detection methods.

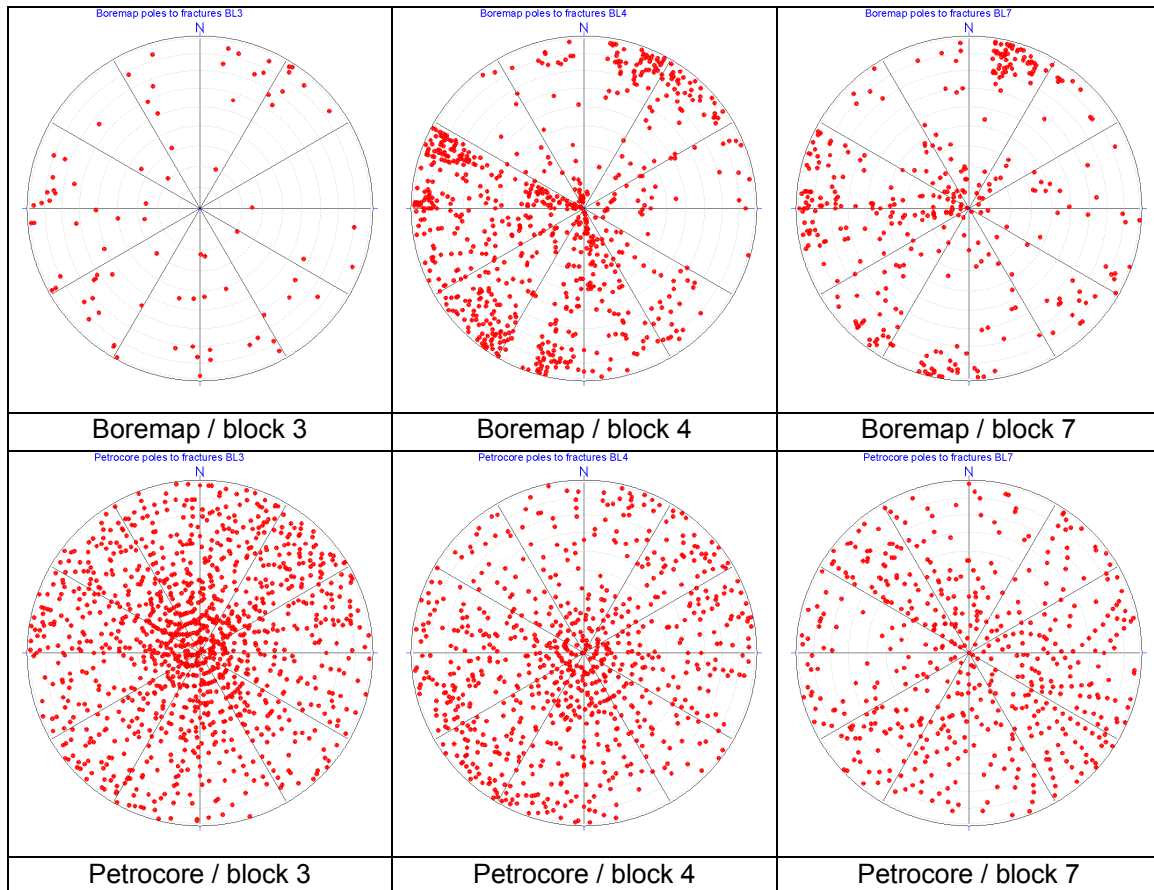


Figure 5-36. Comparison between Boremap and Petrocore fracture orientation data within the same blocks. Lower hemisphere Schmidt plot (polar net) of fracture poles.

Fracture density

Statistical tests

The study on fracture spatial distribution was based on the analysis of the borehole data only. In order to perform a consistent analysis on fracture tunnel data a substantial effort for reprocessing and correcting raw data records was needed and was deemed unrealistic within the timeframe for this study. Further limitations imposed on the density study were that the analysis of 1D fracture density was made using data from Boremap investigations only (see Table 5-17). The reasons for omitting the Petrocore data are given in the reminder of this chapter under section “Confidence, data quality, uncertainties”.

Prior to density analysis, fractures were corrected for the orientation sampling bias following the same correction principles as for the orientation data, i.e. Terzhagi correction with maximum correction factor equal 7. After correcting the fractures their positions along each borehole (or more precisely the between-fracture intervals) were converted to 1D density measure, i.e. number of fractures per meter borehole. As expected, the statistical distribution of fracture density turned out to be positively skewed; in addition the Anderson-Darling normality test /Ryan and Joiner, 2001/ showed that fracture density do not follow normal distribution.

In order to perform a hypothesis test to compare fracture density among blocks a proper statistical test procedure needed to be selected. As the data was non-normal (see *p-value* for Anderson-Darling normality test in Figure 5-38) and strongly asymmetric, only a non-parametric test was to be considered. Any tests based on ranked data (“*Wilcox-family*” tests), were inappropriate since for some of sample populations (fracture density within blocks) the median value was strongly affected by “non-fracture” segments (no fractures detected within 1 m segment along the borehole) and, consequently, this fact made the median a non-representative parameter of the distribution (remind that “*Wilcox-family*” tests are based on comparing medians between tested populations /Box et al., 1978/.

Seeing as it was difficult to find some representative population parameter suitable as a test parameter, a Kolmogorov-Smirnov (*K-S*) test was suggested as according to this procedure more emphasis is put on comparing shape of the populations than any specific population parameter. *K-S* statistics derives a maximum deviation between tested populations found by comparing their cumulative frequency plots and relates this statistics to a critical level for known degrees of freedom and significance level /see Davis, 1986 for details/. Figure 5-38 shows comparison of cumulative frequencies of fracture density for the tested pairs of blocks and Table 5-20 summarizes the results from *K-S* tests. Similarly to *Chi-2* tests on fracture orientations the null hypothesis here assumed that no differences existed between compared sample populations, i.e. in this case: no differences in fracture density between blocks.

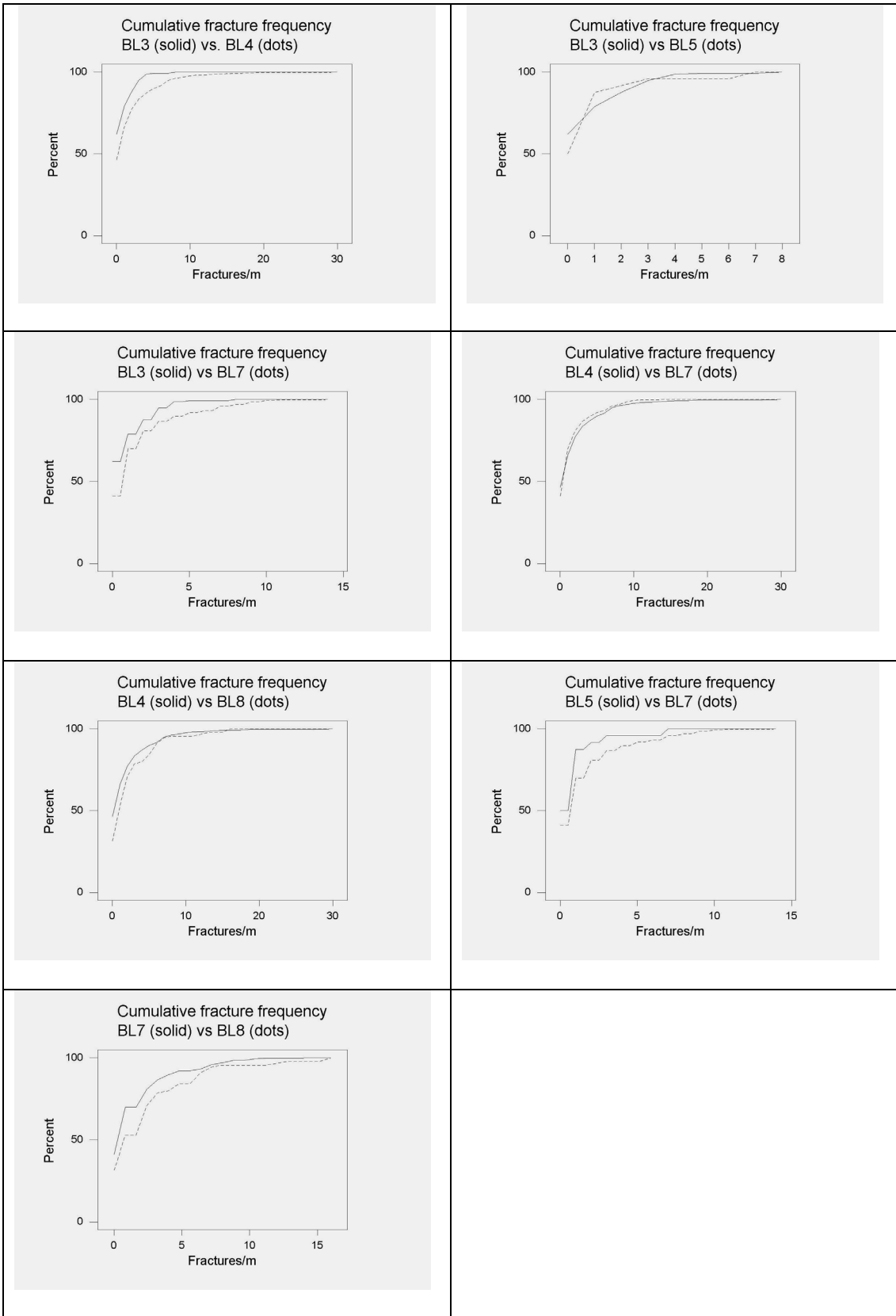


Figure 5-37. Cumulative frequency plots of fracture density. Cumulative plots correspond to pairs of blocks for, which Kolmogorov-Smirnov statistics was computed test a hypothesis on no difference between fracture densities. Only Boremap data considered.

Table 5-20. Kolmogorov-Smirnov statistics computed for pairs of cumulative frequency plot of fracture density within blocks presented in Figure 5-37. Only Boremap data considered.

Compared blocks	K-S statistics	K-S critical at 10% significance level
BL3 vs. BL4	0.16	0.11
BL4 vs. BL8	0.15	0.14
BL3 vs. BL5	0.14	0.27
BL4 vs. BL7	0.05	0.08
BL7 vs. BL8	0.34	0.14
BL3 vs. BL7	0.21	0.12
BL5 vs. BL7	0.07	0.25

According to Table 5-20 several block constellations did not exhibit any strong reasons for rejection the hypothesis on no difference in fracture density. BL3 and BL5 seem to have similar fracture density distribution; the same applies to BL4 and BL7, and, BL5 and BL7.

Confidence, data quality, uncertainties

As mentioned above only the Boremap data were used for fracture density analysis. The Petrocore density data were deemed unreliable since it was observed that nearly all boreholes exhibited several “non-record” intervals (see e.g. depth interval 170 – 250 m in Figure 5-38).

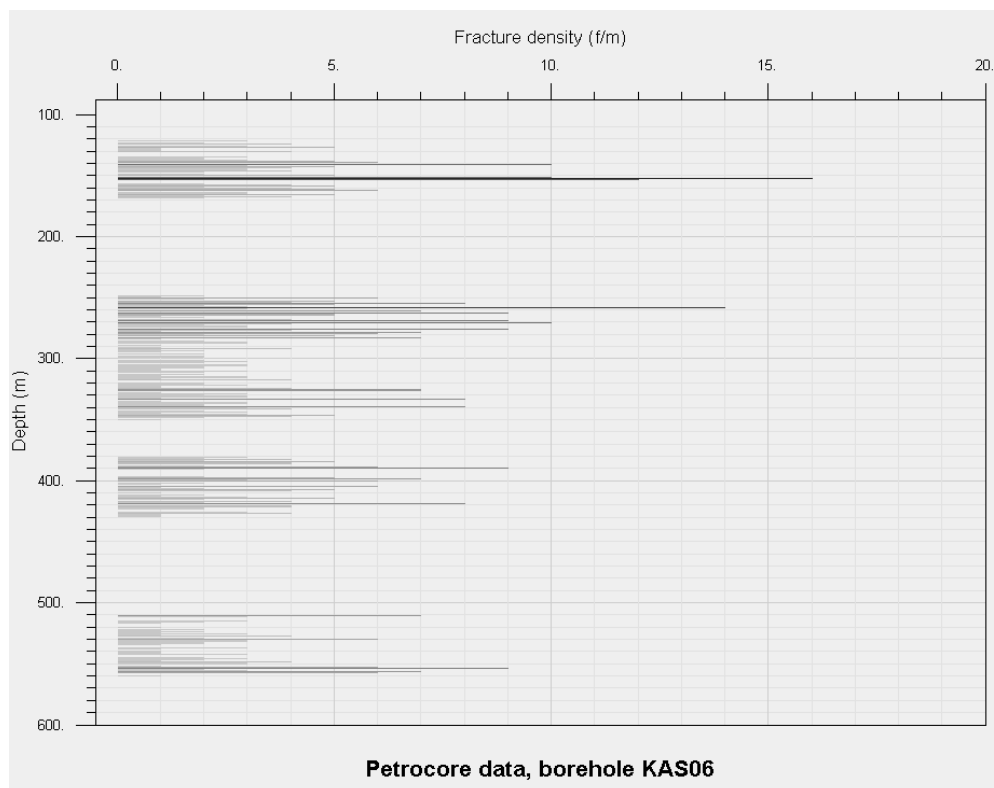


Figure 5-38. Fracture density (fractures/m) as a function of depth in borehole KAS06 (Petrocore data) illustrating “non-records” intervals.

Since no such “zero-fracture” intervals could be observed on the Boremap records it was suspected that the segments of “no-fracture” density must be rather due to recording/detection errors than attributed to a “naturally unfractured” rock mass. This judgment was later confirmed by a deeper analysis of the KAS-boreholes constituting the majority of the Petrocore data. While the fracture records for KAS-boreholes had their origin in two different source files the “missing” fractures (those that represented “non-records” intervals) in one of those files were found in the other though with no record of strike and dip. A possible remedy to circumvent this concern (and continue with statistical analysis on the Petrocore data) was to exclude all “non-record” intervals in the Petrocore data and do statistical analysis on the remaining data. To test if such approach could be still reasonable two Petrocore boreholes were randomly selected from the both above mentioned source files and all the “non-record” intervals were removed from the first file. Subsequently, the corresponding depth segments were excluded from the second source file (even if there were fractures detected within those segments). After this extraction was done, the fracture density data from the first and second file were compared and tested with *K-S* statistics. *K-S* statistic resulted in rejection of the hypotheses on no difference, which lead to a conclusion that fracture records coming from two source files are different even outside the non-record intervals. This test definitely supports the decision to exclude the Petrocore data from statistical analysis on fracture density in this study.

Remember that despite the “non-record” problem the statistical analysis of fracture orientations was performed also on Petrocore data. The reason for this was that the “zero-fracture” intervals have much less impact on fracture orientation statistics than on fracture density. This is of course based on the assumption that the recording/detection errors occur randomly and are not related to any geological structure intersecting a borehole.

Summary

In Table 5-21 an outline of the statistical test results are presented.

Table 5-21. Result summary of fracture statistic tests. The analyzed data and the results are associated with uncertainties et cetera; see related chapters for each statistical test.

#	Null hypothesis	Rejected hypothesis	Data	Comments
1a	No difference in fracture orientations between blocks. Pair blocks comparison.	Yes	Tunnel	The visual interpretation of the Schmidt plots may lead to a conclusion that some blocks consists of the same orientation sets (see Figure 5-24 - Figure 5-31). However, the <i>Chi-2</i> statistics provide that none of the blocks have the same fracture orientation.
1b	No difference in water-bearing fracture orientations between blocks. Pair blocks comparison.	Yes and no	Tunnel	Water-bearing fracture orientations seem to be similar in some blocks (block 1 and 2, 3 and 4 and 4 and 7, respectively).
1c	No difference in non water-bearing fracture orientations between blocks. Pair blocks comparison.	Yes	Tunnel	Non water-bearing fracture orientations seem to be different in all blocks. On the whole, the similarity in orientation between waterbearing fractures was stronger than between non water-bearing fractures.
1d	No difference in non water-bearing fracture orientations between blocks. Multi blocks comparison.	Yes	Tunnel	Non water-bearing fracture orientations seem to be different in all blocks.
1e	No difference in fracture orientations between different depths/tunnel sections. Pair section comparison.	Yes	Tunnel	Fracture orientations seem to change with depth. Generally, the test indicates that the differences in orientations with depth are less obvious then the differences in orientations between blocks.
2a	No difference in fracture orientations between blocks (Boremap and Petrocore data). Pair blocks comparison.	Yes	Borehole	Fracture orientations seem to be different in all blocks. Approximately half of registered fracture population had to be excluded from the analysis due to poor data quality.
2b	No differences in fracture density between blocks (Boremap data) Pair blocks comparison	Yes and no	Borehole	Block 3 and 5, 4 and 7 and 5 and 7, respectively, seem to have similar fracture density distribution.

5.7 Comparison with Äspö96

To a large extent there are only minor adjustments made to deformation zones in model Äspö02 regarding their geometries and characteristics, as compared to the geological model in model Äspö96.

The new data since Äspö96, as described in chapter 4, is limited compared to the amount of data that existed then and essentially all major geological elements were identified already in Äspö96. Two new deformation zones have been modelled in Äspö02, NW1 and NEHQ3. The intersections in the tunnel were there, but no interpolations or extrapolation from them was made.

The RVS-model includes a lot of visualisation, both parameters in boreholes from SICADA, created local parameters in boreholes, reference design files and parameters visualized locally in this project based on data derived from SICADA, TMS, reports, existing design-files and BIPS. The gathering of visualized background data in 3D was not at hand for Äspö96. Some of these data are new.

In Äspö02 a precise location is chosen at each intersection, to be used when the 3D model of a zone is created. The selection is primarily based on the geometry of certain intersections of each zone and to a lesser extent also of the character of each intersection, as described in the zone descriptions earlier in this chapter. In Äspö96 on the other hand the location at a certain level is presented and the general orientation of each zone. Intersections in boreholes are normally given as a wide, approximate borehole length.

Overall the fracture orientations for natural reasons are very similar to what was presented in Äspö96, although there is a difference because the block geometries in the Geomod base model are not the same and the population of fractures therefore differ. The fractures in block 2 have an orientation that is notably different from the average, and partly also block 8. Also the fractures in many of the zones have orientations different from the average.

6 Recommendation for further work

The published model Äspö02 should of course not be regarded as the “final model” of Äspö, but as a living model that should be updated continuously as new data becomes available and interpreted at the site. Protocols should be prepared for all observations of structures that possibly could be modelled deterministically.

This report compiles the present rank of the geological issues that have been considered in the Geomod project. Some work had to be left out because of the cut down of the project. Still other work is desired work that is needed in order to increase the knowledge of the geology at the Äspö site and thus to increase confidence in 3D models presented, both this particular one and others that may come. Work that remains to be done are suggested in this final chapter in the report.

Suggested increase and improvement of background data:

- A compilation of a complete description of TMS, Petrocore and Boremap (and other?) parameters through time; development of terminology and parameters and how they have been are used/not used in specific boreholes/tunnels.
- Comprehensive documentation of mapping methodology.
- Development of a generally accepted geological synthesis and conceptual geological evolution model, comprising lithology, brittle and ductile deformations, alterations and fracture mineralogy.
- A thorough magnetic susceptibility study, which make clear the effect of separate geological phenomena upon the magnetic signature from the total magnetic field upon magnetic maps.
- Expansion of the FCC database with detailed mapping and characterisation of water-conducting features in the lower (chainage 2950 and downward) part of Äspö HRL.
- Expansion of the FCC database with regards to information on grouted sections and fractures.
- Compile interference tests and suggest tests to facilitate modelling of water-bearing structures in the blocks between modelled deformation zones.

Suggested work for model description:

- Statistics within blocks, domains and units.
- Statistics of alteration
- A geological description of the local lithologies and tectonics Äspö HRL is a work that should be extended in the near future to get a more complete understanding of the area.
- Lithological statistics and possibly also modelling. The latter probably require a reinterpretation of the lithological mapping.
- Development of a stringent definition of the deformation zone concept (brittle and ductile), including characteristics and boundary definition.
- Standardized WellCad (or similar) presentation for all boreholes including lithological, minearlogical and structural data as well as selected geophysical logs.
- The cores ought to be reexamined for ductile deformation and the SICADA database complemented. Especially boreholes mapped with Boremap and BIPS images, since there are several indications of ductile deformation that is not found in SICADA. The ductile deformation zones most certainly played an important role during the formation of fractures at Äspö and probably also play an important role in the present day (and future) stress situation and thus the hydraulology.
- A thorough discussion of biases related to modelling of zones based upon different information.
- Development of one or several detailed sub-models, located in areas where background data are concentrated.
- Integrating models between separate geodiciplins.
- A review and modelling of all geophysical investigations at Äspö: this may not be new data but it should be compared with the 'final model' for any discrepancies.

7 References

- Annertz K, 1994.** Manual för tunnelkartring av front, nischer och sidotunnlar. SKB Tekniskt PM Nr 25-95-018, Svensk Kärnbränslehantering AB.
- Aaltonen Jaana, Gustafsson Christer, Nilsson Per, 2003.** Oskarshamn site investigation. RAMAC and BIPS logging and deviation measurements in boreholes KSH01A, KSH01B and the upper part of KSH02. SKB P-03-73
- Andersson J, Ström A, Almén K-E, Ericsson L O, 2000.** Vilka krav ställer djupförvaret på berget? SKB R-00-15, Svensk Kärnbränslehantering AB.
- Andersson P, Byegård J, Dershowitz B, Doe T, Hermanson J, Meier P, Tullborg E-L, Winberg A, (ed.), 2002.** Final report of the TRUE Block Scale project. 1. Characterisation and model development. SKB TR 02-13, Svensk Kärnbränslehantering AB, Stockholm.
- Andersson J, Christiansson R, Hudson J A, 2002.** Site Investigations Strategy for Development of a Rock Mechanics Site Descriptive Model, SKB TR 02-01, Svensk Kärnbränslehantering AB, Stockholm.
- Baker EJ, Lee Y. 1975.** Alternative analysis of geographical contingency tables. The Professional Geographer v.27: 179-188.
- Bergman T, Isaksson H, Johansson R, Lindén A H, Lindgren J, Lindroos H, Rudmark L, Wahlgren C-H, 1998.** Förstudie Oskarshamn. Jordarter, bergarter och deformationszoner. SKB R-98-56, Svensk Kärnbränslehantering AB.
- Bergman T, Isaksson H, Rudmark L, Stanfors R, Wahlgren C-H, Johansson R, 2000.** Förstudie Oskarshamn. Kompletterande geologiska studier. SKB R-00-45, Svensk Kärnbränslehantering AB.
- Bath A, Milodowski A, Ruotsalainen P, Tullborg E-L, Cortés Ruiz A, Aranyossy J-F, 2000.** Evidences from mineralogy and geochemistry for the evolution of groundwater systems during the quaternary for use in radioactive waste repository safety assessment (EQUIP project). EUR report 19613.
- Banwart, S. (ed), 1995.** The Redox experiment in Block scale. SKB Progress Report 25-95-05.
- Beunk F F, Page L M, 2001.** Structural evolution of the accretional continental margin of the Paleoproterozoic Svecofennian orogen in southern Sweden. Tectonophysics 339,67–92.
- Bossart P, Hermansson J, Mazurek M, 2001.** Äspö Hard Rock Laboratory. Analysis of fracture networks based on the integration of structural and hydrogeological observations on different scales. SKB TR 01-21, Svensk Kärnbränslehantering AB.
- Box GEP, Hunter WG, Hunter JS. 1978.** Statistics for Experimenters. Wiley and Sons.

Bäckblom G (ed), 1990. Granskning av Nils-Axel Mörnars arbete avseende postglaciala strukturer på Äspö. SKB PR AR-90-18, Svensk Kärnbränslehantering AB.

Cochran WG. 1954. Some methods for strengthening the common χ^2 tests. *Biometrics* v.10: 417-451.

Curtis P, Elfström M, Stanfors R, 2003. Oskarshamn site investigation Compilation of structural geological data covering the Simpevarp peninsula, Ävrö and Hälö. SKB P-03-07, Svensk Kärnbränslehantering AB.

Davis JC. 1986. *Statistics and Data Analysis in Geology.* John Wiley & Sons. New York.

Dershowitz W, Lee G, Geier JE, Foxford T, La Pointe P, Thomas A. 1998. FracMan. Interactive Discrete Feature Data Analysis, Geometric Modeling and Exploration Simulation. User documentation, v.2.6. Golder Assoc., Inc. Seattle, Washington.

Ericsson L O, 1988. Fracture mapping study on Äspö Island. Findings of directional data. SKB PR 25-88-10, Svensk Kärnbränslehantering AB.

Follin S, Hermanson J. 1996. A Discrete Fracture Network Model of the Äspö TBM Tunnel Rock Mass. AR D-97-001. Swedish Nuclear Waste Management Co., Stockholm.

Gustafsson G, Stanfors R, Wikberg P, 1989. Swedish Hard Rock Laboratory. Firstevaluation of 1988 year pre-investigations and description of the target area, the island of Äspö. SKB TR 89-16, Svensk Kärnbränslehantering AB.

Hermansson J, 1995. Structural geology of waterbearing fractures. SKB PR25-95-23, Svensk Kärnbränslehantering AB.

Hermansson J, Doe T, 2000. March'00 structural and hydraulic model based on borehole data from KI0025F03.

Hermansson J, Follin S, Nilsson P, Nyberg G, Winberg A, 1996. TRUE Block Scale. Updating of the Structural-Hydraulic model and Compilation of Scoping data set. SKB IPR-02-13, Svensk Kärnbränslehantering AB.

Hudson (ed), 2002. Strategy for a Rock Mechanics Site Descriptive Model. A Test Case based on data from the Äspö HRL, SKB R-02-04, Svensk Kärnbränslehantering AB.

Johansson L, Johansson Å, 1990. Isotope geochemistry and age relationships of mafic intrusions along the Protogine Zone, southern Sweden. *Precambrian Research* 48,395–414.

Kornfält K-A, Persson P-O, Wikman H, 1997. Granitoids from the Äspö area, southeastern Sweden – geochemical and geochronological data. *GFF* 119, 109–114.

Kornfält K-A, Wikman H, 1987a. Description of the map of solid rocks around Simpevarp. SKB PR 25-87-02, Svensk Kärnbränslehantering AB.

Kornfält K-A, Wikman H, 1987b. Description to the map (No 4) of solid rocks of 3 small areas around Simpevarp. SKB PR 25-87-02a, Svensk Kärnbränslehantering AB.

Kornfält K-A, Wikman H, 1988. The rocks at Äspö island, description to the map of solid rocks including 3 uncovered trenches. SKB PR 25-88-12, Svensk Kärnbränslehantering AB.

Kresten P, Chyssler J, 1976. The Götömar massif in southeastern Sweden: A reconnaissance survey. Geologiska Föreningens i Stockholm Förhandlingar 98, 155–161.

Kulatilake PHSW, Wathugala DN, Stephansson O, 1990. Analysis of structural homogeneity of rock mass around ventilation drift Stripa mine. In Barton N, Stephansson O (eds), Rock Joints.

LaPointe P, Wallmann P, Follin S, 1995. Estimation of effective block conductivities based on discrete network analyses using data from the Äspö site, SKB TR-95-15, Svensk Kärnbränslehantering AB.

Laaksoharju M, Gurban I, In press. Update of the hydrogeochemical model 2002. IPR-03-36. Svensk Kärnbränslehantering AB.

Laaksoharju M, Tullborg E-L, Wikberg P, Wallin B and Smellie J, 1999. Hydrogeochemical conditions at Äspö HRL Sweden. Applied Geochemistry, 14, 835-860.

Larson S Å, Tullborg E-L, 1993. Tectonic regimes in the Baltic Shield during the last 1200 Ma – A review. SKB TR 94-05, Svensk Kärnbränslehantering AB.

Maddock R H, Hailwood E A, Rhodes E J, Muir Wood R, 1993. Direct fault dating trials at the Äspö Hard Rock Laboratory. SKB TR 93-24, Svensk Kärnbränslehantering AB.

Mazurek M, Bossart P, Eliasson T, 1996. Classification and characterisation of water-conducting features at Äspö: Results of investigations on the outcrop scale. SKB ICR 97-01, Svensk Kärnbränslehantering AB.

Miller SM. 1983. A statistical method to evaluate homogeneity of structural populations. Mathematical Geology. 15:317-328.

Milnes A G, Gee D G, 1992. Bedrock stability in southeastern Sweden. Evidence from fracturing in the Ordovician limestones of northern Öland. SKB TR 92-23, Svensk Kärnbränslehantering AB.

Milnes A G, Gee D G, Lund C-E, 1998. Crustal structure and regional tectonics of SE Sweden and the Baltic Sea. SKB TR 98-21, Svensk Kärnbränslehantering AB.

Munier R, Riad, L, Tullborg E-L, Wikman H, Kornfält K-A, 1988. Detailed investigation of drill-cores KAS02, KAS03 and KAS04 on Äspö island and KLX01 at Laxemar. SKB PR 25-88-11, Svensk Kärnbränslehantering AB.

Munier R, 1989. Brittle tectonics on Äspö, SE Sweden. SKB PR 25-89-15, Svensk Kärnbränslehantering AB.

- Munier R, 1995.** Studies of geological structures at Äspö. Comprehensive summary of results. SKB PR 25-95-21, Svensk Kärnbränslehantering AB.
- Munier R, Hermansson J, 1994.** Updating of the geological-structural model. Comilation of technical notes. SKB PR25-94-05, Svensk Kärnbränslehantering AB.
- Mörner N-A, 1989.** Postglacial faults and fractures on Äspö. SKB PR 25-89-24, Svensk Kärnbränslehantering AB.
- Nisca, D H, Triumpf, C-A, 1989.** Detailed geomagnetic and geoelectric mapping of Äspö. SKB Progress Report 25-89-01. Swedish Hard Rock Laboratory.
- Nisca, D, 1987.** Aerogeophysical interpretation. SKB Progress Report 25-87-04. Swedish Hard Rock Laboratory.
- Puigdomenech I, Banwart S, Bateman K, Milodowski A E, West J M, Griffault L, Gustafsson E, Hama K, Yoshida H, Kotelnikova S, Pedersen K, Lartigue J- E, Michaud V, Trotignon L, Morosini M, Rivas Perez J, Tullborg E-L, 1999:** Redox experiment in detailed scale. SKB ICR 99-01, Svensk Kärnbränslehantering AB.
- Rhén I, Gustafson G, Stanfors R, Wikberg P, 1997.** Äspö HRL –Geoscientific evaluation 1997/5. Models based on site characterization 1986-1995. SKB TR 97-06, Svensk Kärnbränslehantering AB.
- Rhén I, Forsmark T, 2000.** Äspö Hard Rock Laboratory, High-permeability features (HPF). SKB IPR-00-02, Svensk Kärnbränslehantering AB.
- Ryan B, Joiner BL. 2001.** Minitab™ Handbook. 4th edition. Duxbury Thomson Learning. Canada.
- Rønning J H S, Kihle O, Mogaard J O, Walker P, 2003.** Simpevarp site investigation. Helicopter borne geophysics at Simpevarp, Oskarshamn, Sweden. SKB P-03-25.
- Sehlstedt S, Stråhle A, Triumpf C-A, 1990.** Geological core mapping and geophysical borehole logging in the boreholes KBH02, KAS09, KAS11-KAS14 and HAS18-HAS20 at Äspö. PR 25-90-06, Svensk Kärnbränslehantering AB.
- SKB, 1992.** Passage through water-bearing fracture zones, compilation of technical notes, passage through fracture zone NE-1. Hydrogeology and groundwater chemistry, SKB PR 25-92-18c, Svensk Kärnbränslehantering AB.
- SKB, 2002.** Simpevarp - site descriptive model version O. SKB R-02-35 Svensk Kärnbränslehantering AB.
- Slunga R, 1989.** Analysis of the earthquake mechanisms in the Norrbotten area. In Bäckblom & Stanfors (eds), Interdisciplinary study of post-glacial faulting in the Lansjärv area northern Sweden. 1986–1988. SKB TR 89-31, Svensk Kärnbränslehantering AB.
- Slunga R, Norrman P, Glans A-C, 1984.** Baltic shield seismicity, the results of aregional network. Geophysical research letters 11, 1247–1250.

- Smellie J A T and Stuckless J S, 1985.** Element mobility studies of two drillcores from the Götemar granite, southeast Sweden. *Chemical Geology*, **51**, 55-78.
- Stanfors R, Liedholm M, Munier R, Olsson P, Stille H, 1993.** Geological-structural and rock mechanical evaluation of data from tunnel section 1475-2265 m. PR 25-93-10, Svensk Kärnbränslehantering AB.
- Stanfors R, Rhén I, Forsmark T, Wikberg P, 1994.** Evaluation of fracture zone EW1, based on the cored boreholes KA1755A, KA1751A and KAS04. PR 25-94-39, Svensk Kärnbränslehantering AB.
- Stanfors R, Rhén I, Tullborg E-L, Wikberg P, 1999.** Overview of geological and hydrogeological conditions of the Äspö hard rock laboratory site.
- Staub I, Fredriksson A, Outters N, 2002.** Strategy for a Rock Mechanics Site Descriptive Model – Development and testing of the Theoretical Approach SKB R-02-02, Svensk Kärnbränslehantering AB.
- Stephansson O, Dahlström L-O, Bergström K, Sarkka P, Vitinen A, Myrvang A, Fjeld O, Hansen T H, 1987.** Fennoscandian Rock Stress Database – FRSDDB. Researchreport TULEA 1987:06, Luleå University of Technology, Luleå.
- Stephens M B, Wahlgren C-H, 1996.** Post-1.85 Ga tectonic evolution of the Svecofennian orogen with special reference to central and SE Sweden. *GFF* 118, Jubilee Issue, A26–27.
- Stigsson M, Outters N, Hermanson J. 2001.** Äspö Hard Rock Laboratory. Prototype Repository. Hydraulic DFN model no:2. IPR-01-39. Swedish Nuclear Waste Management Co., Stockholm.
- Stråhle A, 2001.** Definition och beskrivning av parametrar för geologisk, geofysisk och bergmekanisk kartering av berg. SKB R-01-19, Svensk Kärnbränslehantering AB.
- Talbot C, Riad L, Munier R, 1988.** The geological structures and tectonic history of Äspö, SE Sweden. PR 25-88-05, Svensk Kärnbränslehantering AB.
- Talbot C, Munier R, 1989.** Faults and fracture zones in Äspö. SKB PR 25-89-11, Svensk Kärnbränslehantering AB.
- Talbot C, Ramberg H, 1990.** Some clarification of the tectonics of Äspö and its surroundings. SKB PR 25-90-15, Svensk Kärnbränslehantering AB.
- Tirén S A, Beckholmen M, Isaksson H, 1987.** Structural analysis of digital terrain models, Simpevarp area, southeastern Sweden. Method study EBBA II. SKB PR 25-87-21, Svensk Kärnbränslehantering AB.
- Tiren S A, Beckholmen M, 1987.** Structural analysis of contoured maps. Äspö and Ävrö, southeastern Sweden. PR 25-87-22, Svensk Kärnbränslehantering AB.
- Triumf, C-A, Thunehed, H, Kero, L, Persson, L, 2003.** Oskarshamn site investigation. Interpretation of airborne geophysical survey data. Helicopter borne survey data of gamma ray spectrometry, magnetics and EM from 2002 and fixed wing airborne survey data of the VLF-field from 1986. SKB P-03-XXX

- Tullborg E-L, 1997.** Recognition of low-temperature processes in the Fennoscandianshield. Ph.D. thesis at Geological Department at the Institution for Geosciences.Geovetarcentrum, Göteborgs Universitet, 41381 Göteborg, Sweden.
- Tullborg E-L, Larson S Å, Stiberg J-A, 1996.** Subsidence and uplift of the presentland surface in the southeastern part of the Fennoscandian Shield. GFF 118, 126–128.
- Wahlgren C-H, Danielsson P, Berglund J, Triumf C-A, Mattsson H, Thunehed H, 2003.** Geologiskt underlag för val av prioriterad plats inom området väster om Simpevarp. Delrapport 1-4. SKB P-03-06, Svensk Kärnbränslehantering AB.
- Wallin B and Peterman Z, 1999.** Calcite fracture fillings as indicators of Palaeohydrogeology at Laxemar at the Äspö Hard Rock Laboratory, southern Sweden. Applied Geochemistry, 14, 953-962.
- Vidstrand P, In press.** Update of the hydrogeological model 2002. IPR-03-35. Svensk Kärnbränslehantering AB.
- Wikberg P (ed), Gustafsson G, Rhén I, Stanfors R, 1991.** Äspö Hard Rock Laboratory. Evaluation and conceptual modelling based on the pre-investigations. SKB TR 91-22, Svensk Kärnbränslehantering AB.
- Wikman H, Kornfält K-A, 1995.** Updating of a lithological model of the bedrock of the Äspö area. SKB PR 25-95-04, Svensk Kärnbränslehantering AB.
- Wikström A, 1989.** General geological-tectonic study of the Simpevarp area with special attention to the Äspö island. SKB PR 25-89-06, Svensk Kärnbränslehantering AB.
- Winberg A, Andersson P, Hermanson J, Byegård J, Cvetkovic V, Birgersson L, 2000.** Final report on the first stage of the tracer retention understanding experiments. SKB TR 00-07, Svensk Kärnbränslehantering AB.
- Winberg A, Hermansson J, 1996:** TRUE Block Scale Experiment. Allocation of Experimental Volume. SKB IPR-02-14, Svensk Kärnbränslehantering AB.
- Åberg G, Löfvendahl R and Levi B, 1984.** The Göttemar granite - isotopic and geochemical evidence for a complex history of an orogenic granite. Geologiska Föreningens i Stockholm Förhandlingar, 106, 297-400.

Appendix 1

Waterbearing fractures

WATER BEARING FRACTURES

Äspö Main tunnel

Applied volume- subgeomod, start at ch 1+450m

Resources:

TMS 2D mapping and attached database in Microstation V8

TMS 3D selective mapping results in Microstation V8

RVS V3.2 (Curtis)

RVS tool used: create lens, length 30m, width 30m, depth 0.1m,

Position: each lens placed on the water bearing fracture trace line (not at the tunnel centreline intersection)

Orientation: Strike and dip taken from the TMS 2D database and graphics

Note: recorded strikes appear to be inconsistent with respect to the digitised graphics

Selection: fractures crossing the entire tunnel width or greater than 7m length in database.

Note: the recorded length appears to be inconsistent with respect to the graphical digitised length.

3D mapping files used:

TK1FRD

TK2FRD

TK3FRD

TK4FRD

TK5FRD

TTBMFR3D

	Allready modelled zone; dont use these values
	Water conducting features with ductile precursor
	Water conducting features with T larger than 10 -6, or indications of flowing wat

Note: TASA (m) approx, only as a localisation aid

Data from TMS			Correlation with ICR97-01 (database ends at approximately TASA3000)	
TASA (m)	strike	dip		Zone
1-482		262	52	
1-538		4	63	1536
1-556		330	84	1555
1-568		108	86	
1-586		360	48	
1-643		287	88	
1-697		121	74	1698
1-714		56	25	
1-750		1	80	
1-845		32	79	1845
1-875		110	84	1876
1-906		350	82	
1-925		346	80	
1-988		10	66	
1-990		288	88	1990
2-027		330	77	
2-060		346	85	
2-088		280	80	2090
2-148		311	90	
2-155		323	88	2154
2-157		282	90	
2-163		126	90	2163
2-178		107	80	
2-197		306	80	2198
2-208		107	90	
2-210		340	85	
2-211		300	85	
2-220		309	70	2220
2-230		125	80	2230
2-283		137	88	2282
2-295		135	30	
2-296		177	78	
2-302		360	68	
2-305		133	68	2305
2-338		125	75	2338
2-352		351	90	2351
2-371		322	88	
2-383		146	90	
2-459		173	60	
2-465		245	65	
2-470		186	70	
2-510		160	88	
2-517		43	90	
2-549		247	67	
2-577		302	68	2575
2-580		288	56	
2-585		300	88	2585
2-621		300	76	2620
2-628		138	89	
2-643		140	90	
2-645		133	79	
2-650a		310	69	
2650b		285	74	
2-665		309	80	2667
2-680a		67	25	
2-680b		15	32	

2-720	123	6	
2-726	310	88	
2-732	290	85	
2-765	4	82	
2-847	354	78	missing from 3D, not modelled
2-850	354	78	missing from 3D, not modelled
2-876	356	85	
2-910	101	90	
2-940	311	84	2935
3-060	131	85	
3-093	140	88	
3-101a	101	79	
3-101b	304	82	
3-111	107	78	
3-125	318	87	
3-132	111	79	
3-135	110	80	
3-147	109	78	
3-150	300	90	
3-153	303	90	
3-154	205	90	
3-160	301	90	
3-164	130	80	
3-194	118	74	
3-205	110	90	
3-229	28	68	
3-276	85	80	
3-278	108	88	
3-280	125	90	
3-284	350	90	
3-290	352	2	
3-292	130	86	
3-296	296	88	
3-305	111	65	
3-313	306	82	
3-314	155	90	
3-362	305	85	
3-364	311	86	
3-393	282	52	
3-401	104	90	
3-405	279	86	
3-445a	281	82	
3-460	112	88	
3-467	116	82	
3-502	105	88	
3-536	150	87	
3-570	45	20	poor positioning
3-585	45	15	
3-591	318	74	
3-600	298	23	
END			

Appendix 2

Protocols over observations of deformation zones (not completed for all observation points, data available in SICADA).

Zone	Protocol Id
ZAS0002A0 (NE1)	TASA1290
ZAS0003A0 (EW3)	TASA1407 KAS06
ZAS0004A0 (NE2)	Surface_trench TASH150 TASA3336 TASA2862 TASA2476 TASA1844 TASA1602 KC0045
ZAS0007A0 (NW1)	TASA3083 TASA1979 TASA1876 KAS06 KA3105 KA2050
ZAS0005A0 (NNW4)	TASA2914 TASA2120 TASA2020 KA2048
ZAS0008A0 (NW2)	TASA2914
ZAS0006A0 (NEHQ3)	TASF15 TASA3518 KJ0044F01 KA3510A
ZAS0001A0 (EW1)	-

TASA1290

Protocol Id:

Deformation zones, single observations

Observation based on
 TMS-mapping: tkart2.dgn
 TMS-database: tms.mdb
 Design-file: Frac_Cat_2002_J_Ä96.dgn Source: This project
 Parameters from SICADA:
 Coremapping protocol- Source:
 BIPS pictures- Source: Äspö archive
 Other: Fracture Zone Catalogue Reference: PR25-95-21

<i>Tunnel section(s):</i>	<i>Borehole section(s):</i>	<i>Other:</i>
TASA 1290-1325m	-	-

Zone name: NE1 (Z6, Z7) *Uncertainty (C/P/Po/N):*

<i>Host rock type</i> PSF (~55%), HSC (~40 %), VB (~5%)	P																				
<i>Width</i> 27.8 metre	P																				
<i>Alteration</i> Weak (Z6) –complete (Z7)	P																				
<i>Zone orientation</i> 230//70	P																				
<i>No of sets:</i> 6 (Z6-5, Z7-1)	P																				
<i>Fracture intensity, Spacing, m (number of fractures if recorded)</i>	N/P																				
<table border="0"> <thead> <tr> <th></th> <th>set 1</th> <th>set 2</th> <th>set 3</th> </tr> </thead> <tbody> <tr> <td></td> <td>NA, 0.4(77), 0.15(80), 0.15(80)</td> <td>0.2(94), 0.2(94)0.1(256)</td> <td>0.1(109) 0.2(77), 0.2(99)</td> </tr> <tr> <td></td> <th>set 4</th> <th>set 5</th> <th>set 6</th> </tr> <tr> <td></td> <td>0.2(144), 0.2(42)</td> <td>0.2(65)</td> <td>0.002(933)</td> </tr> </tbody> </table>			set 1	set 2	set 3		NA, 0.4(77), 0.15(80), 0.15(80)	0.2(94), 0.2(94)0.1(256)	0.1(109) 0.2(77), 0.2(99)		set 4	set 5	set 6		0.2(144), 0.2(42)	0.2(65)	0.002(933)				
	set 1	set 2	set 3																		
	NA, 0.4(77), 0.15(80), 0.15(80)	0.2(94), 0.2(94)0.1(256)	0.1(109) 0.2(77), 0.2(99)																		
	set 4	set 5	set 6																		
	0.2(144), 0.2(42)	0.2(65)	0.002(933)																		
<i>Orientation</i>	P																				
<table border="0"> <thead> <tr> <th></th> <th>set 1</th> <th>set 2</th> <th>set 3</th> </tr> </thead> <tbody> <tr> <td></td> <td>230/70, 341/45</td> <td>94/55</td> <td>60/32</td> </tr> <tr> <td></td> <td>230/35, 120/35</td> <td>50/55, 310/75</td> <td>230/45, 220/55</td> </tr> <tr> <td></td> <th>set 4</th> <th>set 5</th> <th>set 6</th> </tr> <tr> <td></td> <td>284/90, 30/25</td> <td>310/38</td> <td>230/70</td> </tr> </tbody> </table>			set 1	set 2	set 3		230/70, 341/45	94/55	60/32		230/35, 120/35	50/55, 310/75	230/45, 220/55		set 4	set 5	set 6		284/90, 30/25	310/38	230/70
		set 1	set 2	set 3																	
	230/70, 341/45	94/55	60/32																		
	230/35, 120/35	50/55, 310/75	230/45, 220/55																		
	set 4	set 5	set 6																		
	284/90, 30/25	310/38	230/70																		

Length (average) set 1-6
Variability (+/- 2 sigma) NA

Water
(Y/N, l/min)
 Total 2000 l/min in FZC

Mineralogy
(percentage NA)

set 1	set 2	set 3
Y, NA	N	N
set 4	set 5	set 6
N	N	Y, NA
set 1	set 2	set 3
Fe, Ca Chl	Fe, Ca Qz, Chl	Ep, Qz, My
Set 4	set 5	set 6
Ca, Fe	Ca, Chl	Cy, Chl, My

C
P
P

Grouting: Y

Remark: The mylonitic, 1-2 metres wide Z7 lies in the centre of a fine grained granite, in the central part of NE1 and is strongly-completely clay altered. It has the same orientation as Z6. The zone is strongly water bearing and there are also fractures around the zone with various orientation, which are water bearing. Ca 10 metres south of the zone there is also a fractured and water bearing fine grained granite (Z5), with the same strike as the zone (Z6).

Protocol Id:**Deformation zones, single observations***Observation based on*

TMS-mapping: tkart2.dgn

TMS-database: tms.mdb

Design-file: Frac_Cat_2002_J_Ä96.dgn Source: This project

Parameters from SICADA:

Coremapping protocol-

Source:

BIPS pictures-

Source: Äspö archive

Other: Fracture Zone Catalogue

Reference: PR25-95-21

*Tunnel section(s):**Borehole section(s):**Other:*

TASA 1407-1422m	-	-
-----------------	---	---

Zone name:EW3 (Z9, Z0)

Uncertainty (C/P/Po/N):

Host rock type

PSF (~80%), HSC (~15 %), PSE (~5%)

P

Width

12.1 metre

P

Alteration

Weak-medium

P

Zone orientation

89/73 (Z9), 71/76 (Z0)

P

No of sets:

5 (Z9-4, Z0-1)

P

*Fracture intensity,*Spacing, m set 1 set 2 set 3
NA, 0.05(232) 0.1(71) 0.2(55)*(number of fractures
if recorded)*set 4 set 5
0.3(41) 0.002(760)

N/P

*Orientation*set 1 set 2 set 3
89/73, 19/74 58/45 62/70set 4 set 5
290/78 71/76

P

Length (average)

set 1-5

Variability (+/- 2 sigma) NA

C

Water
(Y/N, l/min)
Total 90 in FZC

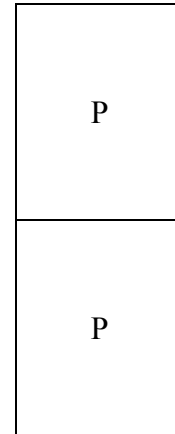
set 1	set 2	set 3
Y, NA	N	NA

set 4	set 5
NA	Y, NA

Mineralogy
(percentage NA)

set 1	set 2	set 3
Chl	Fl, Chl, Ca	Chl

set 4	set 5
Fl, Chl	Chl, Cy



Grouting: Y

Remark: Z0 is a partly clay altered, 1.5-2 metres wide zone in the central part of EW3. The zone is strongly water bearing, and there are also many fractures on each side of the zone that are water bearing. Most of them are sub-parallel to EW3.

Protocol Id:

KAS06

Deformation zones, single observations

Related protocols: -

<i>Observation based on</i> TMS-mapping: TMS-database: Design-file: Source: Parameters from SICADA:corelogging Method: pc_logging_new and petrocore Coremapping protocol- Source: BIPS pictures- Source: Äspö archive Other: Reference:	
--	--

<i>Tunnel section(s):</i>	<i>Borehole section(s):</i>	<i>Other:</i>
	59.8-72.5	-

Zone name: EW3

Uncertainty (C/P/Po/NA):

<i>Host rock type (%)</i>		P
<i>Width</i>		NA
<i>Alteration</i>	Medium to strong tectonisation	NA
<i>Zone orientation</i>		NA
<i>No of sets: NA</i>		NA
<i>Fracture intensity, Spacing, m (number of fractures if recorded)</i>	NA 119 natural fractures	P
<i>Orientation</i>	NA	NA
<i>Length (average) Variability (+/- 2 sigma)</i>	NA	NA
<i>Water (Y/N, l/min)</i>	NA	NA
<i>Mineralogy (percentage NA)</i>	NA	NA
<i>Grouting: NA</i>		

Remark:

Protocol Id:

Surface_trench

Deformation zones, single observations

Observation based on
 TMS-mapping:
 TMS-database:
 Design-file:AS_crop.dgn, AS_trench.dgn Source: Sycon
 Parameters from SICADA:
 Coremapping protocol- Source:
 BIPS pictures- Source: Äspö archive
 Other: Geological map over Äspö and uncovered trench Reference: PR25-88-12
 Technical note 25-93-07i PR25-94-05

<i>Tunnel section(s):</i>	<i>Borehole section(s):</i>	<i>Other:</i>
		Surface outcrop

Zone name: NE2 *Uncertainty (C/P/Po/NA):*

<i>Host rock type</i>	Granodiorite to granite (100%)	Po
<i>Width</i>	4 metre	P
<i>Alteration</i>	NA	NA
<i>Zone orientation</i>	35/80	P/Po
<i>No of sets:</i>	NA	NA
<i>Fracture intensity, Spacing, m (number of fractures if recorded)</i>	NA	NA
<i>Orientation</i>	NA	NA
<i>Length (average) Variability (+/- 2 sigma)</i>	NA	NA
<i>Water (Y/N, l/min)</i>	NA	NA
<i>Mineralogy (percentage NA)</i>	NA	NA
<i>Grouting:</i>	NA	

Remark: This mylonite was mapped in an excavated trench at the surface. NE2 is also discussed in PR25-94-05, where the dip value is derived from. The location used in the pointtable for RVS is from the central part of the mylonite in the trench.

Protocol Id:

TASH150

Deformation zones, single observations

<i>Observation based on</i>	
TMS-mapping:	
TMS-database:	
Design-file: AS_crop.dgn, AS_trench.dgn	Source: Sycon
Parameters from SICADA:	
Coremapping protocol-	Source:
BIPS pictures-	Source: Äspö archive
Other: Technical note 25-93-07i	Reference: PR25-94-05

<i>Tunnel section(s):</i>	<i>Borehole section(s):</i>	<i>Other:</i>
		Surface outcrop
<i>Zone name: NE2</i>		<i>Uncertainty (C/P/Po/NA):</i>

<i>Host rock type</i>	Mylonite (100%)	P
<i>Width</i>	5.5 metre	P
<i>Alteration</i>	Strong	P
<i>Zone orientation</i>	20/75	P/Po
<i>No of sets:</i>	NA	NA
<i>Fracture intensity, Spacing, m (number of fractures if recorded)</i>	NA	NA
<i>Orientation</i>	NA	NA
<i>Length (average) Variability (+/- 2 sigma)</i>	NA	NA
<i>Water (Y/N, l/min)</i>	Y, NA	NA
<i>Mineralogy (percentage NA)</i>	NA	NA
<i>Grouting:</i>	NA	NA

Remark: This wide mylonite in the elevator shaft was mapped as a separate project from the ordinary tunnel mapping. The zone is here primarily ductile and is actually not very fractured. In total it contains 5-6 fractures. There is however a central fault-related fracture that parallels the zone and this is water bearing.

Protocol Id:

TASA3336

Deformation zones, single observations

<i>Observation based on</i>	
TMS-mapping: tkart4.dgn	
TMS-database: tms.mdb	
Design-file: tkarttbm_ls.dgn	Source: Äspö TBM database
Parameters from SICADA:	
Coremapping protocol-	Source:
BIPS pictures-	Source: Äspö archive
Other:	Reference:

Tunnel section(s):

Borehole section(s):

Other:

TASA 3333-3341	-	-
----------------	---	---

Zone name: NE2 (Fracture_ID 14)

Uncertainty (C/P/Po/N):

Host rock type

PSF (~97%), HSC (~3%)

P

Width

<0.5 metre

C

Alteration

Medium

P

Zone orientation

31/85

P

No of sets: NA

NA

Fracture intensity,

set 1

Spacing, m

NA

(number of fractures if recorded)

NA

Orientation

set 1

NA

NA

Length (average)

set 1

Variability (+/- 2 sigma)

NA

NA

Water

set 1

(Y/N, l/min)

N

P

Mineralogy

set 1

(percentage NA)

Ep, Ka

Kl, My, Ox

P

Grouting: N

Remark: This fracture with mylonite may be a possible location for NE2, thinning out towards depth. Four more fractures show evidence of displacement in the immediate vicinity of this fracture. None of the fractures are waterbearing. Water bearing fractures close to this fracture have high angle to it, Their relation to this mylonite is not clear.

Protocol Id:

TASA2862

Deformation zones, single observations

Related protocols: -

Observation based on
 TMS-mapping: tkart4.dgn
 TMS-database: tms.mdb
 Design-file: Frac_Cat_2002_J_Ä96.dgn Source: This project
 Parameters from SICADA:
 Coremapping protocol- Source:
 BIPS pictures- Source: Äspö archive
 Other: Fracture Zone Catalogue Reference: PR25-95-21

<i>Tunnel section(s):</i>	<i>Borehole section(s):</i>	<i>Other:</i>
TASA 2858-2864m	-	-

Zone name: NE2 (Z8) *Uncertainty (C/P/Po/N):*

<i>Host rock type</i> PSE (~80%), PSF (~15 %), HSC (~5%)	P
<i>Width</i> 0.5 metre (0.25-0.5)	P
<i>Alteration</i> Medium	P
<i>Zone orientation</i> 8/50 (12/64)	P
<i>No of sets: 3</i>	P
<i>Fracture intensity, set 1</i> <i>Spacing, m</i> 0.01 <i>(number of fractures if recorded)</i> (8)	N/P
<i>Orientation</i> set 1 8/50	P
<i>Length (average)</i> set 1 <i>Variability (+/- 2 sigma)</i> NA	C
<i>Water</i> set 1 <i>(Y/N, l/min)</i> Y (0.03, 0.01)	P
<i>Mineralogy</i> set 1 <i>(percentage NA)</i> K1	P
<i>Grouting: N</i>	

Remark: The zone is marked as waterbearing, coming from two dripping diffuse points in the roof.

Ca 10 m west of the zone there are two subparallel water bearing fractures and just east of the zone a waterbearing fracture have the same strike as the zone but dip west. The zone is mapped as ductile. No water bearing fractures is in contact with or penetrates the zone.

Protocol Id:

TASA2476

Deformation zones, single observations

Observation based on
 TMS-mapping: tkart4.dgn
 TMS-database: tms.mdb
 Design-file: Frac_Cat_2002_J_Ä96.dgn Source: This project
 Parameters from SICADA:
 Coremapping protocol- Source:
 BIPS pictures- Source: Äspö archive
 Other: Fracture Zone Catalogue Reference: PR25-95-21

<i>Tunnel section(s):</i>	<i>Borehole section(s):</i>	<i>Other:</i>
TASA 2476-2483m	-	-

Zone name: NE2 (Z7) *Uncertainty (C/P/Po/N):*

<i>Host rock type</i> HSC (~50%), VB (~45 %), PSF (~5%)				P
<i>Width</i> 7 metre (6.5-7.5)				P
<i>Alteration</i> Medium (partly mylonitised)				P
<i>Zone orientation</i> 32/65 (12/64)				P
<i>No of sets: 3</i>				P
<i>Fracture intensity, Spacing, m (number of fractures if recorded)</i>	set 1 0.1, 0.18 (30, 22)	set 2 1.3, 1 (4, 4)	set 3 0.5 (5)	N/P
<i>Orientation</i>	set 1 28/78, 12/64	set 2 347/72, 85/85	set 3 320/12	P
<i>Length (average) Variability (+/- 2 sigma)</i>	set 1-3 NA			C
<i>Water (Y/N, l/min)</i>	set 1 N	set 2 N	set 3 N	P
<i>Mineralogy (percentage NA)</i>	set 1 My, Ep, Kl Ka, Fl	set 2 Ka, Kl, Fl	set 3 Ka	P
<i>Grouting: Y</i>				

Remark: Set 2 with orientation 85/85 has striation with the orientation 85/05.

The zone is marked as water bearing, but the three fracture sets are not. Several diffuse areas in the zone are dripping, altogether giving less than 1 l/min.

Close to the zone there exists both parallel water bearing fractures and water bearing fractures at high angle to the zone. At least one of these ends at the zone boundary and none penetrate the boundary.

Protocol Id:

TASA1844

Deformation zones, single observations

Observation based on
 TMS-mapping: tkart3.dgn
 TMS-database: tms.mdb
 Design-file: Frac_Cat_2002_J_Ä96.dgn Source: This project
 Parameters from SICADA:
 Coremapping protocol- Source:
 BIPS pictures- Source: Äspö archive
 Other: Fracture Zone Catalogue Reference: PR25-95-21

<i>Tunnel section(s):</i>	<i>Borehole section(s):</i>	<i>Other:</i>
TASA 1843-1849m	-	-

Zone name: NE2 (Z7) *Uncertainty (C/P/Po/N):*

<i>Host rock type</i> HSC (~50%), PSF (~50%)	P									
<i>Width</i> 0.6 metre (0.6-2.5)	P									
<i>Alteration</i> Strong	P									
<i>Zone orientation</i> 15/70, 11/68	P									
<i>No of sets: 2</i>	P									
<i>Fracture intensity, Spacing, m (number of fractures if recorded)</i>	N/P									
<table style="width: 100%; border-collapse: collapse;"> <thead> <tr> <th style="width: 60%;"></th> <th style="width: 20%; text-align: center;">set 1</th> <th style="width: 20%; text-align: center;">set 2</th> </tr> </thead> <tbody> <tr> <td>Spacing, m</td> <td style="text-align: center;">0.2, 0.04</td> <td style="text-align: center;">0.05</td> </tr> <tr> <td>(number of fractures if recorded)</td> <td style="text-align: center;">(-, 65)</td> <td style="text-align: center;">(7)</td> </tr> </tbody> </table>		set 1	set 2	Spacing, m	0.2, 0.04	0.05	(number of fractures if recorded)	(-, 65)	(7)	N/P
	set 1	set 2								
Spacing, m	0.2, 0.04	0.05								
(number of fractures if recorded)	(-, 65)	(7)								
<i>Orientation</i>	P									
<table style="width: 100%; border-collapse: collapse;"> <thead> <tr> <th style="width: 60%;"></th> <th style="width: 20%; text-align: center;">set 1</th> <th style="width: 20%; text-align: center;">set 2</th> </tr> </thead> <tbody> <tr> <td></td> <td style="text-align: center;">11/68, 15/70</td> <td style="text-align: center;">288/68</td> </tr> </tbody> </table>		set 1	set 2		11/68, 15/70	288/68	P			
	set 1	set 2								
	11/68, 15/70	288/68								
<i>Length (average)</i>	C									
<i>Variability (+/- 2 sigma)</i>	C									
<table style="width: 100%; border-collapse: collapse;"> <thead> <tr> <th style="width: 60%;"></th> <th style="width: 20%; text-align: center;">set 1</th> <th style="width: 20%; text-align: center;">set 2</th> </tr> </thead> <tbody> <tr> <td><i>Water (Y/N, l/min)</i></td> <td style="text-align: center;">Y</td> <td style="text-align: center;">NA</td> </tr> <tr> <td>(18 l/min in FZC)</td> <td></td> <td></td> </tr> </tbody> </table>		set 1	set 2	<i>Water (Y/N, l/min)</i>	Y	NA	(18 l/min in FZC)			P
	set 1	set 2								
<i>Water (Y/N, l/min)</i>	Y	NA								
(18 l/min in FZC)										
<i>Mineralogy (percentage NA)</i>	P									
<table style="width: 100%; border-collapse: collapse;"> <thead> <tr> <th style="width: 60%;"></th> <th style="width: 20%; text-align: center;">set 1</th> <th style="width: 20%; text-align: center;">set 2</th> </tr> </thead> <tbody> <tr> <td></td> <td style="text-align: center;">Cy, Kl, Ka, Qz</td> <td style="text-align: center;">Kl</td> </tr> </tbody> </table>		set 1	set 2		Cy, Kl, Ka, Qz	Kl	P			
	set 1	set 2								
	Cy, Kl, Ka, Qz	Kl								

Grouting: N

Remark: A thinner fracture zone (Z6, ~0.5 m wide) with the orientation 45/28 affects the tunnelsystem over a long section including this zone. Although mapped partly at the same location, the relation between the present zone and Z6 is not clear.

The zone is marked as water bearing and there are two fractures close to the zone which also are water bearing, one subparallel and one at high angle. These are not in contact with the zone.

Protocol Id:

TASA1602

Deformation zones, single observations

Observation based on
 TMS-mapping: tkart3.dgn
 TMS-database: tms.mdb
 Design-file: Frac_Cat_2002_J_Ä96.dgn Source: This project
 Parameters from SICADA:
 Coremapping protocol- Source:
 BIPS pictures- Source: Äspö archive
 Other: Fracture Zone Catalogue Reference: PR25-95-21

<i>Tunnel section(s):</i>	<i>Borehole section(s):</i>	<i>Other:</i>
TASA 1602-1603m	-	-

Zone name: NE2 (Z5) *Uncertainty (C/P/Po/N):*

<i>Host rock type</i> HSC (~90%) PSF (~10 %)	Po
<i>Width</i> 0.6 metre (0.6-1.2)	P
<i>Alteration</i> Medium	P
<i>Zone orientation</i> 36/82	P
<i>No of sets: 4</i>	P
<i>Fracture intensity, Spacing, m (number of fractures if recorded)</i>	N/P
set 1 0.03 (36)	
set 2 0.07 (16)	
set 3 0.07 (9)	
set 4 0.07 (181)	
<i>Orientation</i>	P
set 1 34/82, 36/82	
set 2 36/83	
set 3 220/10	
set 4 320/80	C
<i>Length (average)</i>	P
set 1-4 Variability (+/- 2 sigma) NA	
<i>Water (Y/N, l/min)</i>	P
set 1-4 N	

<i>Mineralogy</i> (percentage NA)	set 1 Kl, Cy	set 2 Kl, Ep, Fl	Set 3 Kl, Ka, Fl
	set 4 Kl, Ka		

Grouting: N

Remark:

The zone itself is not marked as water bearing, but a water ID (B) is mapped in the northern wall as v.

No waterbearing fracture exist close to the zone.

Protocol Id:

KC0045

Deformation zones, single observations

Related protocols: -

<i>Observation based on</i>	
TMS-mapping:	
TMS-database:	
Design-file:	Source:
Parameters from SICADA:corelogging Method: pc_logging_new and petrocore	
Coremapping protocol-	Source:
BIPS pictures-	Source: Äspö archive
Other:	Reference:

<i>Tunnel section(s):</i>	<i>Borehole section(s):</i>	<i>Other:</i>
	Not assaigned	-

Zone name: NE2 Uncertainty (C/P/Po/NA):

<i>Host rock type</i>	
Fine grained granite (100%)	P
<i>Width</i>	
NA	NA
<i>Alteration</i>	
NA	NA
<i>Zone orientation</i>	
NA	NA
<i>No of sets: NA</i>	NA
<i>Fracture intensity, Spacing, m (number of fractures if recorded)</i>	P
<i>Orientation</i>	NA
<i>Length (average) Variability (+/- 2 sigma)</i>	NA
<i>Water (Y/N, l/min)</i>	NA
<i>Mineralogy (percentage NA)</i>	NA
<i>Grouting: NA</i>	

Remark: The borehole KC0045 seems to have been drilled subparallel with a dike of fine grained granite. There are a few thin crush zones in the vicinity of the supposed location of NE2, but otherwise no indications of deformation or alteration of the kind characterising NE2 at nearest observation locations. No one of the crush zones has been assigned to NE2 since there are no evidences or indications of which of them that may relate to the zone.

Protocol Id:

TASA3083

Deformation zones, single observations

Observation based on
 TMS-mapping: tkart5.dgn
 TMS-database: tms.mdb
 Design-file: Frac_Cat_2002_J_Ä96.dgn Source: This project
 Parameters from SICADA:
 Coremapping protocol- Source:
 BIPS pictures- Source: Äspö archive
 Other: Fracture Zone Catalogue Reference: PR25-95-21, HRL-16-19

<i>Tunnel section(s):</i>	<i>Borehole section(s):</i>	<i>Other:</i>
TASA 3082-3084m	-	-

Zone name: (Z1) *Uncertainty (C/P/Po/NA):*

<i>Host rock type</i> Basic volcanite (45%), Granite (~50%) Pegmatite (<5%)		P
<i>Width</i>	~0.5 m	P
<i>Alteration</i>	Weak	P
<i>Zone orientation</i>	302/75	P
<i>No of sets:</i>	1	P
<i>Fracture intensity, Spacing, m (number of fractures if recorded)</i>	set 1 0.003(5)	P
<i>Orientation</i>	set 1 302/75	P
<i>Length (average) Variability (+/- 2 sigma)</i>	NA	NA
<i>Water (Y/N, l/min) Total ~10 l/min</i>	set 1 Y, NA	P
<i>Mineralogy (percentage NA)</i>	set 1 Ep, Ca, Chl	P
<i>Grouting:</i>	Y	P

Remark: The zone is water bearing and there are a few waterbearing fractures and another narrow zone close to the south. These are all at low angle to the zone and are not in contact with it in the tunnel. The fractures in the zone are mapped as ductile. The pegmatite is faulted by the zone.

Protocol Id:

TASA1979

Deformation zones, single observations

Observation based on
 TMS-mapping: tkart3.dgn
 TMS-database: tms.mdb
 Design-file: Frac_Cat_2002_J_Ä96.dgn Source: This project
 Parameters from SICADA:
 Coremapping protocol- Source:
 BIPS pictures- Source: Äspö archive
 Other: Fracture Zone Catalogue Reference: PR25-95-21, HRL-16-19

<i>Tunnel section(s):</i>	<i>Borehole section(s):</i>	<i>Other:</i>
TASA 1979-2004	-	-

Zone name: (Z9)

Uncertainty (C/P/Po/NA):

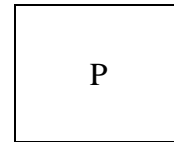
<i>Host rock type</i>	Granodiorite (~35%), Granite(~65%)	P									
<i>Width</i>	~0.5 metre	P									
<i>Alteration</i>	Partly	P									
<i>Zone orientation</i>	290/85, 109/88, 100/85, 110/85	P									
<i>No of sets: 3</i>		P									
<i>Fracture intensity, Spacing, m (number of fractures if recorded)</i>	<table style="width: 100%; border-collapse: collapse;"> <thead> <tr> <th style="width: 33%;">set 1</th> <th style="width: 33%;">set 2</th> <th style="width: 33%;">set 3</th> </tr> </thead> <tbody> <tr> <td>0.04(10), 0.02(15)</td> <td>0.13(8)</td> <td>0.125(5)</td> </tr> <tr> <td>0.125(9)</td> <td></td> <td></td> </tr> </tbody> </table>	set 1	set 2	set 3	0.04(10), 0.02(15)	0.13(8)	0.125(5)	0.125(9)			P
set 1	set 2	set 3									
0.04(10), 0.02(15)	0.13(8)	0.125(5)									
0.125(9)											
<i>Orientation</i>	<table style="width: 100%; border-collapse: collapse;"> <thead> <tr> <th style="width: 33%;">set 1</th> <th style="width: 33%;">set 2</th> <th style="width: 33%;">set 3</th> </tr> </thead> <tbody> <tr> <td>288/88, 290/85, 109/88, 100/85, 110/85</td> <td>322/78</td> <td>260/49</td> </tr> </tbody> </table>	set 1	set 2	set 3	288/88, 290/85, 109/88, 100/85, 110/85	322/78	260/49	P			
set 1	set 2	set 3									
288/88, 290/85, 109/88, 100/85, 110/85	322/78	260/49									
<i>Length (average) Variability (+/- 2 sigma)</i>	<table style="width: 100%; border-collapse: collapse;"> <thead> <tr> <th style="width: 33%;">set 1</th> <th style="width: 33%;">set 2</th> <th style="width: 33%;">set 3</th> </tr> </thead> <tbody> <tr> <td>NA</td> <td></td> <td></td> </tr> </tbody> </table>	set 1	set 2	set 3	NA			P			
set 1	set 2	set 3									
NA											
<i>Water (Y/N, l/min)</i>	<table style="width: 100%; border-collapse: collapse;"> <thead> <tr> <th style="width: 33%;">set 1</th> <th style="width: 33%;">set 2</th> <th style="width: 33%;">set 3</th> </tr> </thead> <tbody> <tr> <td>Y, NA</td> <td>N</td> <td>N</td> </tr> </tbody> </table>	set 1	set 2	set 3	Y, NA	N	N	NA			
set 1	set 2	set 3									
Y, NA	N	N									
<i>Total ~10 l/min</i>		P									

Mineralogy
(percentage NA)

set 1
Chl, Ca, Ox,
My,Ep, Ij

set 2
Ca, Ox

set 3
Chl, Ca, Ij



Grouting: Y

Remark: The zone is water bearing and there are a few waterbearing fractures close and at high angle to the zone. The long water bearing fracture seems to crosscut the zone. The waterbearing fractures outside the zone are sub-parallel to NNW4, which is ca 20 metres east of the zone. Fractures in set 1. with orientation 109/88, have mylonite as fracture mineral

Protocol Id:

TASA1876

Deformation zones, single observations

Observation based on
 TMS-mapping: tkart3.dgn
 TMS-database: tms.mdb
 Design-file: Frac_Cat_2002_J_Ä96.dgn Source: This project
 Parameters from SICADA:
 Coremapping protocol- Source:
 BIPS pictures- Source: Äspö archive
 Other: Fracture Zone Catalogue Reference: PR25-95-21, ICR97-01

<i>Tunnel section(s):</i>	<i>Borehole section(s):</i>	<i>Other:</i>
TASA 1872-1878m	-	-

Zone name: (Z8)

Uncertainty (C/P/Po/NA):

<i>Host rock type</i>	Granodiorite (100%)	P
<i>Width</i>	0.2 metre (0.2--~1.5)	P
<i>Alteration</i>	Medium	P
<i>Zone orientation</i>	110/84, 110/80 (112/80)	P
<i>No of sets:</i>	1	P
<i>Fracture intensity, Spacing, m (number of fractures if recorded)</i>	set 1 0.02(10), 0.08(9)	NA/P
<i>Orientation</i>	set 1 110/84, 110/80	P
<i>Length (average) Variability (+/- 2 sigma)</i>	set 1 NA	NA
<i>Water (Y/N, l/min) Total 102 in FZC</i>	set 1 Y, NA	P
<i>Mineralogy (percentage NA)</i>	set 1 Ep, Ij, Rf, Ca, Chl, Cy	P
<i>Grouting:</i>	Y	P

Remark: The zone is water-bearing and there are also several water-bearing fractures close to the zone. Most of them are to the south-west of and sub-parallel with the zone. However, there is also a water bearing fracture at high angle to the zone, west of it, and according to the design-files from the mapping it is not in contact with the zone.

Protocol Id:

KAS06

Deformation zones, single observations

<i>Observation based on</i>	
TMS-mapping:	
TMS-database:	
Design-file:	Source:
Parameters from SICADA:Method: pc_logging_new	
Coremapping protocol-	Source:
BIPS pictures-	Source: Äspö archive
Other:	Reference:

<i>Tunnel section(s):</i>	<i>Borehole section(s):</i>	<i>Other:</i>
-	595.9-598.4	-

Zone name: NW1

Uncertainty (C/P/Po/NA):

<i>Host rock type</i>	Granodiorite (100%)	P
<i>Width</i>	>=1.4 m	P
<i>Alteration</i>	Tectonisation	P
<i>Zone orientation</i>	NA	NA
<i>No of sets:</i>	NA	NA
<i>Fracture intensity, Spacing, m (number of fractures if recorded)</i>	NA NA 11 fractures	P
<i>Orientation</i>	NA	NA
<i>Length (average) Variability (+/- 2 sigma)</i>	NA	NA
<i>Water (Y/N, l/min)</i>	NA	NA
<i>Mineralogy (percentage NA)</i>	Chl, Ca, Ep, Py, Hm	P
<i>Grouting</i>	N	P

Remark: The angle between the model zone and the borehole is ca 35 degrees

Protocol Id:

KA2050

Deformation zones, single observations

<i>Observation based on</i>	
TMS-mapping:	
TMS-database:	
Design-file:	Source:
Parameters from SICADA: Method: pc_logginng_new	
Coremapping protocol-	Source:
BIPS pictures-	Source: Äspö archive
Other:	Reference:

<i>Tunnel section(s):</i>	<i>Borehole section(s):</i>	<i>Other:</i>
-	6.28-8.16	-

Zone name: NW1

Uncertainty (C/P/Po/NA):

<i>Host rock type</i>	Fine-grained granite (~50%), granite	P	(100%)
<i>Width</i>	NA	NA	
<i>Alteration</i>	No	P	
<i>Zone orientation</i>	NA	NA	
<i>No of sets:</i>	NA	NA	
<i>Fracture intensity, Spacing, m (number of fractures if recorded)</i>	NA NA 17 fractures, crush not included.	P	
<i>Orientation</i>	NA	NA	
<i>Length (average) Variability (+/- 2 sigma)</i>	NA	NA	
<i>Water (Y/N, l/min)</i>	NA	NA	
<i>Mineralogy (percentage NA)</i>	Ca, Chl, Ep, Ox	P	
<i>Grouting</i>	No		

Remark: Only indications of brittle deformations in this observation.

Protocol Id:

TASA2914

Deformation zones, single observations

Observation based on
 TMS-mapping: tkart5.dgn
 TMS-database: tms.mdb
 Design-file: Frac_Cat_2002_J_Ä96.dgn Source: This project
 Parameters from SICADA:
 Coremapping protocol- Source:
 BIPS pictures- Source: Äspö archive
 Other: Fracture Zone Catalogue Reference: PR25-95-21, HRL 96-01

<i>Tunnel section(s):</i>	<i>Borehole section(s):</i>	<i>Other:</i>
TASA 2911-2931m	-	-

Zone name: (Z9)

Uncertainty (C/P/Po/N):

Host rock type

PSF (~85%) HSC (~15 %)

P

Width

7.8 metre

P

Alteration

Weak

P

Zone orientation

128/80

P

No of sets: 5

P

Fracture intensity,

set 1

set 2

set 3

Spacing, m

0.08(29)

0.03(9)

0.2(8)

(number of fractures if recorded)

set 4

set 5

0.15(10)

0.5(6)

N/P

Orientation

set 1

set 2

set 3

98/73

237/25

128/80

P

set 4

set 5

130/50

239/90

C

Length (average)

set 1-5

Variability (+/- 2 sigma)

NA

P

Water

set 1-5

(Y/N, l/min)

N

P

Total 500 l/min in FZC

<i>Mineralogy</i> (percentage NA)	set 1	set 2	set 3
	Chl, Ca	Ca	Ca
	set 4	set 5	
	Ca	Ca	

Grouting: Y

Remark: Although the fracture sets is not water bearing according to the database, the zone is strongly water bearing. There are several water bearing fractures around the zone, most at high angle to it. None of these seem to be in contact with the zone, but several dry fractures are. Two zones pass through Z9 here according to HRL96-01 (fig. 6.2), one approximately N-S and another at NW-SE.

Protocol Id:

TASA2120

Deformation zones, single observations

Observation based on
 TMS-mapping: tkart3.dgn
 TMS-database: tms.mdb
 Design-file: Frac_Cat_2002_J_Ä96.dgn Source: This project
 Parameters from SICADA:
 Coremapping protocol- Source:
 BIPS pictures- Source: Äspö archive
 Other: Fracture Zone Catalogue Reference: PR25-95-21

<i>Tunnel section(s):</i>	<i>Borehole section(s):</i>	<i>Other:</i>
TASA 2113-2137m	-	-

Zone name: (Z3) *Uncertainty (C/P/Po/N):*

<i>Host rock type</i> PSE	P																				
<i>Width</i> 0.6 metre (~0.5-1 metre)	P																				
<i>Alteration</i> Medium-strong	P																				
<i>Zone orientation</i> 355/80, 345/80, 350/88	P																				
<i>No of sets: 5</i>	P																				
<table style="width: 100%; border-collapse: collapse;"> <thead> <tr> <th style="text-align: left;"><i>Fracture intensity,</i></th> <th style="text-align: left;">set 1</th> <th style="text-align: left;">set 2</th> <th style="text-align: left;">set 3</th> </tr> </thead> <tbody> <tr> <td><i>Spacing, m</i></td> <td>0.1(5), 0.15(6), 0.5(3),</td> <td>0.3(7),</td> <td>0.2(11)</td> </tr> <tr> <td><i>(number of fractures if recorded)</i></td> <td>0.1(10), 0.06(15), 0.15(6)</td> <td>0.18(18)</td> <td>0.33(15)</td> </tr> <tr> <td></td> <td>set 4</td> <td>set 5</td> <td></td> </tr> <tr> <td></td> <td>0.5(3)</td> <td>0.67(4)</td> <td></td> </tr> </tbody> </table>	<i>Fracture intensity,</i>	set 1	set 2	set 3	<i>Spacing, m</i>	0.1(5), 0.15(6), 0.5(3),	0.3(7),	0.2(11)	<i>(number of fractures if recorded)</i>	0.1(10), 0.06(15), 0.15(6)	0.18(18)	0.33(15)		set 4	set 5			0.5(3)	0.67(4)		P
<i>Fracture intensity,</i>	set 1	set 2	set 3																		
<i>Spacing, m</i>	0.1(5), 0.15(6), 0.5(3),	0.3(7),	0.2(11)																		
<i>(number of fractures if recorded)</i>	0.1(10), 0.06(15), 0.15(6)	0.18(18)	0.33(15)																		
	set 4	set 5																			
	0.5(3)	0.67(4)																			
<table style="width: 100%; border-collapse: collapse;"> <thead> <tr> <th style="text-align: left;"><i>Orientation</i></th> <th style="text-align: left;">set 1</th> <th style="text-align: left;">set 2</th> <th style="text-align: left;">set 3</th> </tr> </thead> <tbody> <tr> <td></td> <td>355/80, 340/80, 190/90</td> <td>310/89,</td> <td>128/80</td> </tr> <tr> <td></td> <td>334/88, 150/87</td> <td>27/62</td> <td>195/60</td> </tr> <tr> <td></td> <td>set 4</td> <td>set 5</td> <td></td> </tr> <tr> <td></td> <td>26/24</td> <td>294/88</td> <td></td> </tr> </tbody> </table>	<i>Orientation</i>	set 1	set 2	set 3		355/80, 340/80, 190/90	310/89,	128/80		334/88, 150/87	27/62	195/60		set 4	set 5			26/24	294/88		P
<i>Orientation</i>	set 1	set 2	set 3																		
	355/80, 340/80, 190/90	310/89,	128/80																		
	334/88, 150/87	27/62	195/60																		
	set 4	set 5																			
	26/24	294/88																			
<table style="width: 100%; border-collapse: collapse;"> <tbody> <tr> <td style="width: 70%;"><i>Length (average)</i></td> <td style="width: 30%;">set 1-5</td> </tr> <tr> <td><i>Variability (+/- 2 sigma)</i></td> <td>NA</td> </tr> </tbody> </table>	<i>Length (average)</i>	set 1-5	<i>Variability (+/- 2 sigma)</i>	NA	P																
<i>Length (average)</i>	set 1-5																				
<i>Variability (+/- 2 sigma)</i>	NA																				

<i>Water</i> (Y/N, l/min) Total 57 l/min in FZC	set 1 Y, NA	set 2 N	set 3 N	P
	set 4 N	set 5 N		
<i>Mineralogy</i> (percentage NA)	set 1 Ca, Chl, Ij, Ep	set 2 Chl, Ca	set 3 Chl, Ca	P
	Set 4 Chl	set 5 Chl		

Grouting: Y

Remark: There is a zone of increased fracturing south of the zone, which is marked as water bearing in the mapping design file. There are also several minor water bearing, sub-parallel fractures on both sides of the zone. Several dry fractures intersect the zone boundary.

TASA2020

Protocol Id:

Deformation zones, single observations

Observation based on
 TMS-mapping: tkart3.dgn
 TMS-database: tms.mdb
 Design-file: Frac_Cat_2002_J_Ä96.dgn Source: This project
 Parameters from SICADA:
 Coremapping protocol- Source:
 BIPS pictures- Source: Äspö archive
 Other: Fracture Zone Catalogue Reference: PR25-95-21, ICR97-01

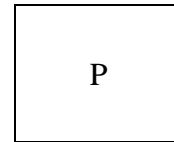
<i>Tunnel section(s):</i>	<i>Borehole section(s):</i>	<i>Other:</i>

Zone name: NNW4 (Z1) Uncertainty (C/P/Po/U):

<i>Host rock type</i> PSE	P
<i>Width</i> 0.6 metre (0.5~1) (1-3 m in ICR97-01)	Po
<i>Alteration</i> Weak-medium	P
<i>Zone orientation</i> 335/80, 154/83, 342/72	P
<i>No of sets:</i> 1 (From ICR97-01: secondary 10/70)	Po
<i>Fracture intensity, set 1</i> <i>Spacing, m</i> 0.13(7), 0.06(18), 0.065(7) <i>(number of fractures if recorded)</i>	P
<i>Orientation set 1</i> 335/80, 154/83, 342/72	P
<i>Length (average) set 1</i> <i>Variability (+/- 2 sigma)</i> NA	C
<i>Water set 1</i> <i>(Y/N, l/min)</i> Y, NA Total 10 l/min in FZC	P

Mineralogy
(percentage NA)

set 1
Chl, Ca, Cy,
Ij, Fe



Grouting: Y

Remark: The zone is water bearing and partly crushed. There is also a surrounding zone (Z0) of increased fracturing. There are several water bearing fractures close to and sub-parallel to the zone and 1-2 are in contact with the zone.

There are no indications of a ductile precursor in the database, but abrupt end of lithologies towards the zone indicate significant faulting.

Protocol Id:

KA2048

Deformation zones, single observations

<i>Observation based on</i>	
TMS-mapping:	
TMS-database:	
Design-file:	Source:
Parameters from SICADA: Method: pc_logging_new	
Coremapping protocol-	Source:
BIPS picture:	Source: Äspö archive
Other:	Reference:

<i>Tunnel section(s):</i>	<i>Borehole section(s):</i>	<i>Other:</i>
-	27.5-46.8 metre	-

Zone name: (NWW4) *Uncertainty (C/P/Po/NA):*

<i>Host rock type</i>	Granite (~45%), pegmatite (~20%) and fine grained granite	P
<i>Width</i>	NA	NA
<i>Alteration</i>	Oxidisation	P
<i>Zone orientation</i>	NA	NA
<i>No of sets:</i>	NA	NA
<i>Fracture intensity, Spacing, m (number of fractures if recorded)</i>	(Average ~9 fractures/m, crush excluded) Crush zone totally 1.16m A total of 173 fractures	NA
<i>Orientation</i>	NA	NA
<i>Length (average) Variability (+/- 2 sigma)</i>	NA	NA
<i>Water (Y/N, l/min)</i>	NA	NA
<i>Mineralogy (percentage NA)</i>	Chl, Ca, Hm, Ep, Fl	P
<i>Grouting</i>	No	P

Remark: The fine grained granite is brecciated and there is a thin breccia (vein) at 30.77. Six narrow crush zones. Low RQD:s between c.27.5 and 45.7. No indications

Protocol Id:

TASA2914

Deformation zones, single observations

Observation based on
 TMS-mapping: tkart5.dgn
 TMS-database: tms.mdb
 Design-file: Frac_Cat_2002_J_Ä96.dgn Source: This project
 Parameters from SICADA:
 Coremapping protocol- Source:
 BIPS pictures- Source: Äspö archive
 Other: Fracture Zone Catalogue Reference: PR25-95-21, HRL 96-01

<i>Tunnel section(s):</i>	<i>Borehole section(s):</i>	<i>Other:</i>
TASA 2911-2931m	-	-

Zone name: (Z9) *Uncertainty (C/P/Po/NA):*

<i>Host rock type</i> PSF (~85%) HSC (~15 %)	P	
<i>Width</i> 7.8 metre	P	
<i>Alteration</i> Weak	P	
<i>Zone orientation</i> 128/80	P	
<i>No of sets: 5</i>	P	
<i>Fracture intensity, Spacing, m (number of fractures if recorded)</i>	P	
set 1 0.08(29)	set 2 0.03(9)	set 3 0.2(8)
set 4 0.15(10)	set 5 0.5(6)	
<i>Orientation</i>	P	
set 1 98/73	set 2 237/25	set 3 128/80
set 4 130/50	set 5 239/90	NA
<i>Length (average)</i>	P	
<i>Variability (+/- 2 sigma)</i>	P	
set 1-5 NA		
<i>Water (Y/N, l/min)</i>	P	
set 1-5 N		
Total 500 l/min in FZC		

<i>Mineralogy</i> (percentage NA)	set 1 Chl, Ca	set 2 Ca	set 3 Ca
	set 4 Ca	set 5 Ca	

Grouting: Y

Remark: Although the fracture sets is not water bearing according to the database, the zone is strongly water bearing. There are several water bearing fractures around the zone, most at high angle to it. None of these seem to be in contact with the zone, but several dry fractures are. Two zones pass through Z9 here according to HRL96-01 (fig. 6.2), one approximately N-S and another at NW-SE.

Protocol Id:

TASF15

Deformation zones, single observations

<i>Observation based on</i>	
TMS-mapping: nkart3.dgn	
TMS-database: tms.mdb	
Design-file:	Source:
Parameters from SICADA:	Source:
Coremapping protocol-	Source: Äspö archive
BIPS pictures-	

<i>Tunnel section(s):</i>	<i>Borehole section(s):</i>	<i>Other:</i>
TASF 3-14 TASJ 11-23	-	-

Zone name: (Z4)

Uncertainty (C/P/Po/NA):

<i>Host rock type</i>	Granodiorite with some fine-grained granite (<5%)	P												
<i>Width</i>	1.2 metre (0.6-1.5)	P												
<i>Alteration</i>	Medium	P												
<i>Zone orientation</i>	216/90	P												
<i>No of sets:</i>	3	P												
<i>Fracture intensity, Spacing, m (number of fractures)</i>	<table style="width: 100%; border-collapse: collapse;"> <tr> <td style="width: 33%;">set 1</td> <td style="width: 33%;">set2</td> <td style="width: 33%;">set3</td> </tr> <tr> <td>0.07(16)</td> <td>0.8(5)</td> <td>0.2(6)</td> </tr> <tr> <td>set 4</td> <td></td> <td></td> </tr> <tr> <td>0.02(60)</td> <td></td> <td></td> </tr> </table>	set 1	set2	set3	0.07(16)	0.8(5)	0.2(6)	set 4			0.02(60)			P
set 1	set2	set3												
0.07(16)	0.8(5)	0.2(6)												
set 4														
0.02(60)														
<i>Orientation</i>	<table style="width: 100%; border-collapse: collapse;"> <tr> <td style="width: 33%;">set 1</td> <td style="width: 33%;">set2</td> <td style="width: 33%;">set 3</td> </tr> <tr> <td>216/90</td> <td>281/29</td> <td>300/90</td> </tr> <tr> <td>set 4</td> <td></td> <td></td> </tr> <tr> <td>204/90</td> <td></td> <td></td> </tr> </table>	set 1	set2	set 3	216/90	281/29	300/90	set 4			204/90			P
set 1	set2	set 3												
216/90	281/29	300/90												
set 4														
204/90														
<i>Length (average) Variability (+/- 2 sigma)</i>	<table style="width: 100%; border-collapse: collapse;"> <tr> <td style="width: 33%;">set 1-4</td> <td></td> <td></td> </tr> <tr> <td>NA</td> <td></td> <td></td> </tr> </table>	set 1-4			NA			NA						
set 1-4														
NA														
<i>Water (Y/N, l/min)</i>	<table style="width: 100%; border-collapse: collapse;"> <tr> <td style="width: 33%;">set1-4</td> <td></td> <td></td> </tr> <tr> <td>N</td> <td></td> <td></td> </tr> </table>	set1-4			N			P						
set1-4														
N														

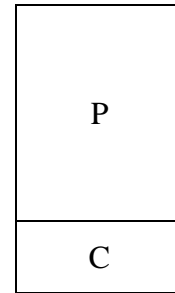
Mineralogy
(percentage NA)

set 1
Chl, Ca

set 2
Chl

set 3
Ca

set 4
Chl, Ca



Grouting: Y

Remark: This is a zone of ductile deformation essentially consisting of mylonitic granodiorite. The zone is not water bearing. There are several water bearing fractures close to the zone on both sides. Most are at high angle to the zone and four of these ends towards the zone. No one of these fractures are mapped to crosscut the

Protocol Id:

TASA3518

Deformation zones, single observations

Observation based on
 TMS-mapping: tkart5.dgn
 TMS-database: tms.mdb
 Design-file: Frac_Cat_2002_J_Ä96.dgn Source: This project
 Parameters from SICADA:
 Coremapping protocol- Source:
 BIPS pictures- Source: Äspö archive
 Other: Fracture Zone Catalogue Reference: PR25-95-21

<i>Tunnel section(s):</i>	<i>Borehole section(s):</i>	<i>Other:</i>
TASA 3518-3522m	-	-

Zone name: (Z4) *Uncertainty (C/P/Po/NA):*

<i>Host rock type</i> PSF		P
<i>Width</i> 3.0 metre (-3.5)		P
<i>Alteration</i> Medium		P
<i>Zone orientation</i> 218/88		P
<i>No of sets:</i> 1		P
<i>Fracture intensity,</i> <i>Spacing, m</i> <i>(number of fractures)</i>	set 1 0.3(8)	P
<i>Orientation</i>	set 1 218/88	P
<i>Length (average)</i> <i>Variability (+/- 2 sigma)</i>	set 1 NA	NA
<i>Water</i> <i>(Y/N, l/min)</i> Total 6 l/min in FZC	set 1 N	P
<i>Mineralogy</i> <i>(percentage NA)</i>	set 1 Ca	P

Grouting: Y

Remark: A zone of ductile deformation consisting of mylonitic Granodiorite.
The zone is not water bearing according to the database. There are two water bearing fractures close to the west of the zone. One of these with extensive seepage (2.9 l/min) ends towards the zone.

Protocol Id:

KJ0044F01

Deformation zones, single observations

<i>Observation based on</i>	
TMS-mapping:	
TMS-database:	
Design-file:	Source:
Parameters from SICADA: Alteration, Natural fractures, Rock type	
Coremapping protocol-	Source:
BIPS pictures-	Source: Äspö archive
Other:	Reference:

<i>Tunnel section(s):</i>	<i>Borehole section(s):</i>	<i>Other:</i>
-	KJ0044F01, 14-17.26 m	-

Zone name: NEHQ3

Uncertainty (C/P/Po/NA):

<i>Host rock type</i>	Granite (100%), mylonitic.	P
<i>Width</i>	(Between 16.7-17.26 in borehole) NA	NA
<i>Alteration</i>	14-17.26, Oxidation, Medium	P
<i>Zone orientation</i>	NA	NA
<i>No of sets:</i>	NA	NA
<i>Fracture intensity, Spacing, m (number of fractures if recorded)</i>	4 natural fractures	P
<i>Orientation</i>	NA	NA
<i>Length (average) Variability (+/- 2 sigma)</i>	NA	NA
<i>Water (Y/N, l/min)</i>	NA	NA
<i>Mineralogy (percentage NA)</i>	Chl, Ca, oxidised walls	P
<i>Grouting</i>	N	C

Remark: The mylonitic granodiorite at the bottom of this hole may continue beyond the borehole depth. The width of the zone is thus not indicated here. The angle between the model zone and the borehole is ca 35 degrees

Protocol Id:

KA3510A

Deformation zones, single observations

<i>Observation based on</i>	
TMS-mapping:	
TMS-database:	
Design-file:	Source:
Parameters from SICADA: Alteration, Natural fractures, Rock type.	
Coremapping protocol-	Source:
BIPS pictures: Attached	Source: Äspö archive
Other:	Reference:

<i>Tunnel section(s):</i>	<i>Borehole section(s):</i>	<i>Other:</i>
-	KA3510A, 13.63-42.16(?)m	-

Zone name: NEHQ3

Uncertainty (C/P/Po/NA):

<i>Host rock type</i>	Fine grained granite (100%)	P
<i>Width</i>	ca 0.7 metre (Mylonitic part)	NA
<i>Alteration</i>	13.63-22.87 m, Oxidation, medium 22.92-42.16 m, Epidotised, strong	P/Po
<i>Zone orientation</i>	228/85 (from BDT-file) 232/89 (IPR-00-34)	P
<i>No of sets:</i>	NA	NA
<i>Fracture intensity, Spacing, m (number of fractures if recorded)</i>	34 natural fractures 17 sealed fracture	P
<i>Orientation</i>	NA	NA
<i>Length (average) Variability (+/- 2 sigma)</i>	NA	NA
<i>Water (Y/N, l/min)</i>	NA	NA
<i>Mineralogy Natural fractures (percentage NA)</i>	Chl, Ca, Py, Ep, Hm	P
<i>Grouting</i>	N	C

Remark: The zone appears to end at ca 25 metres length as do the epidotisation according to the BIPS image. The figure 42.16 may therefore be erroneous. Fractures and mineralogy are collected between 13.63 and 25 metre in the core.

The fine grained granite is mapped as mylonitic (between 22.87 to 25 m). From the BIPS-image alone it is evident that there also is a mylonitic section immediately above this granite in the borehole. It is ca 1.5 metres long in the core. Further up there is still another mylonitic section in the oxidised part of core, between ca 15.6 and 17 metre. This latter section contains several open fractures and may therefore potentially be hydraulically active.